GEOLOGICA ULTRAIECTINA

Mededelingen van het
Instituut voor Aardwetenschappen der
Rijksuniversiteit te Utrecht

No. 38

A GEOPHYSICAL STUDY OF THE ATLANTIS-METEOR SEAMOUNT COMPLEX

JAAP VERHOEF

STELLINGEN

(1)

Het Atlantis-Meteor gebergte kan gekenmerkt worden als een structureel geinduceerde warmteanomalie (secundaire hotspot). De geconstateerde NO-ZW rek die aan het gebergte ten grondslag ligt kan geplaatst worden in een driedimensionaal afkoelingsmodel van de oceanische lithosfeer. Interferentie met bewegingen tussen de Europese en Afrikaanse plaat kan niet uitgesloten worden.

-*Dit proefschrift.*
-*Collette B.J., Slootweg A.P., Verhoef J., Roest W.R. 1984. Geophysical investigations of the floor of the Atlantic Ocean between 10° and 38°N (Kroonvlag-project), Proc. Kon. Akad. Wet., series B, 87, 1-76.*

(2)

De spanningsverdeling in een elastische plaat met een primaire scheur, onder aanname van een tweedimensionale rekspanningstoestand, is dusdanig dat eventueel aanwezige haarscheurtjes in de richting van de primaire scheur en die onder een hoek met de primaire scheur, welke globaal groter is dan ±45° zich zullen openen.

-*Verhoef J., 1977. Onderzoek naar het zich voortplanten en uitbreiden van enkele soorten breuken in brosse materialen , doctoraal sciptie, Utrecht.*

(3)

Het meten van verplaatsingen in het vlak van het oppervlak van een voorwerp kan, zonder voorbewerking van het voorwerp, worden gedaan met behulp van speckle fotografie en interferometrie; een methode welke relatief ongevoelig is voor verplaatsingen uit het vlak. Bij niet uniforme verplaatsingen van het voorwerp, bijvoorbeeld rotaties of vervormingen, kan de structuur van het oppervlak er de oorzaak van zijn dat de correlatie van het speckle patroon voor en na de verplaatsing sterk vermindert en dat daardoor de maximaal meetbare verplaatsing sterk verkleind wordt.

(4)

Gezien het feit dat theoretische admittantiecurven bij zwaartekrachtsstudies veelal slechts eerste orde benaderingen zijn, is het niet aan te bevelen om uit een vergelijking van deze curven met de experimentele waarden een extrapolatie te maken waaruit de waarde van het dichtheidscontrast kan worden bepaald.

-Cochran J.R., 1979. An analysis of isostasy in the world's oceans 2: Mid-ocean ridge crests., J. Geophys. Res.,84, 4713-4729.

(5)

Het corrigeren van free-air anomalieën gemeten over oceaanbodem jonger dan ongeveer 40 Ma door middel van een experimenteel bepaalde relatie tussen ouderdom en zwaartekracht, zoals gegeven door Cochran en Talwani (1977), maakt het mogelijk zwaartekrachtsanomalieën veroorzaakt door de elevatie van de midoceanische rug en de compensatie ervan te elimineren zonder een compensatiemodel voor de rug te specificeren.

-Dit proefschrift, hoofdstuk III.
-Cochran J.R., Talwani M., 1977. Free-air gravity anomalies in the world's oceans and their relationship to residual elevation., Geophys. J.R. astr. Soc., 50, 495-552.

(6)

Het verwaarlozen van een deel van de homogene oplossing voor de spanningsfunktie bij het oplossen van de Von Kármán vergelijkingen voor een rotatiesymmetrische belasting via verstoringsrekening, zoals gedaan door Lambeck en Nakiboglu (1980) is onjuist en leidt tot verkeerde conclusies.

-Lambeck K., Nakiboglu S.M., 1980. Seamount loading and stress in the ocean lithosphere., J. Geophys. Res., 85, 6403-6418.

(7)

De sedimenten gelegen boven de rondom het Atlantis-Meteor seamount complex aanwezige sterke reflector zijn asymmetrisch verdeeld ten opzichte van dit complex, hetgeen grotendeels verklaard kan worden uit de anomale diepte van het gebied en het daardoor ontstane sedimentatie patroon, gebruikmakend van de CCD- ouderdoms curve van Berger en Von Rad (1972), indien aangenomen wordt dat de anomale diepte niet op de rug ontstaan is.

-Dit proefschrift, hoofdstuk IV.
-Berger W.H., Von Rad U., 1972. Cretaceous and Cenozoic sediments from the Atlantic Ocean., in: Hayes D.E., Pimm A.C., et al, 1972, Initial Reports of the Deep Sea Driling Project, vol XIV, Washington (U.S. Government Printing Office), 787-954.

(8)

Het feit dat de magnetische anomalieën over de seamounts van het Atlantis-Meteor complex, met uitzondering van de tablemounts, na correctie voor het niet vertikaal zijn van de magnetische vectoren, positief zijn en resulteren in effectief positief gemagnetiseerde seamounts versterkt de door Williams et al (1983) gedane suggestie dat de magnetisatie van grote seamounts veroorzaakt wordt door viskeus remanent magnetisme in de richting van het huidige magneetveld.

-Dit proefschrift, hoofdstuk II.
-Williams C.A., Verhoef J., Collette B.J., 1983. Magnetic analysis of some large seamounts in the North Atlantic., Earth Planet Sci. Lett., 63, 399-407.

(9)

De veronderstelling dat de correctie voor het indirecte effect van zwaartekrachtsreducties alleen bestaat uit een free-air correctie is onjuist en leidt tot een overschatting van dit effect.

-Heiskanen W.A., Moritz H. 1967. Physical Geodesy, Freeman and Company, San Fransisco.
-Vening Meinesz F.A., 1949. The isostatic reduction and the indirect or Bowie effect., Bull. Geod., 12, 170-179.

(10)

Met behulp van een kruispunten analyse kan worden aangetoond dat, alhoewel de seculaire variatie correctie van de (nieuwe) magnetische referentie velden DGRF 1965, DGRF 1970, DGRF 1975 en IGRF 1980 beter is dan die van het (oude) referentieveld IGRF 1975, de magnetische anomalieën na reductie via deze nieuwe referentievelden nog een tijdsafhankelijke component hebben.

-Verhoef J., Scholten R.D., Cross over analysis of marine magnetic anomalies, Mar. Geophys. Res., 5, 421-435, 1983.

(11)

De onderschatting van het belang van de ondieptes voor de Vlaamse kust door de Spanjaarden heeft geleid tot het mislukken van het samenkomen van de Spaanse Armada en de in de Vlaamse havens gelegen invasiemacht van de Hertog van Parma.

(12)

Het feit dat Plato naast Atlantis gelegen is hoeft niet te betekenen dat Plato wist waar Atlantis lag.

Utrecht, 4 juli, 1984 J. Verhoef

Stellingen behorende bij het proefschrift: "A geophysical study of the Atlantis-Meteor seamount complex".

GEOLOGICA ULTRAIECTINA

Mededelingen van het
Instituut voor Aardwetenschappen der
Rijksuniversiteit te Utrecht

No. 38

A GEOPHYSICAL STUDY OF THE ATLANTIS-METEOR SEAMOUNT COMPLEX

A GEOPHYSICAL STUDY OF THE ATLANTIS-METEOR SEAMOUNT COMPLEX

EEN GEOFYSISCHE STUDIE VAN HET ATLANTIS-METEOR SEAMOUNT COMPLEX

(MET EEN SAMENVATTING IN HET NEDERLANDS)

PROEFSCHRIFT

TER VERKRIJGING VAN DE GRAAD VAN DOCTOR IN DE WISKUNDE EN NATUURWETENSCHAPPEN AAN DE RIJKSUNIVERSITEIT TE UTRECHT, OP GEZAG VAN DE RECTOR MAGNIFICUS PROF. DR. O.J. DE JONG, VOLGENS BESLUIT VAN HET COLLEGE VAN DECANEN IN HET OPENBAAR TE VERDEDIGEN OP WOENSDAG 4 JULI 1984 DES NAMIDDAGS TE 2.30 UUR

DOOR

JACOB VERHOEF

GEBOREN OP 11 DECEMBER 1950 TE ERMELO

DRUKKERIJ ELINKWIJK BV – UTRECHT

PROMOTOR: PROF. DR. B.J. COLLETTE

VOORWOORD

Veel dank ben ik verschuldigd aan een ieder die heeft bijgedragen aan de totstandkoming van dit proefschrift.

Mijn promotor Prof. Dr. B.J. Collette ben ik zeer erkentelijk voor de suggestie van het onderwerp, voor zijn bijdragen tot mijn wetenschappelijke vorming en voor de constructieve discussies tijdens het totstandkomen van dit proefschrift.

Peter Slootweg, Walter Roest, Juan Dañobeitia en Wim Twigt dank ik voor de vele adviezen en de talloze discussies. Joop Hoofd ben ik erkentelijk voor zijn advies en hulp bij zaken betreffende de computer en Ad Stolk voor zijn hulp bij het vervaardigen van de figuren. Dick Verweij en Henk van der Meer dank ik voor de prettige samenwerking tijdens het zeegaande onderzoek.

Prof. Dr. R. Rummel dank ik voor het beschikbaarstellen van computertijd en -programmatuur voor de geoideberekeningen. Peter van Es dank ik voor het uitvoeren van die berekeningen.

Ik dank de Nederlandse organisatie voor zuiver-wetenschappelijk onderzoek (Z.W.O.) die mij door een promotieplaats in staat heeft gesteld dit werk te doen.

CONTENTS

SAMENVATTING

De diepte van de oceaanbodem neemt in het algemeen systematisch toe met toenemende ouderdom. Deze toename kan verklaard worden door thermische modellen van de evolutie van oceanische lithosfeer. Er zijn echter grote delen van de oceaanbodem met een diepte welke afwijkt van de voorspelde diepte-ouderdomsrelatie (diepteanomalieën). In verschillende studies is er reeds op gewezen dat te ondiepe gedeelten van de oceaan veelal gekenmerkt worden door het optreden van vulkanisme (zie bijv. Sclater et al, 1975; Cochran en Talwani, 1977).

De Atlantis-Meteor seamount groep vormt een groot vulkanisch complex gelegen op ongeveer 700 km ten zuiden van de Azoren in het centrale gedeelte van de Noordatlantische oceaan. Een eerdere studie van Cochran en Talwani (1978) gaf aan dat er in het gebied rondom het Atlantis-Meteor complex onvoldoende zwaartekrachtsgegevens aanwezig zijn om voor dit complex de relatie tussen zwaartekracht, diepteanomalie en vulkanisme te bestuderen. Aanvullende zwaartekrachtsgegevens zijn verkregen in twee onderzoeken in 1979 en 1980, waarbij tevens de seismische reflectiemetingen en de magnetische gegevens verkregen tijdens het Kroonvlag-project (Collette et al, 1984) zijn gecompleteerd.

Een analyse van de seismische en magnetische structuur (hoofdstuk II) toont aan dat het Atlantis-Meteor complex opgebouwd is uit langgerekte onderzeese bergen (seamounts) met een typische lengte van ongeveer 100 km en een algemene NW-ZO richting. Plato seamount heeft enigszins afwijkende richtingen. De seamountgroep kan onderverdeeld worden in 4 subgroepen welke tesamen een mozaikpatroon vormen. De structurele beschrijving van het Atlantis-Meteor complex geeft aanleiding tot de veronderstelling dat het gebied een uitrekking in een NO-ZW richting heeft ondergaan.

Nadat de magnetische anomalieën zijn gekorrigeerd voor het niet vertikaal zijn van de magnetische vectoren (reductie naar de pool) worden zij positief over de seamounts. Dit betekent dat de magnetisatierichting normaal is. Deze uitkomst bevestigt de resultaten van een

voorlopige studie (Williams et al, 1983), waarin werd gesuggereerd dat viskeus remanent magnetisme, afkomstig van de huidige normale periode (Brunhes), verantwoordelijk is voor de overwegend normale polarisatie van de seamounts. Door een normale magnetisatie aan te nemen kunnen we de waargenomen magnetische anomalieën ontdoen van het effect veroorzaakt door de grote seamounts. Dit maakt het mogelijk om spreidingsanomalieën en fracture zone-anomalieën te identificeren. Deze anomalieën werden gebruikt, als onderdeel van een grotere studie, om het structurele patroon en de ouderdom van de oceaanbodem rondom het Atlantis-Meteor complex te bepalen.

In hoofdstuk III bestuderen we de diepte en het zwaartekrachtsveld van het gebied en hun onderlinge correlatie. Het gebied rondom het Atlantis-Meteor seamount complex heeft een positieve diepteanomalie, hetgeen wil zeggen dat dit gebied te ondiep is ten opzichte van de diepte ouderdomsrelatie. De positieve diepteanomalie kan worden beschouwd als een belasting op de oceanische lithosfeer. Door hiervoor te corrigeren vinden we de isostatische anomalie van het gebied welke overwegend positief is.

Uit de zwaartekrachtsgegevens berekenen we de buigstijfheid onder de verschillende seamounts en hieruit de elastische dikte van de oceanische lithosfeer. Met gebruikmaking van de relatie tussen de elastische dikte en de ouderdom van de oceanische lithosfeer, zoals voorgesteld door Watts (1978, zie ook Watts et al, 1980) en verder uitgewerkt door Bodine et al (1981) zijn schattingen voor de leeftijden van de seamounts verkregen. De resultaten maken het onwaarschijnlijk dat de seamounts zijn ontstaan op de Midatlantische Rug. De resultaten laten de mogelijkheid open dat de alle vulkanen in ongeveer dezelfde periode actief zijn geweest.

De relatie tussen de zwaartekrachtsanomalieën en de bathymetrie in het lange golflengtegebied, verkregen met behulp van de admittantiemethode, geeft aan dat de compensatie voldoet aan een plaatmodel. Er zijn aanwijzingen dat de langste golflengten op een dieper niveau zijn gecompenseerd. Dit resultaat wordt ook verkregen uit de geoideanomalieën in dit gebied.

In hoofdstuk IV wordt ingegaan op het sedimentatiepatroon rondom het Atlantis-Meteor seamount complex. Het gebied rondom dit complex wordt gekarakteriseerd door een relatief dikke sedimentlaag met daarin sterke en vaak afschermende reflectoren. Op de meeste plaatsen komen deze reflectoren waarschijnlijk overeen met vulkanoklastische lagen afgezet door turbidietstromen. De contouren van de diepteanomalie correleren goed met de regionale isopachen van het sediment gelegen boven de sterke reflector. Deze correlatie geeft aanleiding tot het opstellen van een carbonaat-sedimentatiemodel, waarin met behulp van paleodiepte reconstructies de carbonaat-sedimentatie wordt berekend. Het model verklaart de belangrijkste aspecten van het sedimentatiepatroon en leidt tot de conclusie dat de leeftijd van de sterke reflector, welke niet overal een tijdhorizon hoeft te zijn, niet veel ouder kan zijn dan Mioceen. Deze conclusie wordt versterkt door de afwezigheid van sedimenten in het zuidwestelijke gedeelte van het gebied. Het is daarom niet waarschijnlijk dat het vulkanisme in dit gebied en de abnormale diepte ervan ontstaan zijn op het spreidingscentrum. Het model is niet gevoelig genoeg om mogelijke leeftijdsverschillen tussen de seamounts aan te geven. De conclusies van dit hoofdstuk bevestigen de resultaten verkregen uit de zwaartekrachtsgegevens betreffende de ouderdom.

In hoofdstuk V worden verschillende studies over diepteanomalieën samengevat en de resultaten ervan vergeleken met die van het Atlantis-Meteor seamount complex. De resultaten van deze studie geven aan dat de "primaire hotspot"-hypothese een onwaarschijnlijke verklaring is voor het ontstaan van het Atlantis-Meteor seamount complex. Als een alternatieve hypothese wordt het opbreken van de oceanische lithosfeer als gevolg van door uitrekking veroorzaakte spanningen voorgesteld. Een bovengrens voor de uitrekking kan verkregen worden uit de nauwkeurigheid van de reconstructie van het spreidingspatroon (Collette et al, 1984), waarbij voor het gebied rondom het Atlantis-Meteor complex geen systematische afwijkingen zijn gevonden. Een mogelijke oorzaak voor de uitrekking kan gevonden worden in voortgaande thermische contractie buiten het transformdomein van de oceanische fracture-zones

(Collette et al, 1984). Interactie met plaatgrensprocessen kan echter niet uitgesloten worden. Deze processen vormen mogelijk zelfs de reden dat restanten van de horizontale contractie van de lithosfeer zich in bepaalde gebieden, zoals het Atlantis-Meteor gebied, concentreren.

CHAPTER I

GENERAL INTRODUCTION AND SUMMARY

The depth of the ocean floor in general increases systematically with increasing crustal age (e.g. Sclater and Francheteau, 1970; Parsons and Sclater, 1977). This increase of depth further away from a mid-ocean ridge crest can be explained by thermal models for the evolution of the oceanic lithosphere. There are, however, large portions of oceanfloor whose depth deviate from the predicted depth-age relation (depth anomalies, Menard, 1973). Cochran and Talwani (1977) examined depth anomalies throughout the world's oceans and noticed a relation between the intermediate wavelength positive features (both gravity and depth) and areas of extensive off-ridge volcanism (c.f. Menard, 1973; Anderson et al, 1973; Sclater et al, 1975). The volcanism which is not associated with plate margin processes is called intra-plate volcanism (Turcotte and Oxburgh, 1978).

The Atlantis-Meteor seamount group forms a large volcanic complex in the central North Atlantic ocean, situated some 700 km south of the Azores (see Figure 1). The whole area around this complex is too shallow in terms of the depth-age curve and constitutes a positive depth anomaly. It actually forms the most southern part of the North Atlantic Gravity High (Cochran and Talwani, 1978), which extends from Iceland to about 30°N and which comprises areas of different plate tectonic setting. The study of Cochran and Talwani (1978) was based upon 1°*1° averages. In the area around the Atlantis-Meteor complex there was not enough gravity data to calculate 1°*1° averages (see Cochran and Talwani, 1978, Figure 1A).

Since there were insufficient data in the Atlantis-Meteor area for studying the relation between gravity, depth anomalies and the occurrence of volcanism, it was decided to complete the continuous seismic reflection and magnetic data obtained in the course of the Kroonvlag-project (Collette et al, 1984) by a special survey of the area combining gravity, seismic and magnetic measurements. In 1979

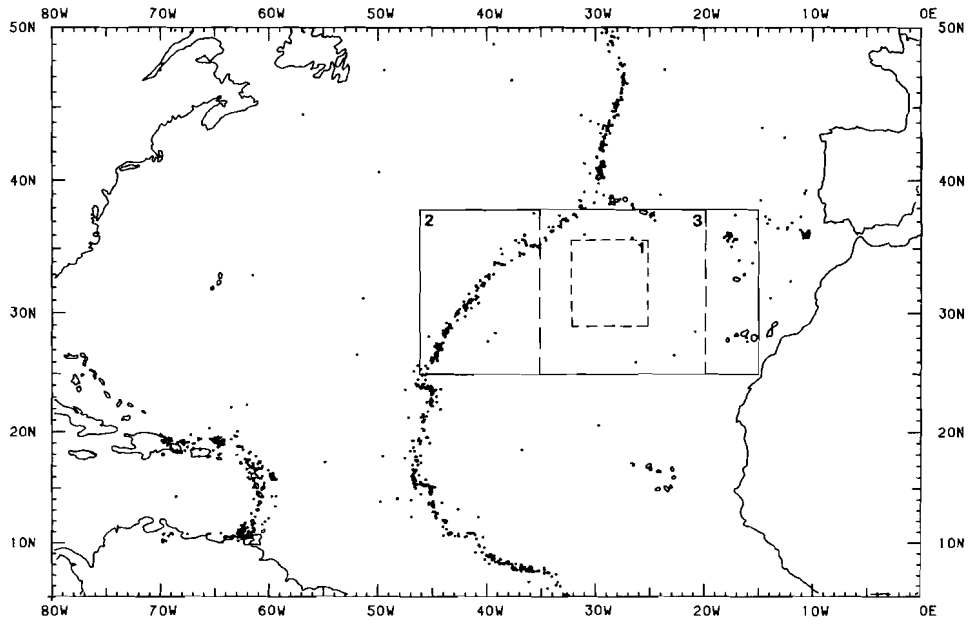

Figure 1: Location of study areas. Dots indicate earthquake epicenters. We studied the Atlantis-Meteor seamount complex in area 1 (chapter II). The gravity field was studied in area 2 (chapter III) and the sedimentation pattern in area 3 (chapter IV).

measurements were carried out on board MV Tyro. In 1980 a further survey was conducted on board HNLMS Tydeman with the special purpose to reconnoitre the Atlantis subgroup.

Several models have been developed to explain the origin of volcanic island and seamount chains. Wilson (1963, 1973) and Morgan (1971, 1972) thought that the volcanism at the surface was produced by movement of the lithosphere over a hotspot or plume, considered to be a thermal anomaly that is fixed in the earth's mantle. Turcotte and Oxburgh (1973) relate the linear volcanism to the development of a propagating fracture with magma rising diapirically through the fractured lithosphere producing the volcanoes at the surface. The propagating fracture in their model is caused by tensional stresses.

Generally, intra-plate volcanism is related to the occurrence of mid-plate swells. Studies of the subsidence of atolls (Detrick and

Crough, 1978; Menard and McNutt, 1982) and heat flow measurements over the Hawaiian swell (Detrick et al, 1981; Von Herzen et al, 1982) seem to indicate that mid-plate swells were formed by a broad-scale reheating and thinning of the lithosphere.

Earlier observations

Several of the seamounts belonging to the Atlantis-Meteor seamount group have already been studied; Great Meteor even in great detail. This large seamount was discovered in 1937 by the German research vessel 'Meteor' (Dietrich, 1939). Early studies concerning this seamount were reported by Heezen et al (1954) and Pratt (1962).

The Great Meteor seamount has a flat summit with an oval shape, reaching 275 m below sealevel (Ulrich, 1970). Seismic reflection and refraction profiles indicate that the Great Meteor seamount mainly consists of volcanic rock superimposed by a cap of sediments probably consisting of biogenic limestones and calcareous sands (Hinz, 1969; Aric et al, 1970; von Rad, 1974). Hinz (1969) gave a sediment isopach map which shows that for the summit terrace the sediment thickness reaches up to 0.3 second two-way travel time (about 450 m). For the flanks of the seamount thicknesses of more than 0.4 s (about 600 m) are found. With these data Haut (1973) constructed magnetic models and tried to explain the magnetic anomalies assuming a normal magnetization of 5 A/m. In order to account for the steep gradients in the anomalies over the central part of the seamount, Haut had to postulate the existence of a body for which there is no seismic evidence. Using the outcome of a gravity survey, Fleischer et al (1970) computed a value of 2.6 g/cm^3 for the density of Great Meteor seamount. Plaumann (1974) arrived at a value of 2.72 g/cm^3, reporting that there are indications for higher densities in the central or in the upper part of the seamount. Watts et al (1975, cf. Bodine and Karner, 1981) computed the flexure from the gravity anomalies and came to an effective flexural rigidity for the lithosphere underneath the Great Meteor seamount of about 6. 10^{29}dyne cm. This value gives an

effective elastic thickness of 19-22 km (Watts et al, 1980; Bodine et al, 1981). Von Stackelbergh (1976, see also 1979) studied the recent sedimentation around Great Meteor seamount. They found sedimentation rates that are generally higher on the eastern than on the western flank of the seamount. As part of the Dutch contribution to the activities of the International Seabed Working Group, detailed investigations were carried out west of Hyères seamount and in the area 30°-33°N/ 23°-26°W, i.e. ENE of Great Meteor seamount (e.g. Kuypers, 1981; Kuypers et al, in prep.; Fermont and Troelstra, 1983).

The occurrence of Miocene foraminifera on the terraces and in reworked sediments of Great Meteor seamount made Pratt (1962) conclude that the minimum age is Miocene. An indirect dating by Hinz (1969) of the volcanic activity from 55 to 35 Ma ago is based on an interpretation of a seismic section to the NE of Great Meteor seamount which is no longer valid. His horizon A3 belongs to the shielding reflectors which are generally found around volcanoes (see also chapter IV) and which are presumably directly related to the volcanic activity as such. Wendt et al (1976) analyzed two basalt samples from the flanks of the Great Meteor seamount and found K-Ar ages of 11 and 16 Ma.

The other seamounts in this area were only briefly explored (Heezen et al, 1954; Heezen and Hollister, 1971). From dredged limestone cobbles Heezen et al concluded that Atlantis seamount must have been an island within the past 12000 years.

Summary

An analysis of the seismic and magnetic structure of the Atlantis-Meteor seamount group (chapter II) reveals that this complex consists of elongated structures of a typical length of about 100 km in a general NW-SE direction. Plato seamount has slightly different directions. The seamount group can be divided into 4 subgroups or blocks, together forming a mosaic pattern. The structural description of the Atlantis-Meteor complex itself is suggestive of extension in a

NE-SW direction. When corrected for skewness the magnetic anomalies become positive over the seamounts. This means that the polarization is normal. This outcome substantiates the results of an earlier study (Williams et al, 1983), in which it was suggested that viscous remanent magnetization dating from the present normal period, the Brunhes, is responsible for the predominance of normal polarization in seamounts. Assuming a normal magnetization the observed magnetic anomalies can be "cleaned" by removing the effect of the huge seamounts. This makes it possible to identify spreading and fracture zone anomalies. These anomalies were used, as part of a larger study, to establish the structural pattern of the oceanfloor around the Atlantis-Meteor seamount complex.

In chapter III we study the depth anomaly and the gravity field of the area. The area around the Atlantis-Meteor seamount complex has a positive depth anomaly. From gravity data we calculated the flexural rigidity under the seamounts, as well as the isostatic anomaly in the area. The relation between the elastic thickness and the age of the oceanic lithosphere, as originally proposed by Watts (1978, c.f. Watts et al, 1980) and elaborated by Bodine et al (1981), was used to obtain age estimates for the seamounts. The isostatic anomaly in the area around the seamount complex is predominantly positive. The flexure study results make it unlikely that the seamounts originated on the Mid-Atlantic ridge. We do not find a clear age migration pattern of the volcanism and our results leave open the possibility that the volcanoes in the area all became active in about the same period. The relation between the long wavelength gravity anomalies and the bathymetry, obtained by using the admittance method, show that the compensation closely follows a plate model. There are indications that the longest wavelengths are compensated at a deeper level. This result is sustained by the geoid anomalies in the area.

In chapter IV the sedimentation pattern around the complex is described. The area around the seamounts is characterized by a relatively thick sedimentary layer containing strong and often shielding reflectors. In most places these reflectors probably

represent volcano-clastic layers deposited by turbidity currents. Locally the presence of sills cannot be precluded. The depth anomaly contours correlate well with the regional isopachs of the sediment above the strong reflector. This correlation led to the construction of a simple carbonate sedimentation model. In this model paleodepth reconstructions were used to calculate the carbonate sedimentation. The model explains the most important aspects of the sedimentation pattern. Besides it led to the conclusion that the age of the strongly reflecting layer cannot be much older than Miocene. This conclusion is sustained by the absence of sediments in the southwestern part of the area. Therefore it is unlikely that the volcanism in this area and the anomalous depth originated on the spreading center. The model is not sensitive enough to detect possible variations in age between the different seamounts.

In chapter V we summarize several studies on depth anomalies and compared their results with those obtained for the Atlantis-Meteor seamount complex. The results obtained in this study make the simple hotspot hypothesis an unlikely explanation for the origin of the Atlantis-Meteor seamount complex. As an alternative hypothesis we suggest lithospheric fracturing.

CHAPTER II:

STRUCTURE OF THE ATLANTIS-METEOR SEAMOUNT COMPLEX FROM SEISMIC AND MAGNETIC DATA

Introduction

The Atlantis Meteor seamount group forms a large volcanic complex to the south of the Azores. In this chapter we will restrict ourselves to the immediate surroundings of the seamount complex. The regional setting of the Atlantis-Meteor seamount complex will be discussed in a later chapter in connection with the free-air gravity measurements.

The tracks surveyed by the Vening Meinesz Laboratorium in the area around the seamounts have an average spacing of 25 km (see Figure 5). This relatively dense spacing led to the discovery of a feature which had not been recognized before, viz. a high degree of linearity of the composing elements of the seamount group. Using the seismic information we will discuss these elements in detail.

The magnetic anomalies in this area are of three different types: seafloor spreading anomalies, fracture zone anomalies and anomalies caused by the seamounts. After correction of the magnetic anomalies for skewness ("reduction to the pole") it appears that there is a correlation between the magnetic anomalies and the topographic expression of the seamounts: all seamounts remarkably have a positive magnetization after deskewing.

Using a simple 3-D magnetic model for the seamounts it was possible to "clean" the observed magnetic anomalies by removing seamount effects. The residual anomalies were then used to analyze the fracture zone pattern in the area.

The magnetic directions can be enhanced by using the absolute value of the analytical signal of the anomaly (Nabighian, 1972). In general the magnetic and seismic directions are the same. The total pattern gives rise to the supposition of an extensional origin for the Atlantis-Meteor seamount complex.

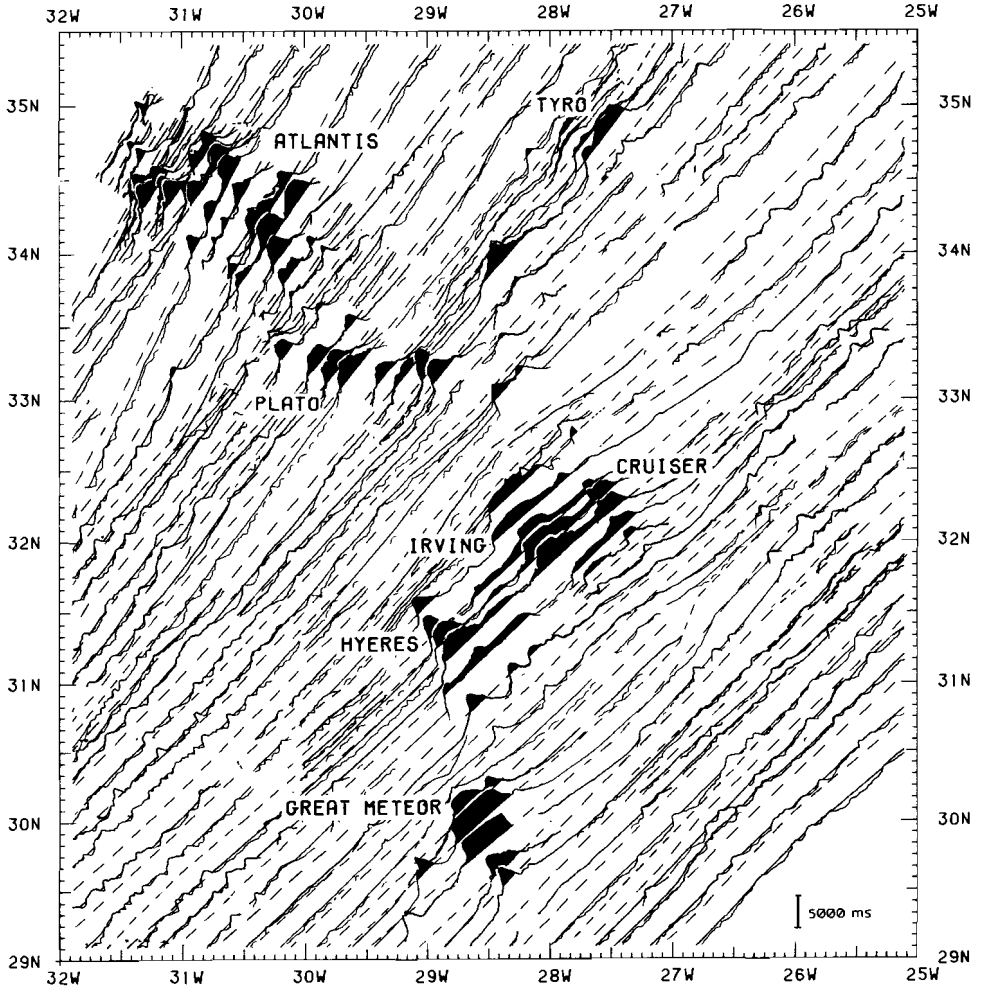

Figure 1: Simplified seismic reflection profiles projected with an azimuth of 315. The offset is 3333 ms (2500 m). Only bottom and the acoustical basement are given. Seamounts less deep than 2500 m have been shaded.

SEISMIC DATA

The greater part of the seismic reflection profiles is shown in Figure 1, projected along the track. Only the ocean bottom and the acoustical basement have been plotted. The shaded parts give the topography less deep than 2500 m. In the immediate surroundings of the seamounts we lose the contact with the oceanic basement, e.g. to the east and southeast of Great Meteor seamount. This is due to flexure of the oceanic lithosphere caused by the load of the seamounts (see chapter III) as well as to the presence of a highly reflective layer, which shields the oceanic or volcanic basement acoustically (see chapter IV).

The bathymetric depths were contoured by hand. The resulting contourchart is given in Figure 2. The contour interval is 500 m. The basement depth was contoured by computer with a method using a digital filter (Slootweg 1978). For the contouring we used a grid of 0.05° and a cut-off wavelength of 45 km, roll-off 6 dB/octave. In parts without basement information, the contouring program extrapolates over distances up to about half the cut-off wavelength. The resulting contour chart with a contour interval of 500 m is given in Figure 3.

The bathymetric contour chart shows that, in general, the eastern and southern parts of the area are deeper than 4000 m. There is a gradual deepening towards the east, i.e. in the direction away from the Mid Atlantic Ridge. Clearly recognizable in the contour charts and also in the seismic profiles of Figure 1 are blocks of high areas, which show definite linear patterns.

Great Meteor seamount

Great Meteor seamount forms part of the most southeastern block. Figure 4A shows the seismic reflection profiles in the area now with internal seismic reflectors. Centered at about 30°N/ 28° 30'W Great Meteor seamount rises up from the adjacent seafloor to a minimum depth of about 275 m below sealevel. The seismic profiles in Figure 4A

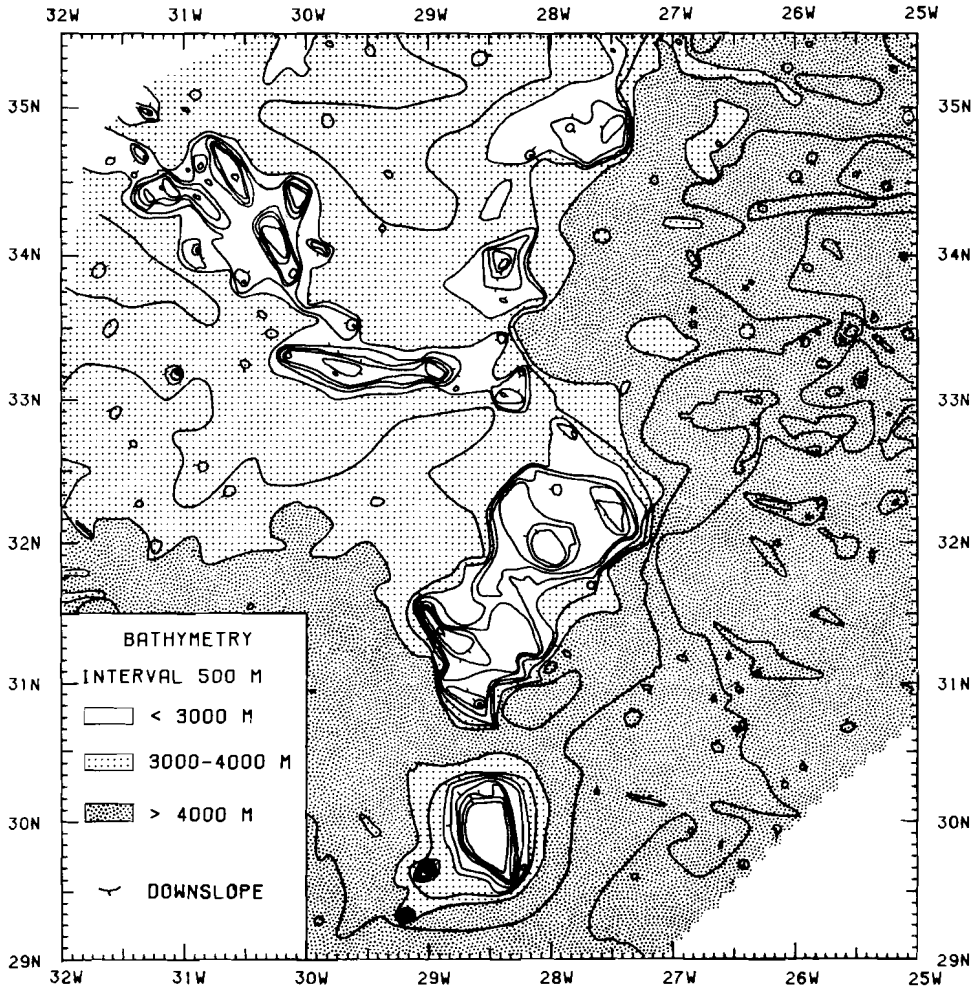

Figure 2: Bathymetric contour chart of the Atlantis-Meteor seamount complex. Contour interval is 500 m. For tracklines see Figure 5.

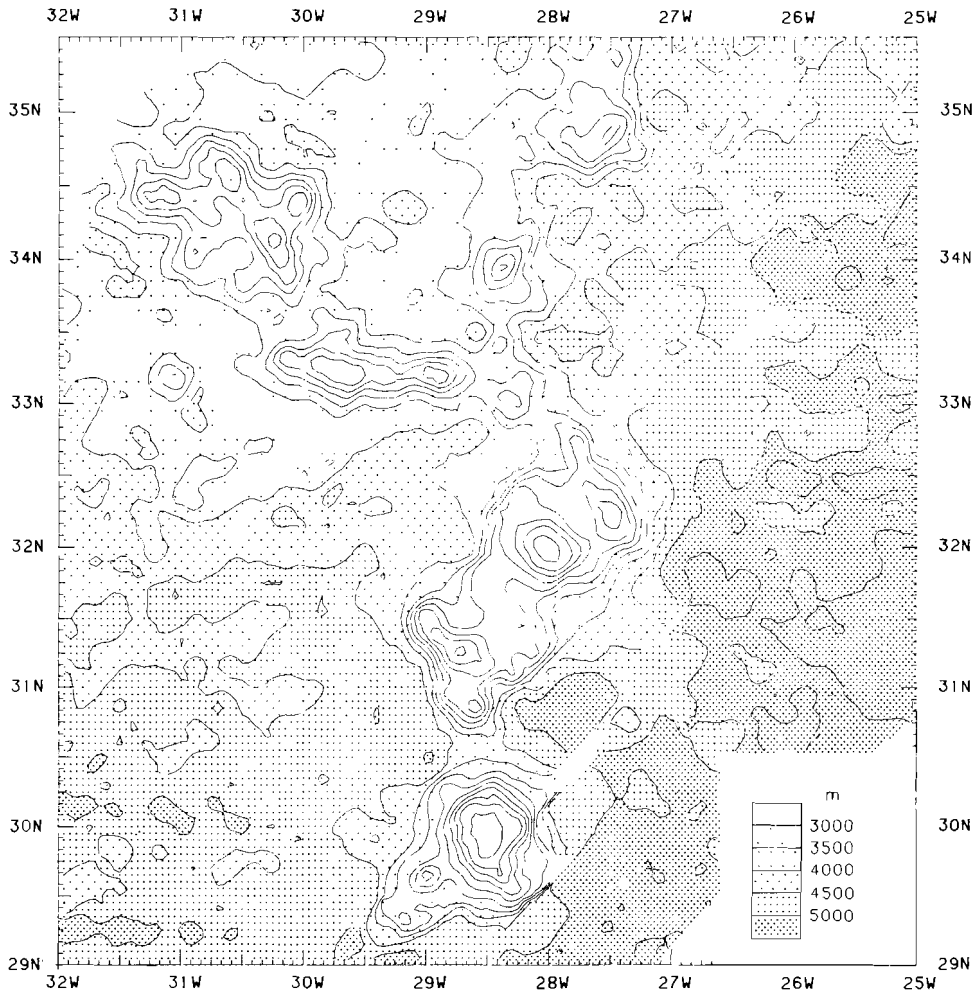

Figure 3: Contour chart of the basement depth of the Atlantis-Meteor seamount complex. Contour interval is 500 m.

clearly show that this seamount has a flat surface and is a tablemount. Both the bathymetric and the basement contours show that Great Meteor seamount is elongate in a NW-SE direction. In general, the basement contours coincide with the bathymetric contours. However as a rule tablemounts are covered by reef sediments and debris thereof on the slopes. In our seismic records we could not distinguish between volcanics and reefs. Hinz(1969) detected a sedimentary layer of a thickness of 0.4 seconds on top of Great Meteor seamount. To the southeast of Great Meteor seamount there are two smaller seamounts: Small Meteor seamount (Kleine Meteor Bank) at about 29°40'N/ 29°W and Closs seamount at 29°20'N/ 29°10'W. Both seamounts have been crossed by only one profile only (see Figure 4A). Therefore the horizontal dimensions of these two seamounts on the contour charts are only schematic.

Cruiser, Irving and Hyères seamounts

Between 30°45'N and 32°50'N and around 28°W lies a complex which in total is less deep than 3000 m. Figure 4B shows the seismic reflection profiles with the internal seismic reflectors. Within this complex we find at least four parallel linear structures.

The most northeastern structure in Figure 4B is Cruiser seamount with a maximum height of 590 m below sealevel. The general strike of this seamount is 320 and its length is about 70 km. Cruiser seamount contains no flat surface.

Irving seamount is situated at about 32°N/ 28°W. It rises up to 250 m below sealevel and is a tablemount. The flat surface of this seamount clearly shows on three seismic profiles in Figure 4B. The general direction of Irving seamount is NW-SE, but due to its oval shape it is difficult to assign a distinct orientation to this seamount. The length of the structure is about 100 km.

Between Irving and Hyères seamounts we find several structures which are not as shallow as the other seamounts. The directions found here are the same as for the other seamounts inside the complex.

Hyères seamount is the most southwestern structure in Figure 4B.

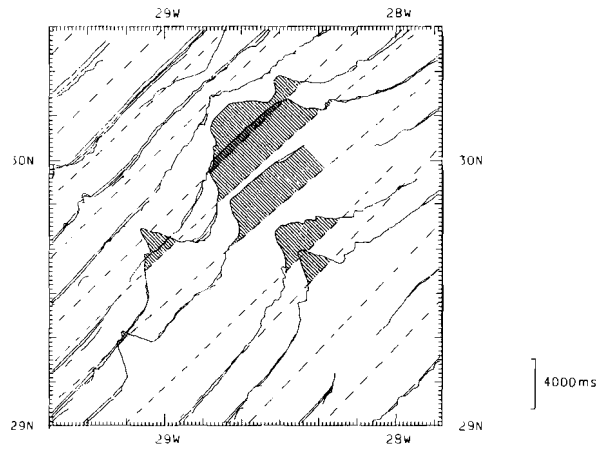

Figure 4A: Seismic reflection profiles over Great Meteor seamount. The offset is 3333 ms (2500 m). Parts less deep than 2500 m have been shaded.

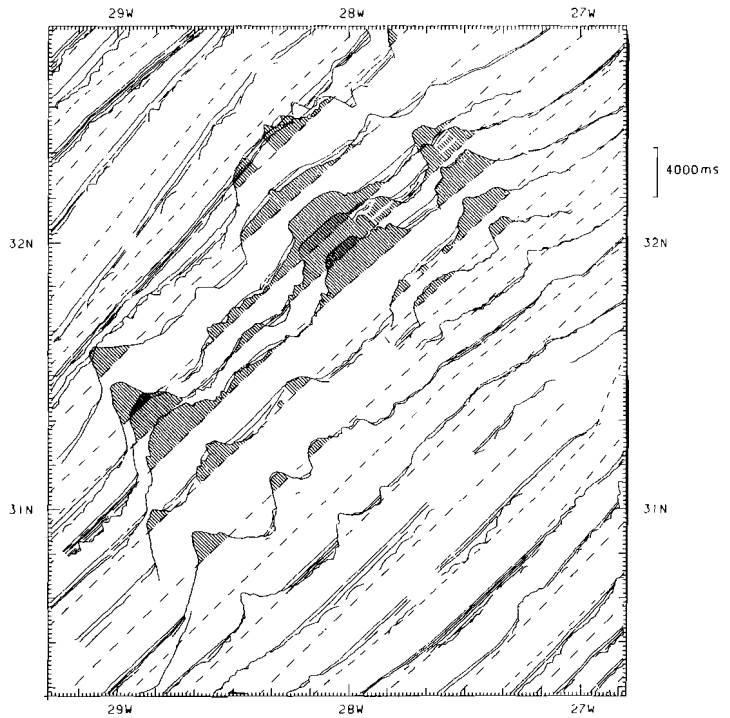

Figure 4B: Seismic reflection profiles over the Cruiser, Irving and Hyères complex. The offset is 3333 ms (2500 m). Parts less deep than 2500 m have been shaded.

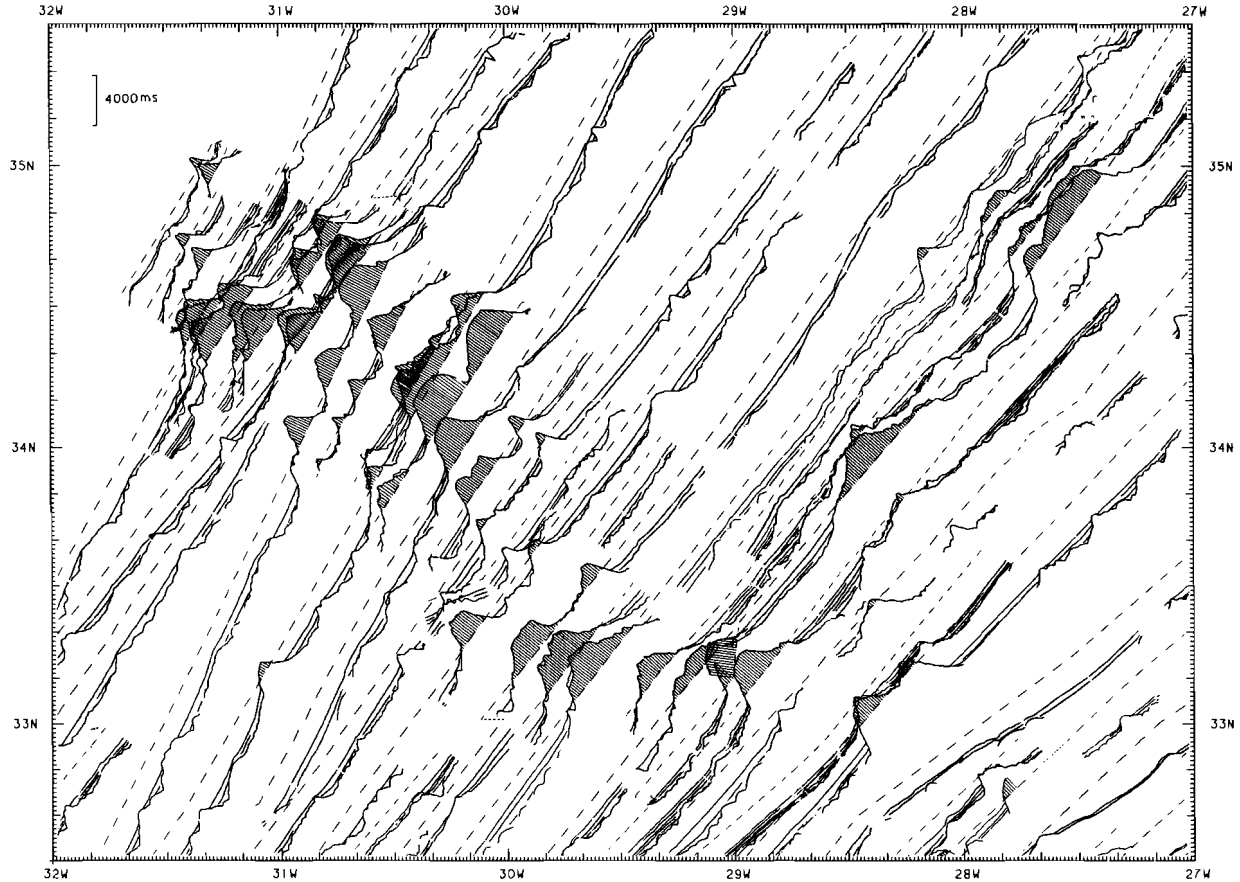

Figure 4C: Seismic reflection profiles over Atlantis, Plato and Tyro seamounts. The offset is 3333 ms (2500 m). Parts less deep than 2500 m have been shaded.

This seamount has a recorded minimum depth of 330 m at 31°20'N/ 28°50'W. The seismic profiles over Hyères seamount show no flat surface. Coming from the northwest Hyères rises up abruptly from the oceanfloor. It then seems to divide in two branches in the south-east. Hyères seamount has a strike of 305 and a length of about 100 km.

Inside the complex formed by Cruiser, Irving and Hyères seamounts, several sedimentary basins are to be found, e.g. between Cruiser and Irving seamounts. On several profiles a sedimentary cover of the seamounts has been recorded, e.g. the profiles over the northwestern part of Irving seamount.

Plato and Tyro seamounts

PLato seamount is aligned in a general E-W direction (see Figure 4C). It consists of en echelon structures with a WNW-ESE direction. The overall length of Plato seamount is about 110 km, the recorded minimum depth is 580 m. At 33°55'N/ 28°25'W there is an "unnamed" seamount with a minimum depth of about 780 m. This seamount shows no clear directions. Tyro seamount is situated at 34°40'N/ 27°30'W with a minimum depth of 1370 m and a not clearly defined NW-SE direction.

Atlantis seamount group

Plato seamount forms the connection with another complex structure, the Atlantis seamount group. The two major elements of this group (see Figure 1) have a NW-SE trend and lengths of about 65 km. Figure 4C shows, that both elements contain flat surfaces and are tablemounts. The southern one, at 34°05'N/ 30°10'W (Atlantis seamount proper) rises up to 250 m below sealevel, the tablemount at 34°30'N/ 30°25'W up to 400 m. The smaller structures in the Atlantis seamount group roughly have the same strike as the major elements. The northwestern limit of the Atlantis seamount is not given in the contour charts of Figures 2 and 3 because of lack of data. The bathymetric charts of this area (cf. Gebco, sheet 5.08, 1982) do not give structures less deep than 2500 m to the west of about 31°30'W.

Minor structures

Also in the deeper parts of the area several NW-SE lineations occur. For instance to the east and northeast of Cruiser seamount (see Figure 1) we see minor structures with a general NW-SE direction and lengths of about 50 km. These lineations can also be recognized in the magnetics (see Figure 5).

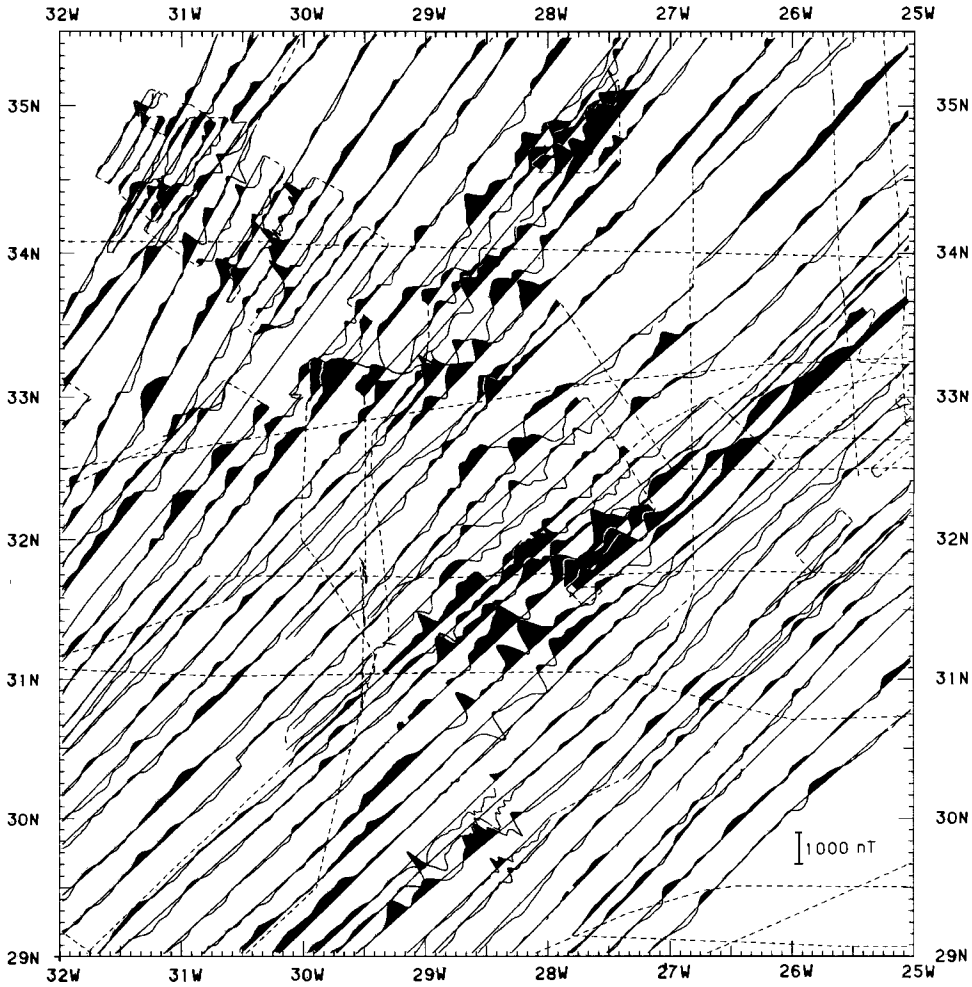

Figure 5: Magnetic anomalies projected perpendicular to the tracks. Positive magnetic anomalies have been shaded. Dotted track lines represent data, both magnetic and seismic, used in the contour charts but not shown in Figures 1, 4 and 5.

MAGNETIC DATA

The total intensity magnetic values were reduced by using the new reference fields: DGRF 1965, DGRF 1970, DGRF 1975, PGRF 1975 and IGRF 1980 (IAGA, Working Group 1, 1981). The magnetic observations in the Atlantis-Meteor seamount area were performed over the period 1965-1982 and so the time dependence of the reference fields, which corrects the secular variation, can become an important factor. The recently adopted reference fields correct the secular variation in a much better way than the older IGRF 1975. Using cross-over analysis Verhoef and Scholten (1983) showed that the involved inaccuracies over the period 1969-1980 amount about 50 nT for the IGRF 1980 fields. Over the same period the IGRF 1975 gives errors up to 200 nT. Before these new reference fields became available Twigt (1980) applied a filter along the track with a cut-off wavelength of 185 km and a roll-off of 24 dB/ octave to remove the regional. As shown by Verhoef and Scholten (1983) such a filter does indeed remove the secular variation completely. However, this method has the disadvantage that the standard deviation at intersection points increases considerably, due to the circumstance that the filtering procedure is dependent on the track orientation. The low cut-off wavelength of the applied filter (185 km) also deforms some of the longer wavelengths effects in the spreading anomalies.

The resulting magnetic anomalies are given in Figure 5, projected perpendicularly to the tracks. Figure 6 gives the computer contour chart (cut-off wavelength 45 km) of the magnetic anomalies, together with the 3000 m basement contour from Figure 3.

Description of the magnetic anomalies

The magnetic anomalies over the seamounts are in the order of 500 nT and are much larger than the seafloor spreading and fracture zone anomalies in the area, which are in general between 100 and 200 nT. Within the seamount area proper the magnetic profiles clearly show the

general NW-SE directions also described in the seismic section. Plato seamount shows a more E-W direction. Here the positive anomaly is clearly offset to the south with respect to the topography (see Figure 6).

The magnetic anomalies over tablemounts contain short wave lengths, e.g. Great Meteor seamount at about 30°N/ 28°30'W and Atlantis seamount at about 34°N/ 30°30'W. The filtering effect of the contour program reduces these short wavelengths almost completely. This means that in the contour chart of Figure 6 the amplitudes of the anomalies over tablemounts are considerably reduced. Atlantis seamount at about 34°N/ 30°30'W for example has only an amplitude of about 300 nT.

In the southeastern part of the area we find several aligning magnetic anomalies in a WNW-ESE direction. These are fracture zone anomalies in the Cretaceous Magnetic Quiet Zone. In the CMQZ the magnetic anomalies over fracture zones are not complicated by polarity reversals and thus only the effect of fracture zones as such does count (Slootweg and Collette, in prep., see also Twigt et al, 1983). To the southeast of the complex formed by Cruiser, Irving and Hyères seamounts several minor lineations are found in the magnetic anomalies, which have a NW-SE direction, e.g. at about 31°N/ 27°W.

The magnetic contour chart clearly shows several anomalies with a general NNE direction, e.g. at about 29°N/ 31°30'W up to about 32°30'N. For instance at about 29°N/ 30°W we find a positive anomaly running NNE which changes its direction into NE at about 32°N. The anomalies are seafloor spreading anomalies, as will be shown later on.

Data analysis

The magnetic anomalies in the area around the Atlantis Meteor seamount complex contain information about the seafloor spreading process (seafloor spreading anomalies), about the fracture zone pattern (fracture zone anomalies) and about the seamounts (seamount

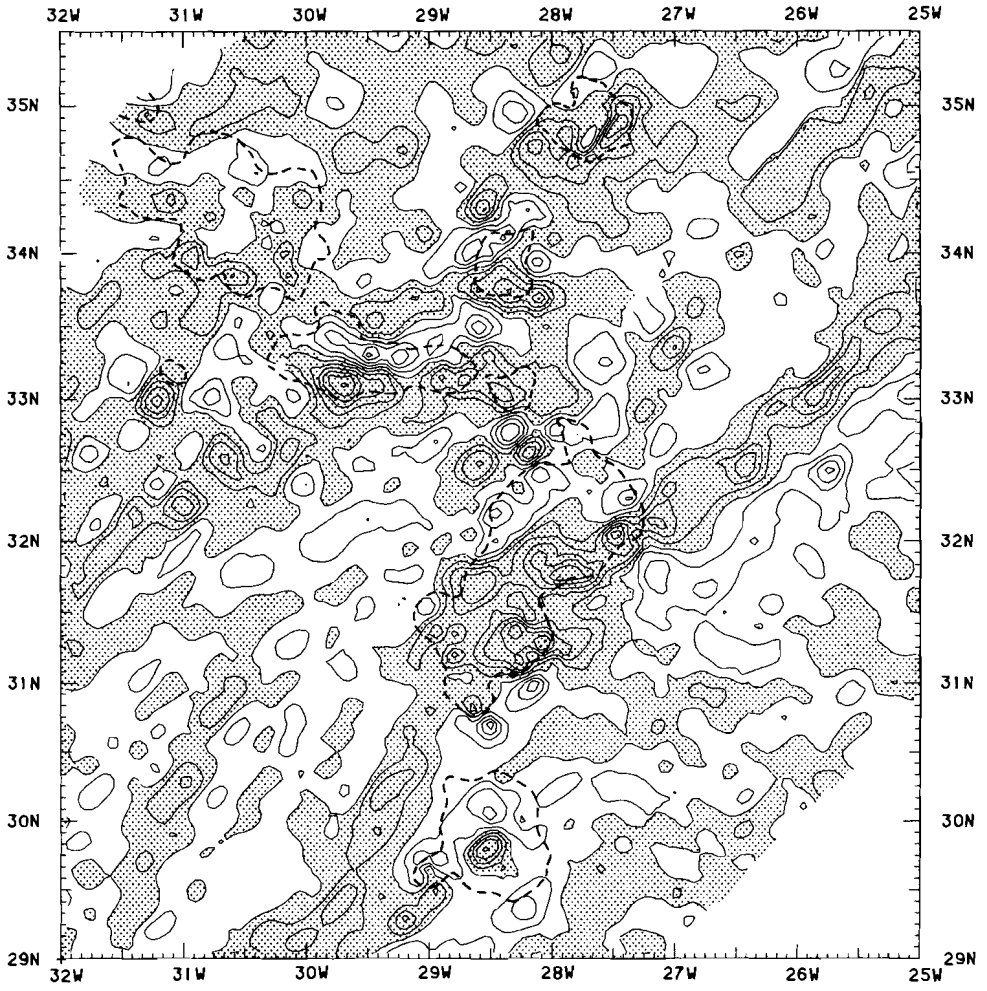

Figure 6: Contour chart of the observed magnetic anomalies. Contour interval 100 nT. Positive magnetic anomalies have been shaded. Heavy dotted line gives generalized 3000 m basement contours from Figure 3.

anomalies). The latter are the larger in amplitude. Identification of the seafloor spreading anomalies is extremely difficult because of the large seamount anomalies. In general the sources, which cause these different type of anomalies, are disjoint. This means that the results of these sources, the anomalies, must be separable, in principle. Magnetic anomalies are shifted with respect to their sources, when not measured on the magnetic pole. This shift, being a function of the orientation of the body (as shown by Schouten, 1971), may sometimes make it hazardous to establish the correlation between magnetic anomalies and the topography causing them.

The shift in position or skewness is caused by the non-parallelism of the involved magnetic vectors. These vectors are the magnetization vector and present magnetic field vector. In the case of thermo-remanent magnetization (TRM), the magnetization direction is given by the magnetic field direction at the time of the cooling of the body below the Curie temperature. Total magnetic intensity measurements give the vector sum of the present field or reference field and the anomaly. As the anomaly usually is much smaller than the reference field, in practice only its projection on the present field vector is measured. Using only this projection as the anomaly introduces the orientation of the present magnetic field as a parameter in the skewness of the anomalies.

The shift of the magnetic anomalies with respect to the sources can in principle be eliminated if the orientation of the two magnetic vectors described above is known. This correction for skewness can be done by assuming that the bodies causing the anomalies are linear structures (Schouten, 1971). Without this assumption the correction for skewness is somewhat more complicated.

Linear structures

The skewness of magnetic anomalies over linear structures can be corrected by applying the phase-shift technique of Schouten (1971). A phase-shift angle theta is calculated from the orientation of the

linear structure with respect to the magnetic north and the present and remanent magnetic field vectors. In addition to a phase-shift, the magnetic anomalies over linear structures are also affected by an amplitude coefficient for the projection of the ancient field in the plane, perpendicular to the azimuth of the body, and for the projections of the anomaly on the present field direction (Schouten, 1971; see also Williams et al, 1983).

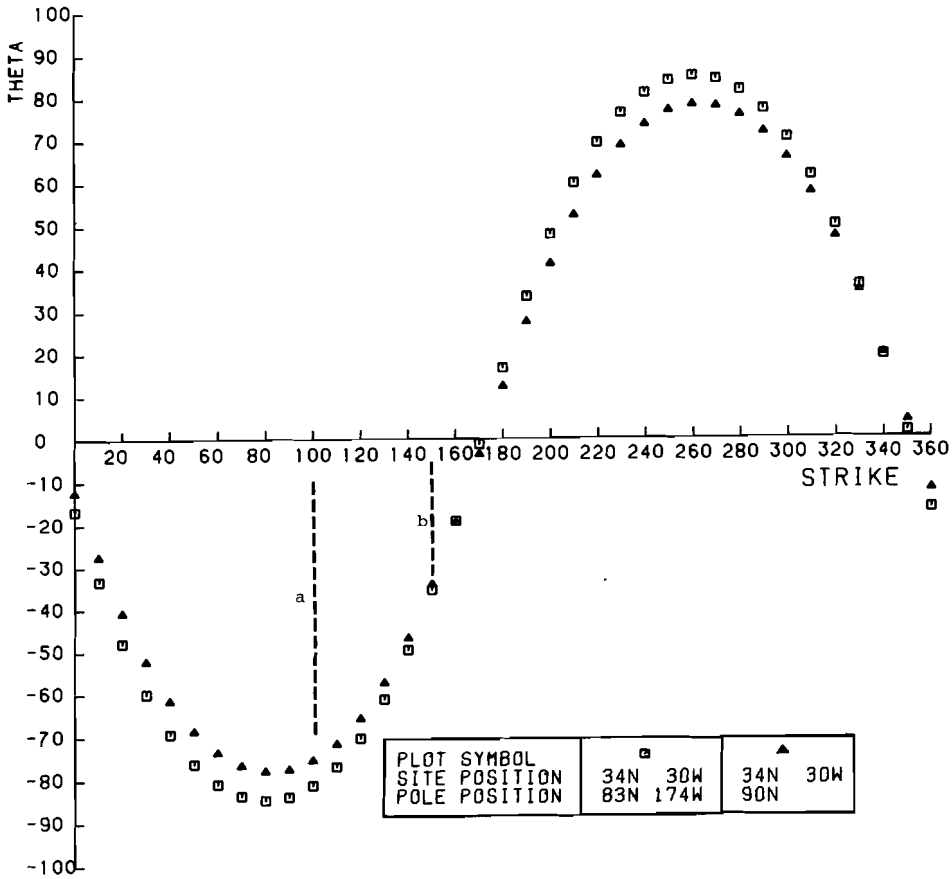

Figure 7: Theta values relative to the azimuth of a linear magnetized body at 34°N/ 30°W. Squares mark theta values for the Late Tertiary pole and triangles for the geographic (= mean Brunhes pole). Dashed lines a and b indicate the azimuths of Plato and Atlantis respectively.

Figure 7 shows the values of the phase-shift angle theta as a function of the strike of a magnetic body at 34°N/ 30°W and relative to the geographic (mean Brunhes) pole and the Late Tertiary pole (83°N/ 174°W, Van den Berg, 1979). For Plato seamount with a strike of about 100 a theta value of -80° is found. Atlantis seamount, striking about 150, has a theta value of only -35°. This can be seen in the observed anomalies (Figure 6): the offset to the south over Plato seamount is larger than the one over Atlantis seamount. Correction for these theta values makes the magnetic anomalies coincide with the topography (Williams et al, 1983).

If one makes the assumption that the structure is linear its direction has to be known to apply a phase shift correction. The seamounts of the Atlantis-Meteor complex form elongate structures with clearly defined directions. However the varying directions of the seamounts make it impossible to assume a same value of theta over the whole area. Also the seafloor spreading and fracture zone anomalies in the area have directions which differ from those of the seamounts. This necessitates the production of several plots, each with the anomalies phase shifted over different theta values, as has been done in the mentioned prelimenary study of the area. In this study we decided to use a three dimensional approach.

Three dimensional structures

For three dimensional structures the correction for the skewness of the magnetic anomalies can be realized by using an operator "reduction to the pole" (e.g. Baranov, 1957, Bhattacharyya, 1965 Le Mouel et al, 1972, Galdeano and Rossignol, 1977). We applied the procedure described by Le Mouel et al (1972). The operator "reduction to the pole" is defined in the Fourier domain. The magnetic anomalies are transformed to the Fourier domain, using a standard 2-D FFT technique. For this it is necessary to have the anomalies defined at rectangular grid points. The contour chart of Figure 6 gives the magnetic anomalies with a grid of 0.05*0.05 degrees. This implies that

all wavelengths smaller than about 10 km are eliminated.

The parameters needed for the operator "reduction to the pole" are inclination and declination of present and remanent field. Table I gives these values for the present field in the center of the area (32°N/ 28°W), together with the variations over the area. For the remanent field parameters the time at which the magnetization originated has to be known. The age of the seamounts belonging to the Atlantis-Meteor complex is only roughly known (see chapter I), the age of the oceanfloor in this area ranges from about 40- 90 Ma. Table I lists the following possibilities:

1): The magnetisation is recent or effectively recent. For this the magnetization direction of the geographic pole (mean Brunhes) should be used. This magnetization direction can only apply to topographic features like the seamounts, since the oceanfloor here is older than about 40 Ma.

2): The magnetization is Tertiary. We used the Early Tertiary pole (83°N/164°E) given by Van den Berg (1979). Values for the Late Tertiary pole (83°N/186°E, see Van den Berg, 1979) are not given since they are virtually the same as the Early Tertiary one.

TABEL I: Magnetic field parameters

	inclination	*declination*
Present pole :	51° ± 4°	-16° ± 1°
Geographic pole :	52° ± 3°	0°
Tertiary pole :	46° ± 3°	- 3° ± 1°
Late Cretaceous pole:	36° ± 3°	-29° ± 1°

Tertiary magnetization might apply to the seamounts and also is valid for the seafloor to the west of the positive magnetic anomaly, which runs from about 29°N/30°30'W to 34°30'N/25°W in Figure 6.

3): The magnetization is Late Cretaceous, with a paleopole situated at 61°N/ 226°E (Van den Berg, 1979). This magnetization direction only

applies to the southeastern part of the area, being Cretaceous of age. As can be seen in Table I the value for the inclination using the geographic pole does not differ significantly from the one for the Tertiary pole. Therefore we only show the phase shifting for the geographic pole magnetization (western part of Figure 8) and for the Late Cretaceous magnetization (southeastern part of Figure 8). In this Figure the 3000 and 2000 m basement contours from Figure 3 indicate the seamount positions.

Anomalies "reduced to the pole"

Figure 8 shows that after reduction to the pole the majority of the structures less deep than 3000 m now have a positive magnetic anomaly over it. Great Meteor seamount has a positive anomaly situated over the center of the seamount, although the lateral extent of the positive anomaly is smaller than the area comprised by the 2000 m basement contour. Cruiser and Irving seamount now also have positive anomalies over the topografic highs. Hyères seamount has a negative anomaly over its southeastern part. Plato, Tyro and Atlantis seamount, together with the "unnamed" seamount at 34°N/ 28°30'W, all have positive magnetic anomalies. The magnetic anomalies outside the 3000 m basement contour hardly change at different places, e.g. the anomaly between 29°N/30°W and 31°N/ 29°W. Between 32° and 33°N and at around 29°W, Figure 8 shows a continuous positive anomaly, which almost has a N-S direction and which is not continuous in the observed anomalies of Figure 6. This behaviour is to be expected from Figure 7. Seafloor spreading directions in this area strike 180-200 degrees. As can be seen in Figure 7, the phase-shift angle is low for these strikes, but it is high for E-W strikes. Therefore the anomaly between 32° and 33°N and around 29°W must be a fracture zone anomaly.

With the Late Cretaceous parameters, the southeastern part of the area shows continuous anomalies, striking about WNW-ESE. These anomalies are mainly caused by fracture zones. The continuity is caused by the absence of polarity reversals in the Cretaceous Magnetic

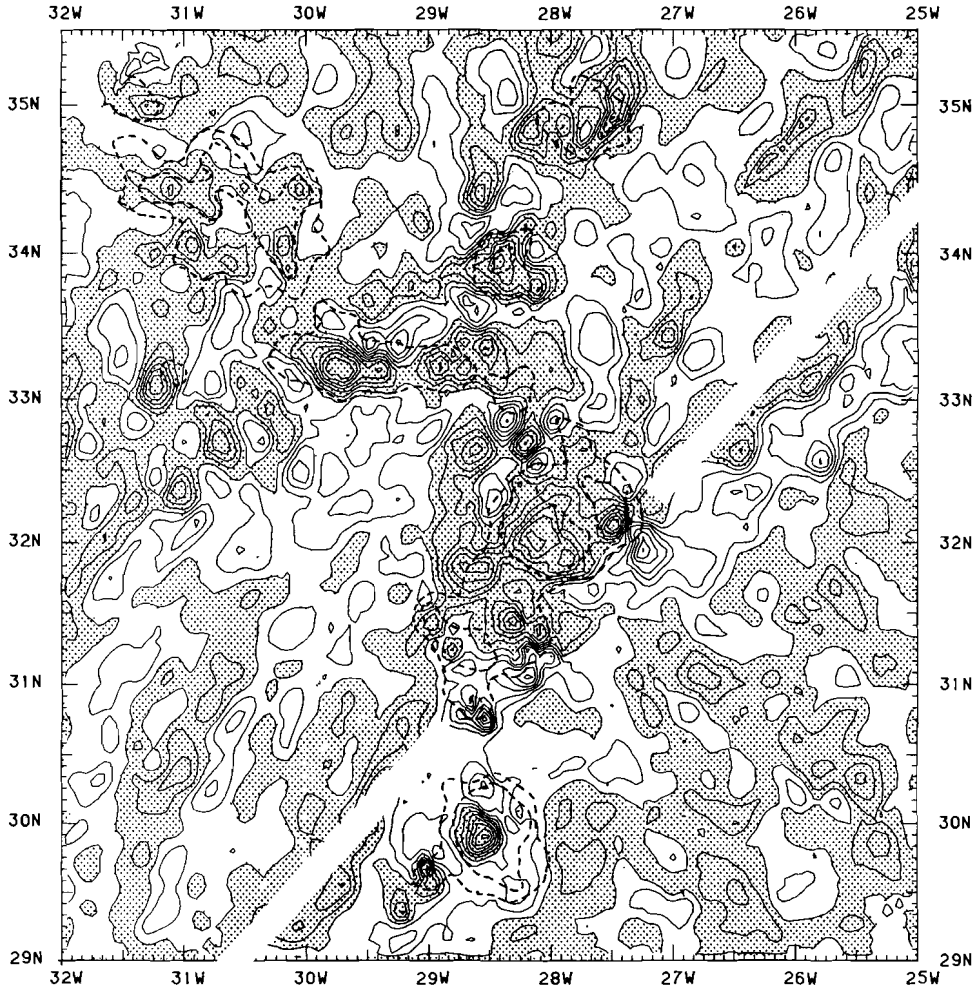

Figure 8: Magnetic anomalies "reduced to the pole". Contour interval 100 nT. Positive magnetic anomalies have been shaded. Dashed lines indicate generalized 3000 and 2000 m basement contours from Figure 3. White band running from 29°N/30°30'W to 34°30'N/25°W denotes transition from magnetization direction corresponding to geographic pole (area to the northwest of white band) to the Late Cretaceous magnetization direction (area to the southeast of white band). Parameters for magnetization directions are listed in Table I.

Quiet Zone.

Reduction of the magnetic anomalies to the pole, as shown in Figure 8, leads to the following observations: the observed magnetic anomalies can be made to coincide with the topography after applying a phase shift with a magnetization direction given by the geographic pole or by the Tertiary pole. In the Atlantis-Meteor seamount complex almost all topographic highs have a positive magnetic anomaly. Hyères seamount seems an exception with a negative anomaly over its southern part (see discussion). Other exceptions are tablemounts where, usually, the magnetic anomalies after phase shifting do not coincide with the topography. Figure 8 doesn't show this, since the short wavelength anomalies over tablemounts have been filtered out in the contouring process.

Correction for seamount anomalies

By applying phase shifting techniques we were able to define the relationship between seamount anomalies and topography. With a three dimensional magnetic model for this topography we can isolate these anomalies and eliminate the effect of the seamounts on the total magnetic anomaly pattern. As input for the magnetic model calculations we used the basement contours of Figure 3. For all basement structures less deep than 4000 m a model anomaly was calculated using a two dimensional Fourier technique. A magnetization of 5 A/m was assumed, except for those parts less deep than 1000 m for which we took a value of 1 A/m. These values were found to give the best overall fit with the observed anomalies. For the magnetization direction we choose those corresponding to the geographic (or Tertiary) pole given in Table I. Figure 9 gives the result with a contour interval of 100 nT. The dashed line surrounds the area inside which the contribution from the magnetic model is significant. In order to make a direct comparison possible between the calculated and the observed anomalies, we constructed profiles from the contours of Figure 9 along the tracks. Major discrepancies in amplitude between the observed and

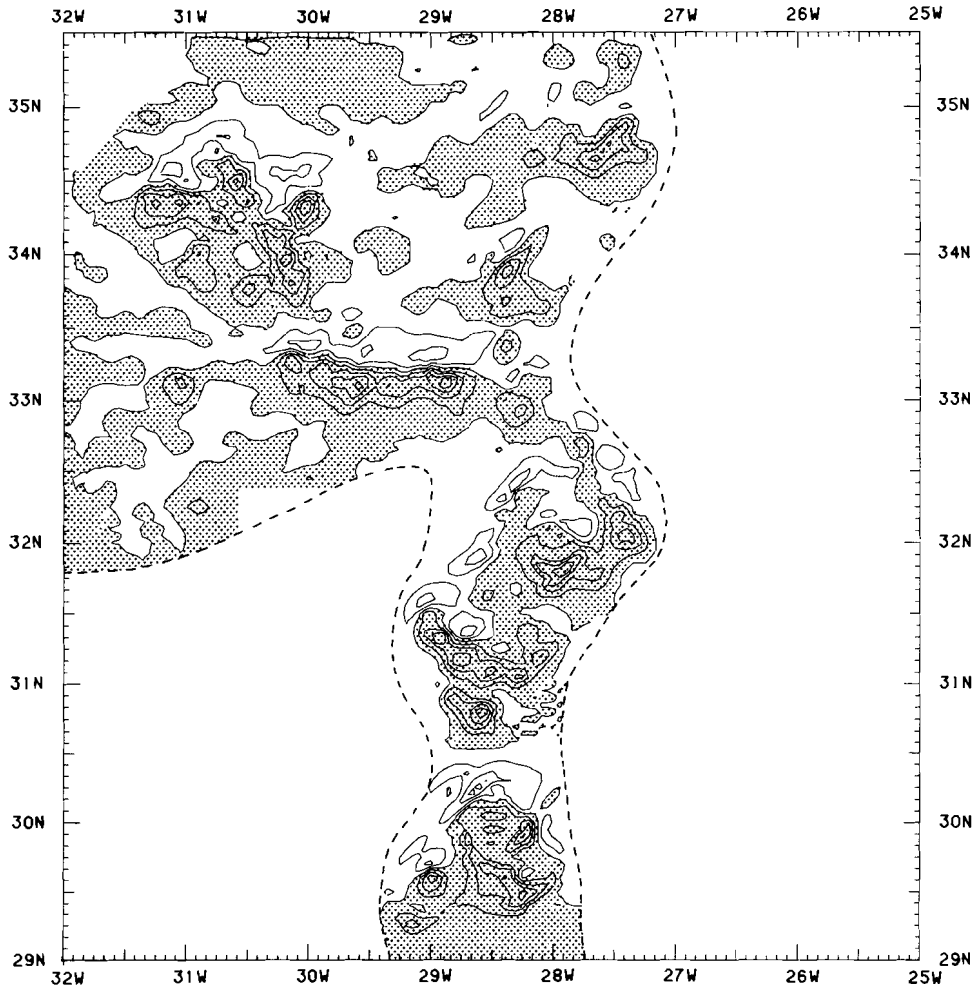

Figure 9: Magnetic model for the seamounts. Contour interval 100 nT. Positive anomalies have been shaded. Dashed line surrounds the area with a significant contribution from the model. The model was calculated from the basement contours of Figure 3, with a magnetization of 5 A/m for the parts less deep than 4000 m and one of 1 A/m for those less deep than 1000 m. Magnetization direction corresponds to the geographic pole.

calculated anomalies occur over tablemounts. Accurate comparison between observed and calculated anomalies is complicated by the "background" level caused by seafloor spreading and fracture zone anomalies. Because of this complication we did not try to refine the magnetic model by varying the magnetization for the different seamount groups.

The magnetic model does not predict some of the observed short wavelength anomalies. This can be caused by: effects of tablemounts, short wavelength structures in the basement, that are not given by the contours in Figure 3, irregularities in the magnetization of the basement, or reversely magnetized bodies in the seamounts. These discrepancies could in principle, be diminished by a refinement of the magnetic model. However, because we don't know the exact cause of the discrepancies and because we don't expect a significant improvement from a model refinement, we have chosen for elimination of the short wavelength discrepancies by filtering. For this we constructed profiles along the tracks from both contour charts of Figure 6 and Figure 9 and filtered these with a low pass filter, cut-off wavelength 22.5 km, roll-off 24 dB/ octave. A residual was calculated and a new contour chart was produced.

Residual magnetic anomalies

Figure 10 gives this contour chart of the magnetic anomalies, i.e the anomalies after elimination of the seamount effects as computed along the tracks and brought back to the geographic position. Inside the area where the model anomaly from Figure 9 has a significant contribution, the short wavelengths in the residual (up to 22.5 km) have been eliminated. Outside this part the residuals in Figure 10 are the same as the observed contours from Figure 6. Here the anomalies also contain information in the wavelength band between 10 and 22.5 km.

The residual anomalies over Great Meteor seamount are positive over the central part of the seamount. As stated before, the procedure

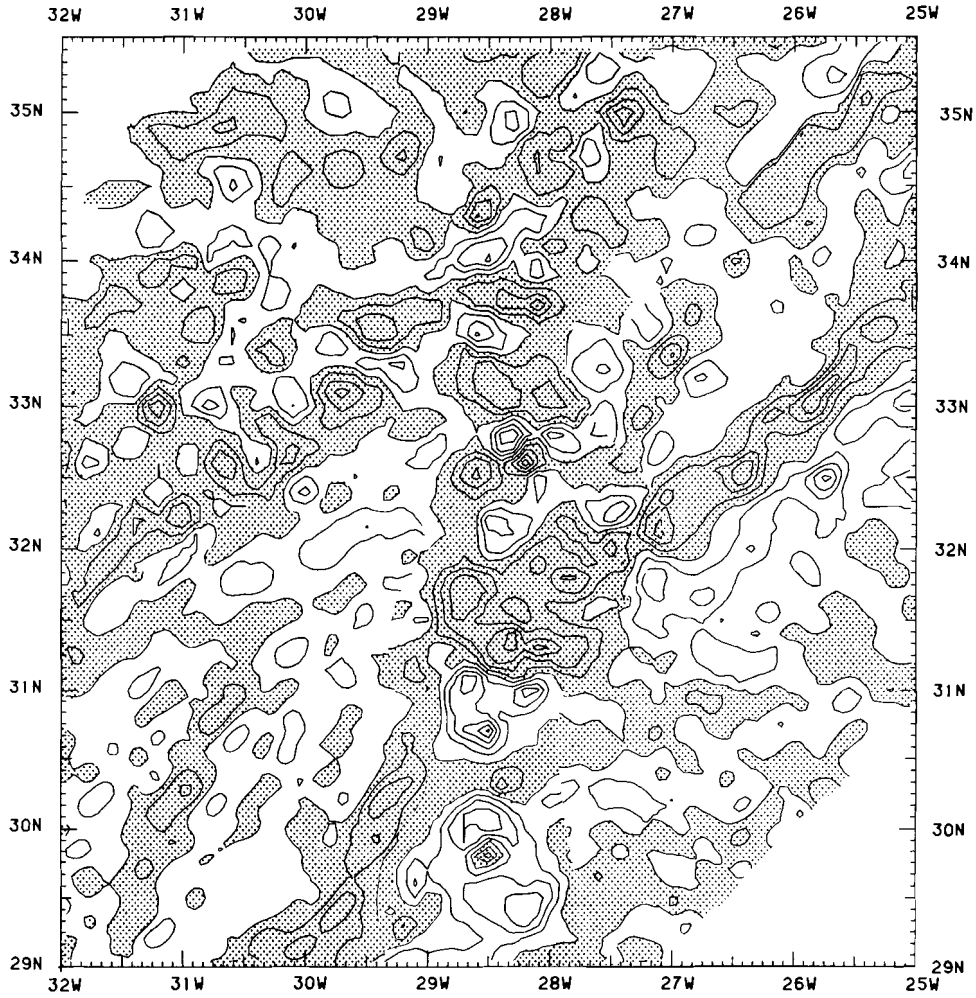

Figure 10: Residual magnetic anomalies, after removing the seamount effects. Contour interval is 100 nT. Positive magnetic anomalies have been shaded. See text for description of the calculation of the residual magnetic anomalies.

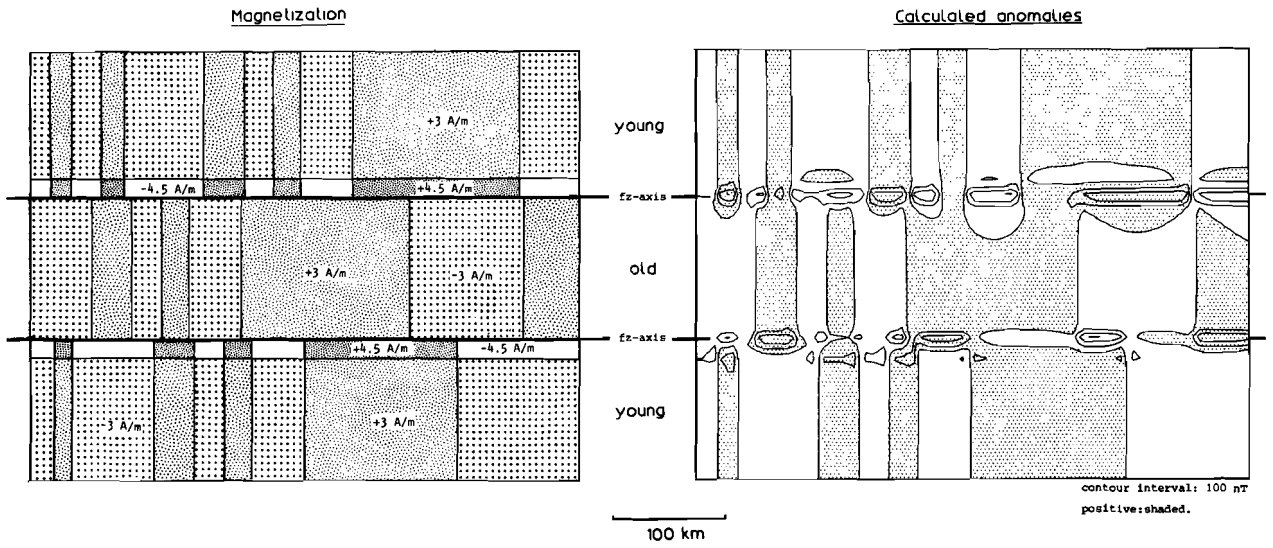

Figure 11: Computed anomalies over a model of the floor of Atlantic Ocean with enhanced magnetization in the fracture zone valley. The northern fracture zone has from north to south a young to old contrast, the southern one an old to young contrast. Magnetization direction corresponds to geographic pole (see Table I for parameters).

of removing the effect of seamounts does not work satisfactorily for tablemounts. The complex formed by Cruiser, Irving and Hyères seamounts has a positive residual, which is part of the elongate positive anomaly, mentioned earlier. The E-W magnetic anomalies over Plato seamount have for the greater part disappeared in the residuals.

The residual anomalies in Figure 10 then are "cleaned" by removing effects of the seamounts. The remainder should now consist of seafloor spreading and fracture zone anomalies. To identify these anomalies Figure 11 shows a simple 3-D magnetic model of spreading and fracture zone anomalies. For this we took a planparallel horizontal layer of 1 km thickness with its top at 4 km and with a magnetization distribution as indicated. The spreading anomalies are caused by contrasts between the positively and negatively magnetized blocks. The fracture zones have been modelled by assuming an enhanced magnetization situated at the younger side of the axis (Twigt et al, 1983, see also Collette et al, 1984). The anomalies over this schematic structure were calculated by using the parameters for the center of the present area. With this model we identified the seafloor spreading and fracture zone anomalies.

Structural pattern

Figure 12 shows the structural pattern, i.e. the sea floor spreading pattern, of the area of Atlantis-Meteor seamount complex. In this Figure the position of the identified magnetic anomalies has not been corrected for skewness. We took the position of the western positive flank of the anomaly. The fracture zone pattern is based on both topographic and magnetic expressions of the fracture zones. Note that with the used vertical exaggeration of about 6 times in Figure 1 the fracture zones only show as minor indentations. The fracture zone pattern in Figure 12 forms part of the analysis of the spreading process in a much larger area in the central North Atlantic Ocean between 10° and 38°N (Collette et al, 1984). The reconstruction of the sea floor spreading pattern in the seamount area formed a crucial part

of this analysis.

The fracture zone pattern in Figure 12 is given in the form of spreading segments. Each segment describes a period of the spreading process. Following a theorem by Morgan (1968), fracture zones must follow a small circle pattern in order to make spreading possible. The movement of the plates can be described on a sphere as a rotation, defined by a pole of rotation and a spreading angle. The spreading segments in Figure 12 define small circle patterns for the different rotation poles which describe the spreading process in the central North Atlantic Ocean. Each spreading segment is subdivided in rotation angles of .25 degrees, except for the poles of anomaly 34 and older where the subdivision represents 1 degree. This has been done since these latter poles are very close to the area.

In the southwestern part of the area at about 29°10' N Atlantis fracture zone can be found. The age of the ocean floor to the north of this fracture zone in the southwestern part of our area, is about 68 Ma (anomaly 30/31, using the timescale of Lowrie and Alvarez, 1981). Anomaly 34 (86 MA), which marks the end of the Cretaceous Magnetic Quiet Zone, appears south of 33°N/ 25°W. Hayes fracture zone enters the area near 32°45'N/ 32°W. In the northwest near 34°30'N/ 32°W Oceanographer fracture zone could be identified (Fox et al, in preparation). To the east this fracture zone disappears underneath the Atlantis seamount group. The age of the ocean floor in the northwestern part is about 48 Ma (anomaly 21). By extrapolation we find an age of 36 Ma (anomaly 13) in the upper northwest corner of the area.

Upper limit of the age of the seamounts

The positions of the different seamounts in the area around the Atlantis-Meteor complex are indicated in Figure 12 by the 3000 and 2000 m basement contours from Figure 3. The age of the ocean floor under the different seamounts forms the upper limit to the age of the seamounts in question. This would be the real age if the seamounts

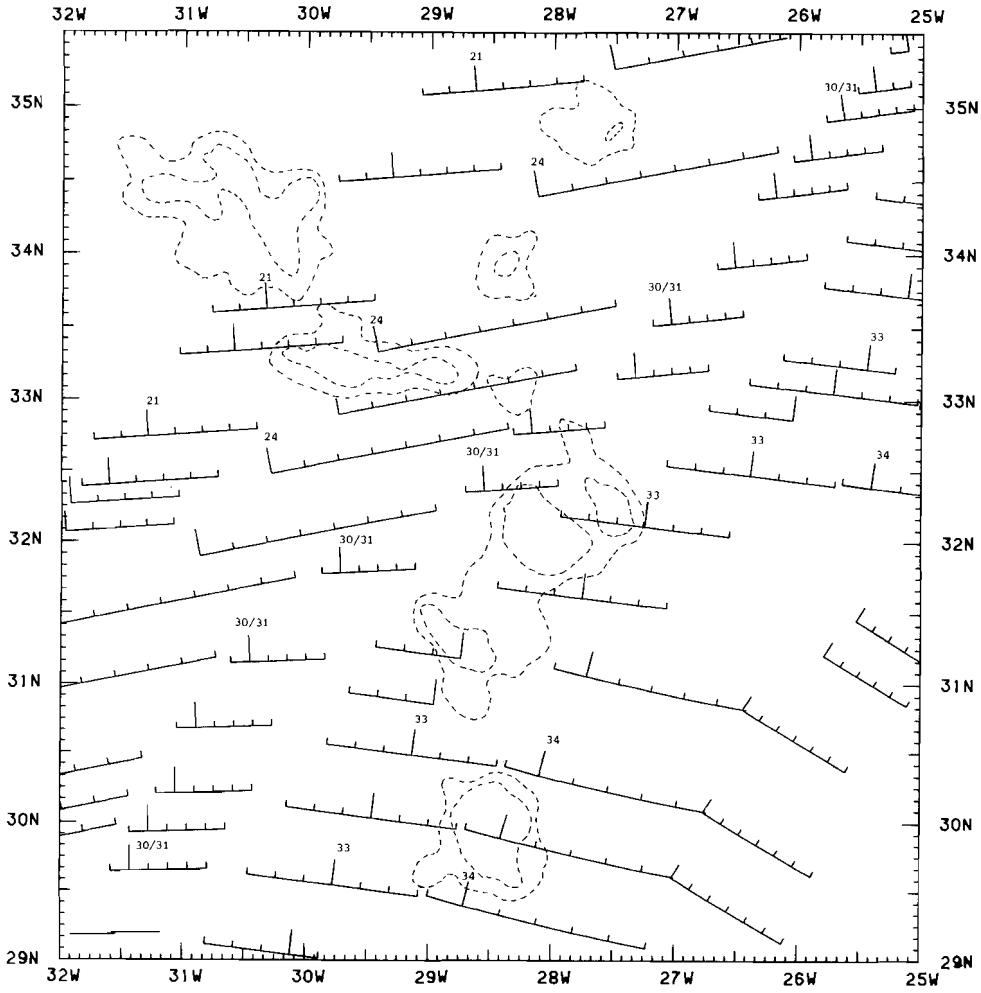

Figure 12: Fracture zone pattern and identified magnetic anomalies in the area around the Atlantis-Meteor seamount complex. Fracture zones are given as spreading segments. The positions of the identified magnetic anomalies have not been corrected for skewness. Dashed lines give the generalized basement contours from Figure 3. See text for explanation of the fracture zone pattern.

originated at the spreading axis. Table II lists these ages as obtained by linear interpolation between magnetic anomalies.

TABEL II: Age of oceanfloor beneath the seamounts.

Great Meteor seamount	:	82-86 Ma
Hyères seamount	:	75-83 Ma
Irving seamount	:	69-78 Ma
Cruiser seamount	:	68-77 Ma
Plato seamount	:	49-60 Ma
"unnamed" seamount (34°N/ 28°30'W)	:	53-56 Ma
Tyro seamount	:	50-56 Ma
Atlantis seamount group	:	37-48 Ma

The "Nabighian"

The structural information which magnetic anomalies contain is often directly visible in the profiles, e.g. Figure 5, where we clearly see lineations in the magnetics over the seamounts. Lineations, for instance in positive anomalies, can be disrupted by magnetization reversals, which change the sign of the anomaly. Nabighian (1972) introduced a method to eliminate the reversal effect. In this method use is made of the analytical signal (Bracewell, 1978) of the magnetic anomaly or of its first derivative. The absolute value of the analytical signal used by Nabighian (1972) is called the "Nabighian". The "Nabighian" taken from the derivative of the anomaly was used in the detection of fracture zones in ocean crust of Cenozioc age. Here the sign of the magnetic contrast over the fracture zone changes as a function of age to both sides (Twigt, 1980, Collette et al, 1984).

Figure 13 shows the "Nabighian" of the derivative of the magnetic anomaly over two 2-D models. The anomalies have been calculated with

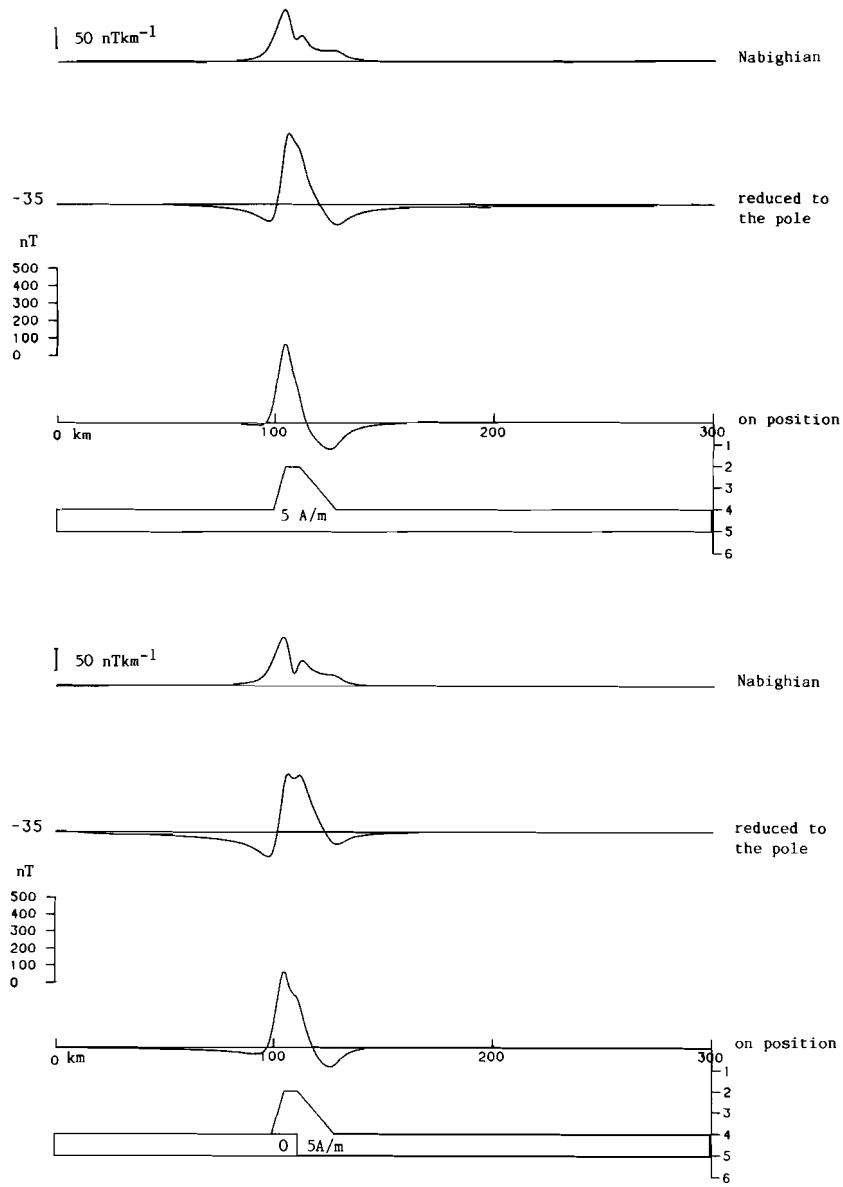

Figure 13: Two dimensional magnetic models over seamounts. Magnetic anomalies are calculated using a magnetization direction corresponding to the geographic pole. Phase shifted anomalies are also given, together with the "Nabighian" of the first derivative of the magnetic anomaly.

the parameters for the present field and for the remanent field (geographic pole) given in Table I. We also show the anomaly "reduced to the pole". The largest peak in the "Nabighian" is situated above the largest change of slope of the seamount. When a less steep change of slope and a deeper contrast occurs, the amplitude of the peak decreases. The flat top of the seamount shows as two maxima. Contrasts can be distinguished as long as the horizontal distance between them is larger than their depth.

In Figure 13B we show a model of a seamount together with a magnetization contrast of the ocean floor. The influence of this contrast on the largest maximum of the "Nabighian" is only small (see discussion).

Figure 14 gives the "Nabighian" of the profiles in the area of the Atlantis-Meteor seamount complex. The "Nabighian" is not a linear operator. This means that the effects caused by seafloor spreading, fracture zone and seamount anomalies are no longer separable. Figure 14 shows that the value of the "Nabighian" is much larger over seamounts than over fracture zone and spreading anomalies. Therefore it may be assumed that the amplitude of the "Nabighian" is mainly caused by seamount anomalies.

The "Nabighian" extrema over Great Meteor seamount don't show as a clear structural direction. The profiles over the central part of the seamount, the tablemount, give several maxima. This might point to a magnetic contrast in the top of the tablemount. The "Nabighian" extrema over the other seamounts give the same NW-SE directions as described before. Plato seamount shows WNW-ESE directions.

Magnetic and seismic directions

Figure 15 gives the directions detected in the seismics together with the ones from the magnetics (using the "Nabighian"). In general, the directions from the seismic data agree well with the ones found in the magnetic anomalies. The magnetic and seismic positions don't always coincide . This might be related to the circumstance that the

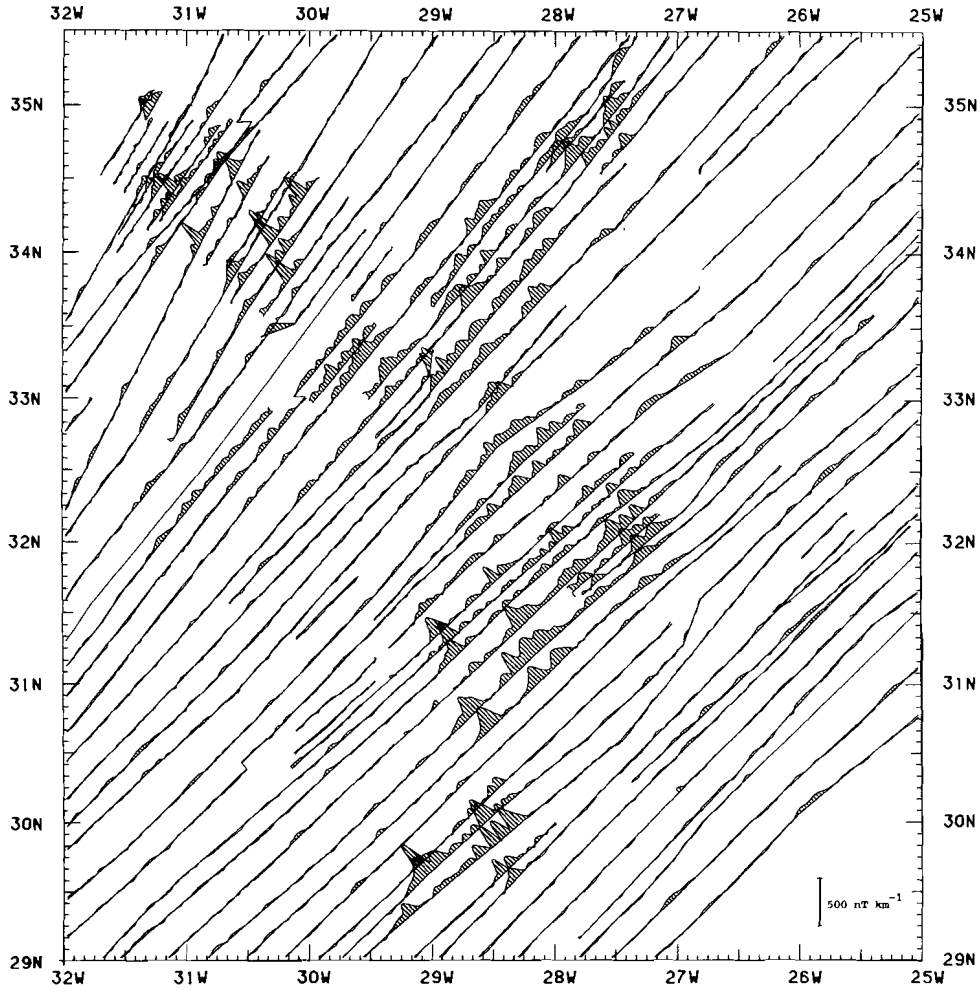

Figure 14: The "Nabighian" of the first derivative of the magnetic anomalies plotted with an offset of 15 nT/km. Amplitudes larger than 15 nT/km have been shaded.

topographic lineations we chose don't necessarily coincide with the position of the steepest slope in the magnetic contrast.

DISCUSSION

The Atlantis-Meteor seamount complex is resting on ocean floor ranging in age from about 37 Ma under the western part of the Atlantis seamount sub group to about 86 Ma under Great Meteor seamount (see Table II). This sets an upper limit to the age of these volcanic complexes. Closer age determinations of the seamounts cannot reliably be made from the magnetic anomalies, since the variation of the position of the paleomagnetic pole during the Cenozoic and Late Cretaceous is not large enough to produce appreciable phase-shift differences in this part of the Atlantic (see Figure 7).

The magnetic anomalies over the Atlantis-Meteor seamount group are in general positive after correction for the skewness. Hyères seamount seems to form an exception. Reduced to the pole we have a negative anomaly over the southern part of this seamount (see Figure 8). The structural pattern, given in Figure 12, shows that the oceanfloor is negatively magnetized under Hyères seamount and also to the south of it (the negative block between anomalies 33 and 34). This negative magnetization results in a negative anomaly on the pole over the southern part of the seamount (see model in Figure 13B), which nevertheless is positively magnetized.

The positive magnetic anomalies, when reduced to the pole, over the seamounts point to a positive magnetization. A magnetization of 5 A/m gives in general the correct amplitude of the anomaly, as can be seen from Figure 9. Anomalies caused by local variations in magnetization cannot be distinguished from "background" level, i.e. the seafloor spreading and fracture zone anomalies. A positive magnetization of 5 A/m was also used by Haut (1973) in a detailed magnetic study over Great Meteor seamount.

In a preliminary study, which only describes the magnetics over Plato and Atlantis seamounts, the positive magnetization over these

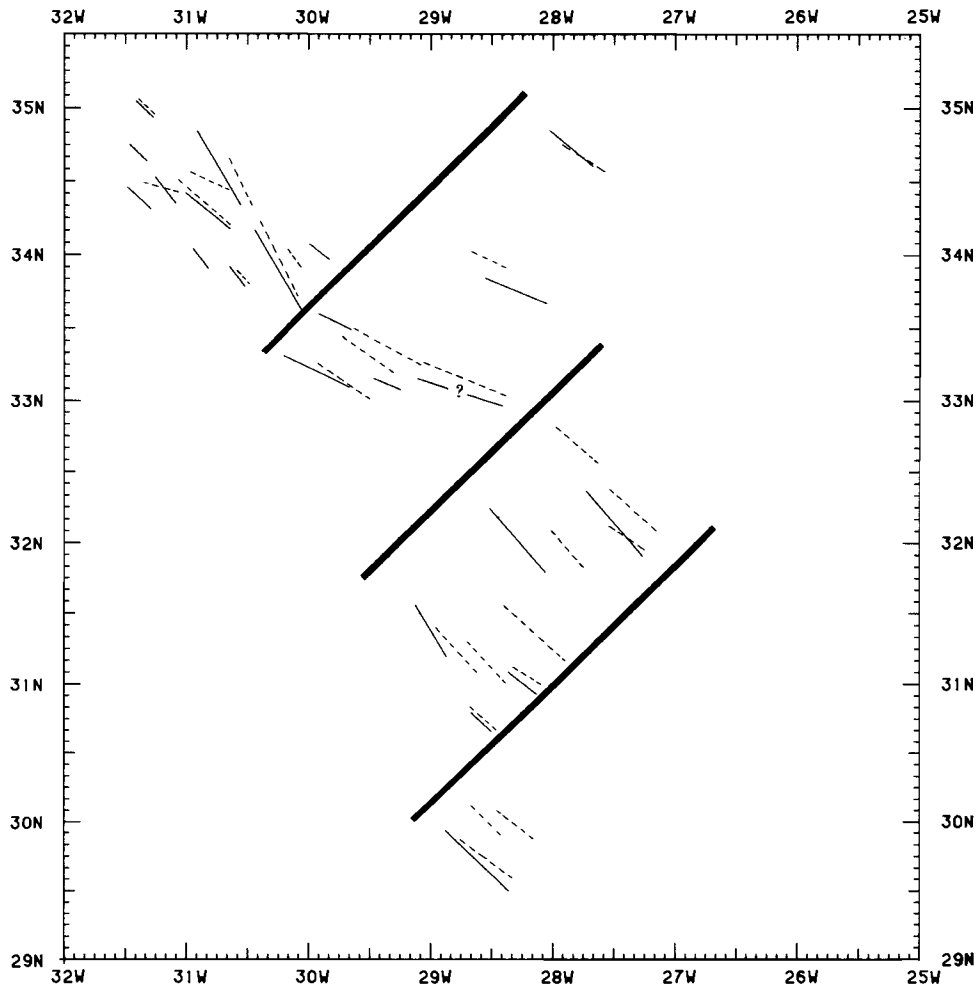

Figure 15: Seismic and magnetic directions found in the Atlantis-Meteor seamount complex. Continuous lines give seismic directions. The magnetic directions (dashed lines) are taken from the "Nabighian". Heavy lines give the boundaries (transform zones) between the seamount groups.

seamounts has already been discussed (Williams et al, 1983). There it was concluded that the coincidence of all volcanoes being active mainly during normal periods was pushing statistics too far. The normal polarity of the seamounts of the Atlantis-Meteor complex can be combined with the observation of Bullard and Mason (1963), that the majority of the seamounts show normal polarization. Francheteau et al (1970) found in the Pacific ocean that for 42 investigated seamounts only 8 have reversed magnetization.

Williams et al (1983) explained the predominance of normal magnetization as the effect of viscous remanent magnetization (VRM) dating from the present normal period (Brunhes). The thermo-remanent magnetization (TRM) of the seamounts would be overprinted then by VRM, thus glossing over reversed thermo-remanent polarizations. This does not preclude the existence of reversed magnetized rocks in seamounts. Small seamounts may have apparent magnetizations in directions that differ from the present field directions, including reverse directions. They may evolve over a relative short period and thus the chances are greater that they have grown in a single polarity interval.

Tablemounts are often characterized by large short wavelength anomalies. Even after "reduction to the pole" a clear correlation with topography is seldom possible. Magnetic modelling over tablemounts showed, that an irregularly shaped magnetic top, not necessarily representing the observed topography, can explain the short wavelength anomalies. The different extrema in the "Nabighian" over tablemounts also point to an irregularly shaped contrast. Free air gravity anomalies often show a relative low over the central flat surface of tablemounts, which indicates a lower density at the surface. Hinz(1969) detected a sedimentary layer with a thickness of 0.4 seconds on top of Great Meteor seamount. This together has led to the hypothesis that the short wavelength magnetic anomalies over tablemounts are caused by buried topography of the original volcanoes, hidden from direct observation by reef sediments and its debris on the slopes.

The seismic profiles in the area around the Atlantis-Meteor seamount complex show this complex to consist of a mosaic of blocks arranged in a general NW-SE direction. The individual seamounts in each block are linear with NW-SE directions and abut against NE-SW zones which separate the blocks and can be followed in the depth contours of Figure 2, especially to the SE and NW of the Cruiser, Irving Hyères block. No evidence has been found for faulting along the separating zones. The total structure of lineated blocks separated by transverse zones is suggestive of extension in a NE-SW direction. Verhoef and Collette (1983) concluded that the Atlantis-Meteor seamount complex is underlain by a tear fault system. The amount of involved extension is not known. In the Cruiser, Irving and Hyères block we found at least four large parallel linear structures. So here we have to reckon with a minimum of four major feeder dikes or dike complexes. For the other blocks this amount could be less. What this means in terms of absolute extension and how this adds up for the total area is hard to say.

A large extension of the area around the Atlantis-Meteor seamount complex may form a source of errors for the reconstruction of the fracture zone pattern. As we did not find any inconsistencies while reconstructing this pattern (Collette et al, 1984) the accuracy of the reconstruction process gives an upper limit for the amount of extension involved. This means that there is space for a few, maybe ten, kilometers NE-SW extension.

In accommodating the extension we can follow two solutions. The first one is to find it in the effect of doming related to the uplift of the area as a whole. The extensional effect of doming is small, geometrically it is an order of magnitude smaller than the uplift, too small to account for the whole phenomenon. The resulting stresses are not even large enough to cause rupture. A second solution lies in finding the cause of the extension in the horizontal plane, i.e. in supposing that the area as such underwent tensional deformation. This places the pattern in a more regional context.

The answer to the question how to accommodate the extension bears

on the problem of whether midplate oceanic volcanism finds its cause in the occurrence of primary hot spots or mantle plumes (cf. Wilson, 1963 and Morgan, 1971), or in midplate tectonism creating a secondary hotspot (Turcotte and Oxburgh, 1973 and 1978). We will come back to the problem in the general discussion of chapter V.

CHAPTER III

THE GRAVITY FIELD OF THE ATLANTIS-METEOR SEAMOUNT COMPLEX

Introduction

The area around the Atlantis-Meteor seamount complex is too undeep compared to the age-depth relationship given by Parsons and Sclater (1977) and forms, following Menard's definition (1973), a positive depth anomaly. This positive depth anomaly forms the southern part of the North Atlantic Gravity High (described by Cochran and Talwani ,1978, from 1°*1° averages), which extends from Iceland to about 30°N. In this chapter we will calculate the depth anomaly of the area in more detail, using the structural pattern from the Kroonvlag-project (Collette et al, 1984).

From the gravity data the isostatic anomaly will be calculated, after correction for topography effects and assuming a regional compensation system. From the elastic response of the lithosphere, the flexure of which causes the regional compensation, we will calculate the elastic thickness under the seamounts of the Atlantis-Meteor complex. Using this thickness we will estimate the age of the seamounts. It will be shown, using the cross spectral technique, that the compensation closely follows a plate model for wavelength smaller than about 1000 km. The gravity data was also used for the calculation of a detailed geoid in the area around the Atlantis-Meteor seamount complex. The geoid anomalies, including altimeter data, confirm that the compensation closely follows a plate model.

STRUCTURAL SETTING AND DEPTH ANOMALY

Structural data

Figure 1 shows the tracklines with seismic and magnetic data. The

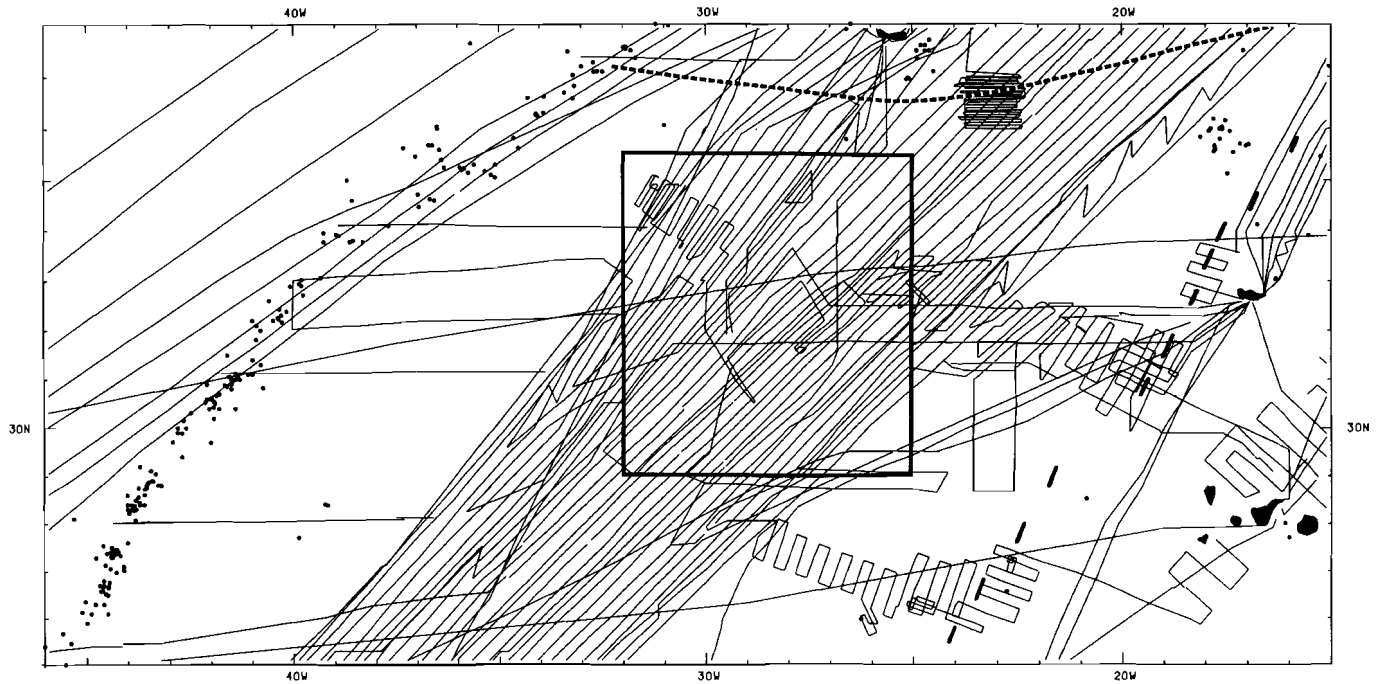

Figure 1: Tracklines with seismic data. The heavy dashes give the East Azores fracture zone, which forms the northern boundary of the study area. The discontinuous heavy line indicate the Mesozoic magnetic anomaly MO (eastern boundary). The Mid-Atlantic ridge is indicated by the earthquake epicenters (western boundary). The central square indicates the seamount area, studied in chapter 2.

average track spacing in the central part of the area with the seamounts, indicated in Figure 1 with the rectangle, is about 25 km. The western boundary of the area for which we will calculate the depth anomaly and the isostatic anomaly is formed by the Mid Atlantic Ridge. The eastern boundary is formed by the isochrone of Mesozoic magnetic anomaly M0 (118 Ma, the identification of M0 is based on Slootweg and Collette, in prep., complemented with identifications of Rabinowitz et al, 1979). East of this boundary the Canary Islands, Madeira and the Madeira Torre Rise are found. The northern boundary of the area is formed by the East Azores fracture zone. To the south the 27°N parallel was taken.

Figure 2 shows a computer contour of the corrected basement depth. Corrected basement depth is defined as the depth to basement after correction for sediment loading. The correction for sediment loading was done by assuming local isostatic compensation. With a waterdepth d, density ρ_w , a sediment thickness s, density ρ_s and a density ρ_m for the asthenosphere we find for the corrected basement depth d_c (e.g Crough, 1983):

$$d_c = d + \frac{\rho_m - \rho_s}{\rho_m - \rho_w} \cdot s \qquad (1)$$

Recent results on sediment velocity and density obtained from DSDP holes indicate that the corrected basement depth can be found by adding 0.6 times the sediment thickness to the observed waterdepth (Crough, 1983). At places where we did not reach the basement, as often happens close to the seamounts due to the presence of an opaque reflector (see chapter IV) and/or the flexure of the oceanic lithosphere (see this chapter), we took the deepest reflector as an indication for the basement depth. This gives a lower limit of the sediment thickness and thus the calculated corrected basement depth will be too low there.

In the western part of the area, at 28°N, 31°N and 34°N, three east-west tracks from the NAVADO project were used (Anonymous, 1967). On these tracks no seismic data were available, only depth

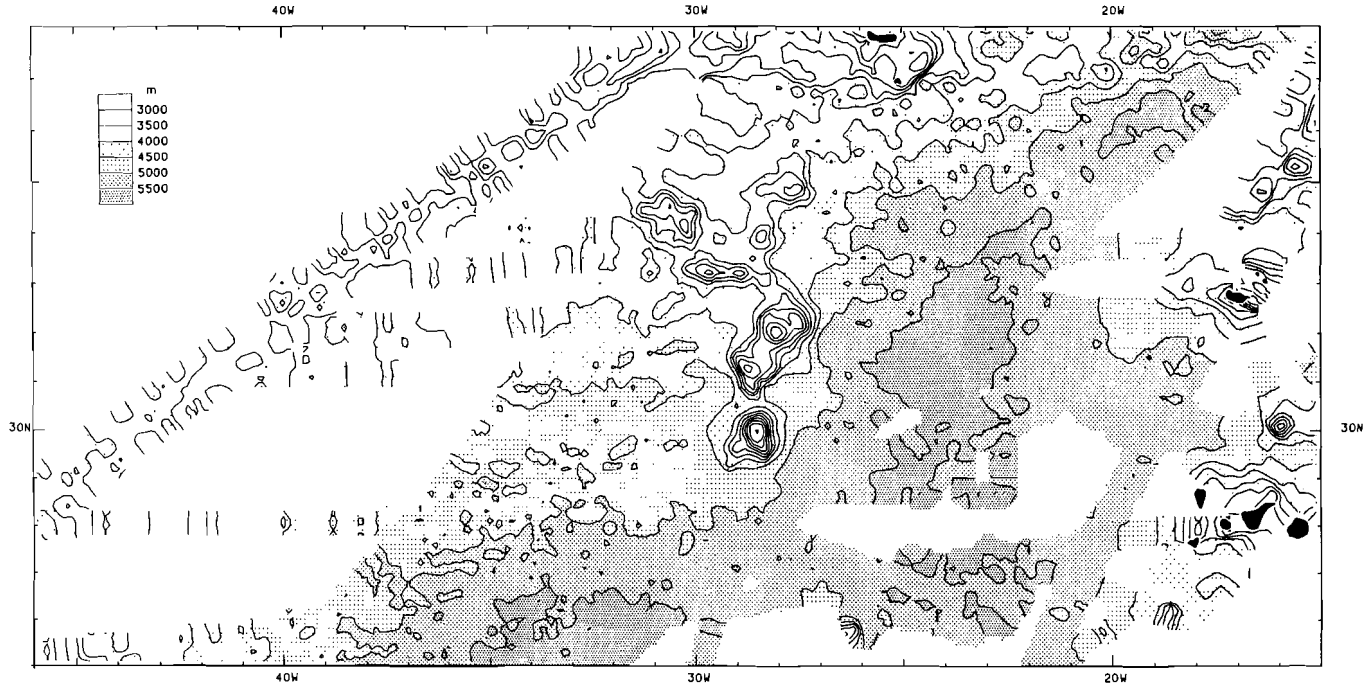

Figure 2: Corrected basement depth. Computer contoured with a cut-off wavelength of 55 km, 6dB/octave. Contour interval 500 m. The corrected basement depth denotes the basement depth after correction for sediment loading (see text). In the contouring we did not incorporate the depth contours of the islands. This is indicated by the white band around the islands.

information. We used these tracks only in those parts of the area with sparse data, i.e. to the west of our dense track bundle. As the sediment thickness in this area, which is close to the Mid Atlantic Ridge, is small in general, we here took the bathymetry as the corrected basement depth.

In figure 2 the Atlantis-Meteor seamount complex is clearly visible as a general rising of the oceanfloor. A description of the individual subgroups can be found in chapter II. To the north, between 24° and 27°W, we find the topographic high of the Azores. The depth contours in the eastern and northeastern part of the area run roughly parallel to the Mid Atlantic Ridge. More to the east the oceanfloor again becomes less deep, due to the presence of Madeira and the Madeira Torre Rise and, in the southeastern part, the western Canary Islands.

Structural pattern

Figure 3 gives the structural pattern of the area around the Atlantis-Meteor seamount complex. The central part is based on an analysis of the data from the Kroonvlag-project between 10° and 38°N (Collette et al, 1984). The fracture zone pattern is shown, based on the magnetic and seismic data. In addition, identified magnetic spreading anomalies are given. The position of the spreading anomalies corresponds to the western positive flanks of the observed anomalies. The gaps in the fracture zone pattern were filled in using the synthetic flow line pattern reconstruction from the Kroonvlag-project (dashed lines). For the continuation of the fracture zones up to the Mid Atlantic Ridge the same flow line pattern was used. For the continuation to the east up to Mesozoic magnetic anomaly M0 a simplified flow line pattern was used, based on an analysis by Slootweg and Collette (in prep.). To the north of the East Azores fracture zone we used the magnetic anomaly identifications of Laughton and Whitmarsh (1974) and of Searle (1980).

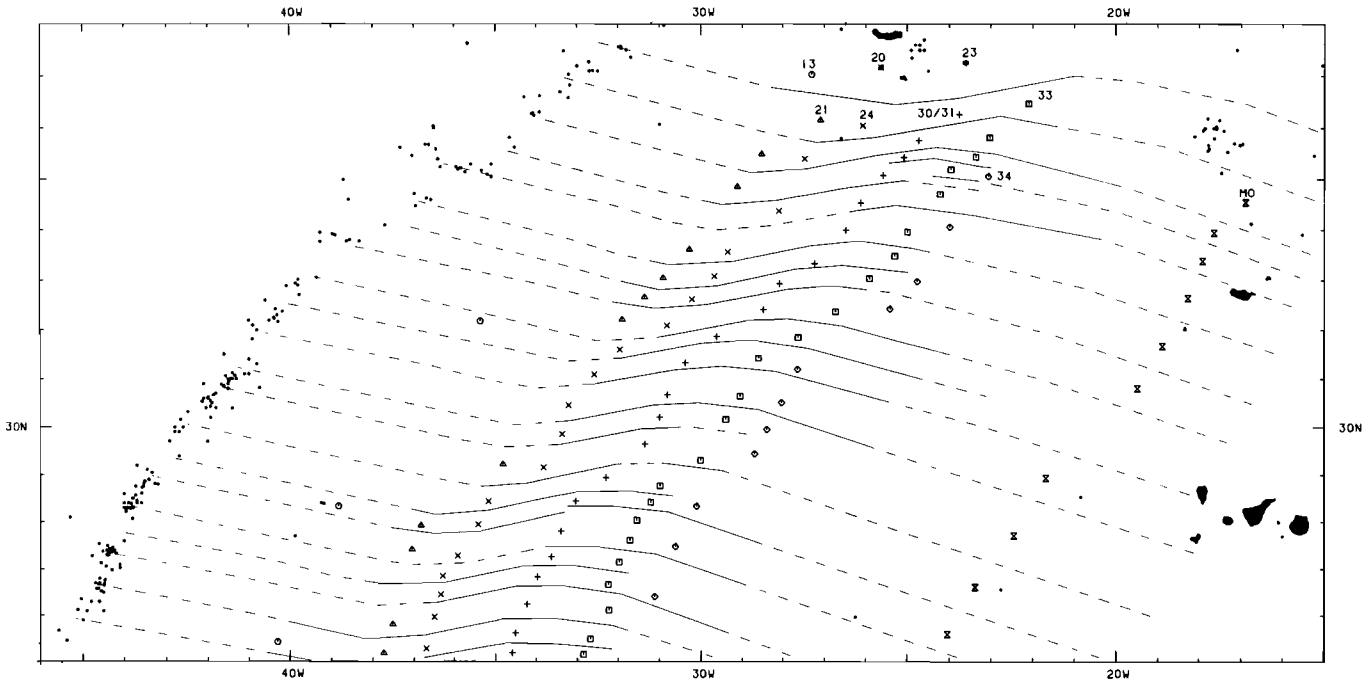

Figure 3: Structural pattern. Continuous lines indicate fracture zones. Dashed lines give flow line continuations of fracture zones. Identified magnetic anomalies are indicated by different symbols. Modified after Collette et al (1984).

Depth anomaly

Using the corrected basement depths of Figure 2 and the ages of the oceanfloor following from Figure 3 we calculated the depth anomaly. The depth anomaly, as defined by Menard (1973), denotes the difference between the depth expected for the ocean floor of a given age and the observed basement depth, corrected for sediment loading. Areas less deep than expected are defined as having positive depth anomalies. We used the depth-age relationship given by Parsons and Sclater (1977), taking the square root relation for ages less than 25 Ma and the exponentional relation for the older oceanfloor. For the conversion of magnetic anomalies to age we used the time scale of Lowrie and Alvarez (1981). The age of the oceanfloor between the identified magnetic anomalies was calculated by linear interpolation, taking the course of the fracture zones into account.

Figure 4 shows the depth anomaly contours. The depth anomaly in the area around the Atlantis-Meteor seamount complex is predominantly positive. Between 30° and 40°W at about 27°N we find the transition to the area with a negative depth anomaly. The area from 30°-33°N/ 23°-25°W also has a negative depth anomaly. The positive depth anomaly increases going to the seamounts and reaches a value of about 1500 m at the base of the seamount complex. Inside the complex we find values of more than 4500 m for the depth anomaly. To the north, a positive depth anomaly of more than 1000 m can also be found: the Azores complex. In the eastern part of the area the positive depth anomaly increases again. This increase is related to Madeira and the Madeira Torre Rise. From the few tracks we have up to the Mid Atlantic Ridge we see that the positive depth anomaly continues up to the ridge. This is in agreement with the findings of Cochran and Talwani (1978). We do not have enough data to establish whether or not the 1500 m positive depth anomaly related to the Atlantis subgroup continues up to the Mid Atlantic Ridge.

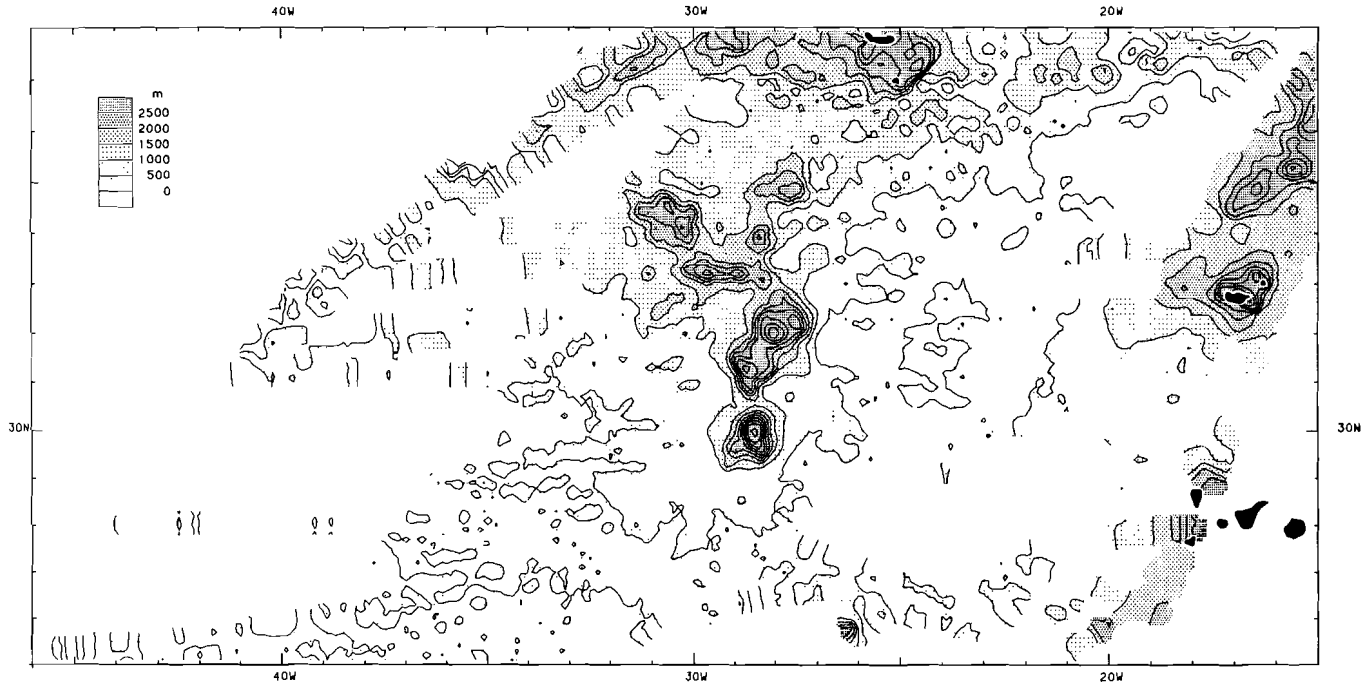

Figure 4: Depth anomaly. Computer contoured with a cut-off wavelength of 55 km, 6dB/octave. Contour interval 500 m. In the contouring we did not incorporate the depth contours of the islands. This is indicated by the white band around the islands.

THE GRAVITY ANOMALIES

The data

Figure 5 gives the track lines with gravity information. The gravity data from the Vening Meinesz Laboratorium, Utrecht, indicated by the continuous lines, consist of detailed surveys in the area (1979 and 1980) together with some tracks right through the area (1977, 1981 and 1982) and four east-west tracks from the NAVADO-project (Anonymous, 1967). The gravity data from the Rijks Geologische Dienst, Haarlem, indicated by the dotted lines, consist of a detailed survey in 1980.

Additional gravity information was obtained from the N.O.A.A.-National Geophysical and Solar-Terrestrial Data Center. These tracks are shown as the dashed lines in Figure 5. Table I summarizes the origin of the gravity data.

TABLE I: Gravity data set.

Origin	*Total of kilometers*
V.M.L., Utrecht.	61 670
R.G.D., Haarlem.	3 330
Lamont-Doherty Geological Observatory.	92 830
Woods Hole oceanographic institute.	44 390
N.O.A.A.	10 110
Bureau Gravimetrique International	6 300
C.N.E.X.O.	3 100
Total	221 730 km

The gravity data were converted to anomalies using the gravity formula adopted in 1967 by the International Association Geodesy (Morelli et al, 1974). Data from the Data Center, reduced with the IGF 1930 (Heiskanen and Moritz, 1967) and based on the Potsdam value were converted with the following formula:

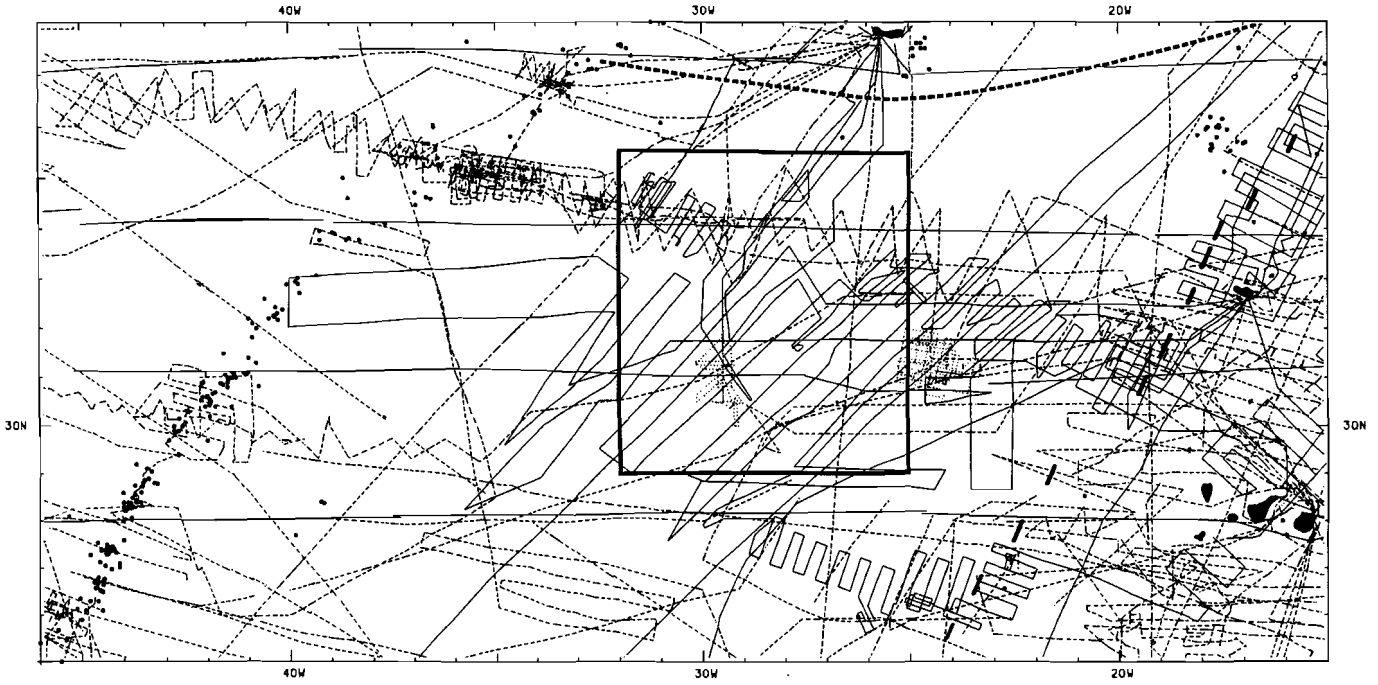

Figure 5: Tracklines with gravity data. Continuous lines indicate tracklines from V.M.L., Utrecht. Dotted lines indicate tracklines from R.G.D., Haarlem. Dashed lines give additional tracks from other institutes (see Table I). Central square indicates seamount area. East Azores fracture zone (heavy dashed line), magnetic anomaly MO (discontinuous heavy line) and Mid-Atlantic Ridge (earthquake epicenters) form boundaries of study area.

$$\delta g = (3.2 - 13.6 \sin^2\Phi) \text{ mGal} \qquad (2)$$

with Φ : geographic latitude.
This correction varies in the area given in Figure 5 from +0.8 mGal in the south to -2.4 mGal in the north.

The total data set given in Figure 5 and Table I is very inhomogeneous: different gravity meters, some with and some without cross-coupling correction devices, as well as different navigation systems were used in collecting the data. The internal accuracy of such a data set is difficult to estimate. We used cross-over analysis as a check for the accuracy. From the navigation points of the track lines we calculated, by computer, the positions of the intersection points of the tracks, together with the difference in the gravity anomaly at these points (see Verhoef and Scholten, 1983, were the same method was used for magnetic data). The cross-over analysis was made for the VML-tracks only, for the tracks of the other institutes and for the total data set. The results, given in Table II, show a small average and a standard deviation of about 8 mGal.

TABLE II: Cross-over analysis gravity data.

Data set	*number of crossings*	*average + deviation*
VML	290	(0.2 ± 6.5) mGal
Other institutes	893	(0.8 ± 7.9) mGal
Total data set	1714	(1.2 ± 8.0) mGal

The standard deviation, although rather high, is not unusual for such an inhomogenous data set, c.f. Prince and Forsyth (submitted). We did not attempt to minimize the errors at the intersection points by an adjustment procedure. Several tracks or part of tracks giving large discrepancies were eliminated from the data set.

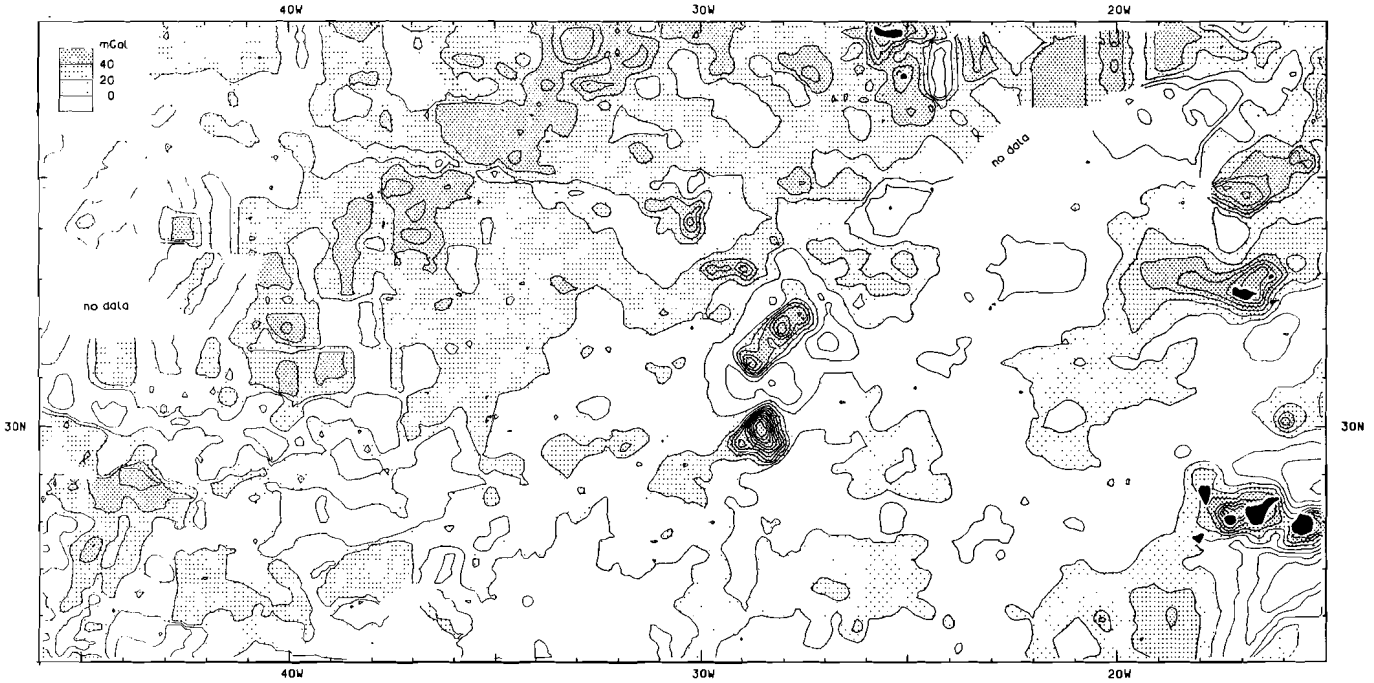

Figure 6: Computer contour of free-air anomalies, cut-off wavelength 80 km, 6 dB/octave. Contour interval 20 mGal. We did not incorporate the gravity information on land of the islands. This is indicated by the white band around the islands.

Free air anomalies

In the area around the Atlantis-Meteor seamount complex, indicated by the rectangle in Figure 5, the average track spacing is about 40 km. In some parts of the area, e.g. around 35°N, between 20° and 25°W the gravity information is scarce. The irregular data spacing make it difficult to define the cut-off wavelength used in the computer contouring. We used a cut-off wavelength of 80 km. Figure 6 gives the resulting gravity contours . We did not incorporate the gravity information on land of the islands.

The gravity contours show strong positive anomalies correlating with the topographic highs formed by the islands and the seamounts. Great Meteor seamount (30°N/ 28°30'W) has a positive gravity anomaly of more than 200 mGal. (N.B.: the amplitude of the anomaly has been reduced by the contouring.) To the north and to the south of Great Meteor seamount we find negative anomalies. Over the complex formed by Cruiser, Irving and Hyères seamounts (32°N/ 28°W) we also find a positive anomaly with an amplitude of about 100 mGal, significantly smaller than the one over Great Meteor seamount. The positive anomaly over the Cruiser, Irving, Hyères complex is completely surrounded by a negative anomaly with an amplitude up to -40 mGal. Plato seamount (33°N/ 29°30'W) and Atlantis seamount (34°N/ 30°W) both have positive gravity anomalies with amplitudes of 80 mGal. Tyro seamount (35°N/ 27°30'W) has a positive anomaly of 60 mGal.

To the east of the seamounts we find predominantly negative gravity anomalies, which further to the east change into the positive anomalies related to Madeira, the Madeira Torre Rise and the Canary Islands. To the south of the seamounts we also find an area with negative gravity anomalies. Here we note the general agreement with the change from positive to negative depth anomaly, already noted by Cochran and Talwani (1977 and 1978). In the northern part of the area we find the positive gravity anomalies related to the Azores. The greater part of the Mid Atlantic Ridge has a positive gravity anomaly.

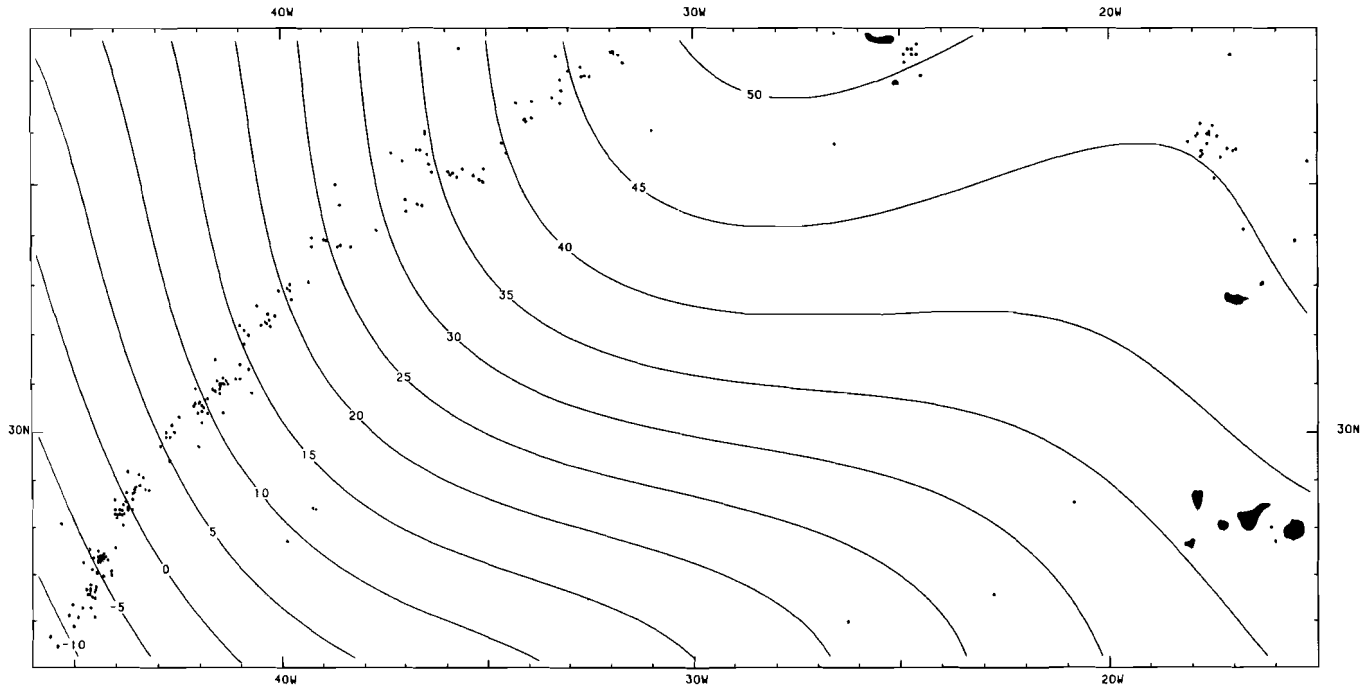

Figure 7: Geoid undulations. Contour interval 5m. Calculated from Gaposchkin (1980). Parameters used in the calculation are listed in table III.

At about 35°N we clearly see Oceanographer fracture zone and at about 30°N Atlantis fracture zone. The active parts of the other fracture zones, like Hayes fracture zone at about 34°N are hardly visible because of the scarceness of gravity data at those places (see Figure 5).

Correction for the indirect effect of geoidal anomalies

Gravity measurements on board of surface ships are by nature performed at sea-level. If we neglect the small deviations caused by sea-surface topography, the sea-surface corresponds with the geoid. We find the gravity anomaly from the observed value by a comparison with a reference value, viz. the normal gravity at the reference ellipsoid. If at the observation point the geoid differs in height from the ellipsoid, a correction must be applied (e.g. Chapman and Bodine, 1979). This correction consists of a term correcting the distance (free air correction) and a term, correcting the excess mass in the case of a positive geoid undulation, or for the mass deficiency in the case of a negative geoid undulation, between geoid and reference ellipsoid (a Bouguer correction). The total correction for a geoid undulation of N meter amounts to 0.2656*N mGal. This correction becomes important in regional studies.

TABLE III: Constants used for calculation of geoid-undulation

a_e	= 6 378 136 m	(equatorial radius)
G.M	= 3.986005 10^{14} m^3s^2	(M:earth mass, G:gravity constant)
f	= 1/298.255	(flattening)
w	= 7.29211514 10^{-5} rad/s	(angular velocity)
g_{eq}	= 978 034 mGal	(equatorial gravity)

We calculated the geoid undulations in the area of Figure 6 from the spherical harmonic coefficients of the geopotential given by Gaposchkin (1980). Figure 7 shows the undulations calculated with the parameters listed in Table III. The geoid undulations in this part of

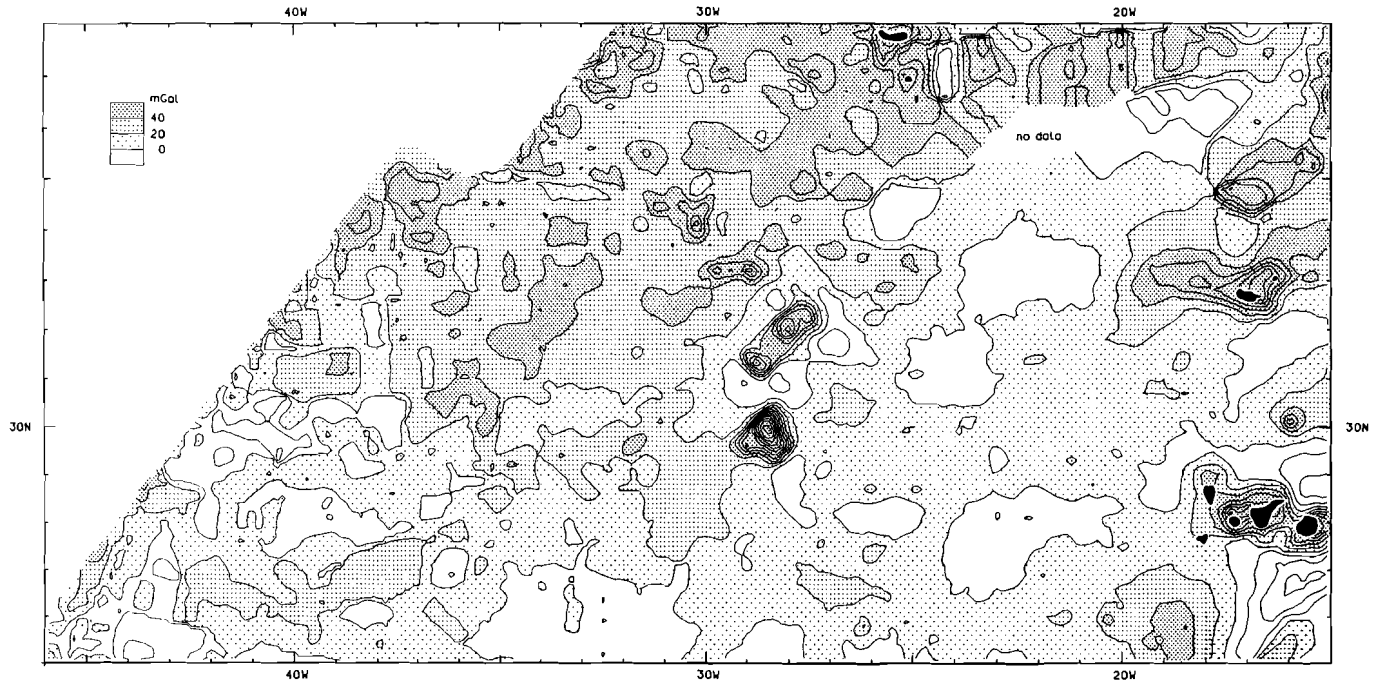

Figure 8: Gravity anomalies after correction for indirect effect and ridge effect (see text). Contour interval 20 mGal. Anomalies on the American plate are not shown.

the Atlantic vary from -10 m in the southwest to +50 m in the northeast. The corresponding indirect effect varies from about -2 mGal in the southwest to about +13 mGal in the northeast. We have corrected the free-air anomalies for this effect.

THE CORRECTIONS FOR TOPOGRAPHY

Correction for the ridge effect

In order to enable a direct correlation between gravity anomalies and depth anomalies, firstly we must correct the former for the gravity-effect of the Sclater-curve. Using 1°*1° averages Cochran and Talwani (1977) examined the empirical gravity-age relation. Their empirical curve has a value of about 20 mGal at the spreading center and decreases to about zero for ages larger than about 40 Ma. Using the structural pattern from Figure 3 we calculated the value of this ridge-effect.

Figure 8 shows the observed gravity anomalies after correction for the indirect effect and for the ridge effect. To the west of the Mid Atlantic Ridge we do not have accurate age determinations, so this part is not shown in Figure 8. The differences with Figure 6 can be found in a long wavelength trend caused by the indirect effect and a contribution from the ridge-effect in the first 400-500 km from the ridge-axis. The anomaly related to the Atlantis subgroup is no longer connected with the ridge anomalies and is now surrounded by relative lower gravity anomalies.

Correction for topography effects

The anomalies shown in Figure 8, inside the area defined when discussing Figure 1, i.e east of the Mid Atlantic Ridge, south of the East Azores fracture zone, west of isochrone M0 and north of 27°N will next be cleansed of topography effects.

For the determination of the gravity effect of topography it is necessary to choose a reference level. On land the geoid is often used as reference level. At sea, use of the geoid results in large positive Bouguer anomalies. In addition, when choosing a reference level at constant depth, the Mid-Atlantic Ridge will show by a strong trend, the topography effect of the Ridge being 150 to 200 mGal. In this study we took the Sclater-curve as a reference level. All topography less deep than predicted by this curve will give a negative correction, all deeper topography a positive one. This choice of reference level became possible, since we already corrected the observed gravity anomalies for the total ridge-effect, i.e. the effect of the topography of the ridge and of its compensation. This correction was realized by applying an empirical gravity age curve without specifying a compensation model for the ridge. By using the Sclater-curve as a reference level the compensation mechanism and the deviations of isostatic equilibrium of our study area can be studied independent of the processes which are active at the Mid-Atlantic Ridge.

For the calculations of the gravity effect of the topography we used a spherical earth model. We distinguished three cases:

-1) correction for topography close to the station (nearby correction). We calculated the nearby correction for topography inside a square with sides of 2.5 degrees around the station S, using 0.1°*0.1° averages for the mass above the reference level (Sclater-curve). The depth of an mass-element P was lowered to correct for the curvature of the earth (see Figure 9). The contribution of the element at P to the total correction in station S was calculated with the equations for the gravity effect of a paralellopiped (Talwani, 1973). To avoid edge effects we extended the area where necessary with topographic data used for the intermediate distance correction (see below).

-2) correction for topography at intermediate distance from the station. At larger distances between station S and mass-element P short wavelength variations in topographic relief only lead to small

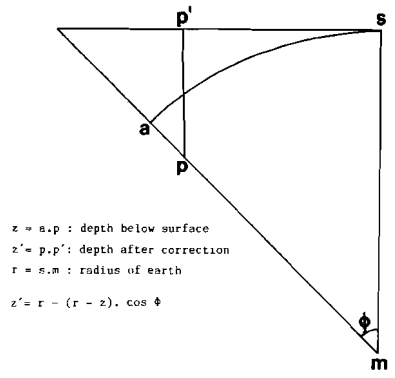

Figure 9: Depth corrections to account for the earth's curvature.

perturbations on the total correction. Now we can use larger elements. To avoid complications in the transition from small (0.1 * 0.1 degree) to larger (0.25 * 0.25 degree) elements we put the transition at a square with sides of 2.5 degrees around the station S. Outside this square up to and including Hayford zone 11, i.e a circle with radius 7°51' around station S we calculated the contribution of the topography using the mass-line formula from Kukkamaki (1955). In order to perform the topography corrections for all points S in the area around the Atlantis-Meteor seamount complex we must know the mass above the Sclater curve in a much larger area. From the VML data set (partly published, Collette et al, 1984) we calculated the corrected basement depth in the area 15°-46°N, 5°-55°W at a grid of 0.25 degrees. Areas with not enough data were interpolated using a two dimensional Gausian interpolation routine. We added heights for the African continent and the Iberian peninsula, as well as for the islands in the area. We used the identified magnetic anomalies from Collette et al (1984) supplemented with identifications from Perry et al (1981) to calculate the theoretical depth in the whole area.

-3) correction for topography farther away than Hayford zone 11 from the station, i.e. a distance of more than 7°51' (about 870 km). We added this correction later, together with the isostatic effect.

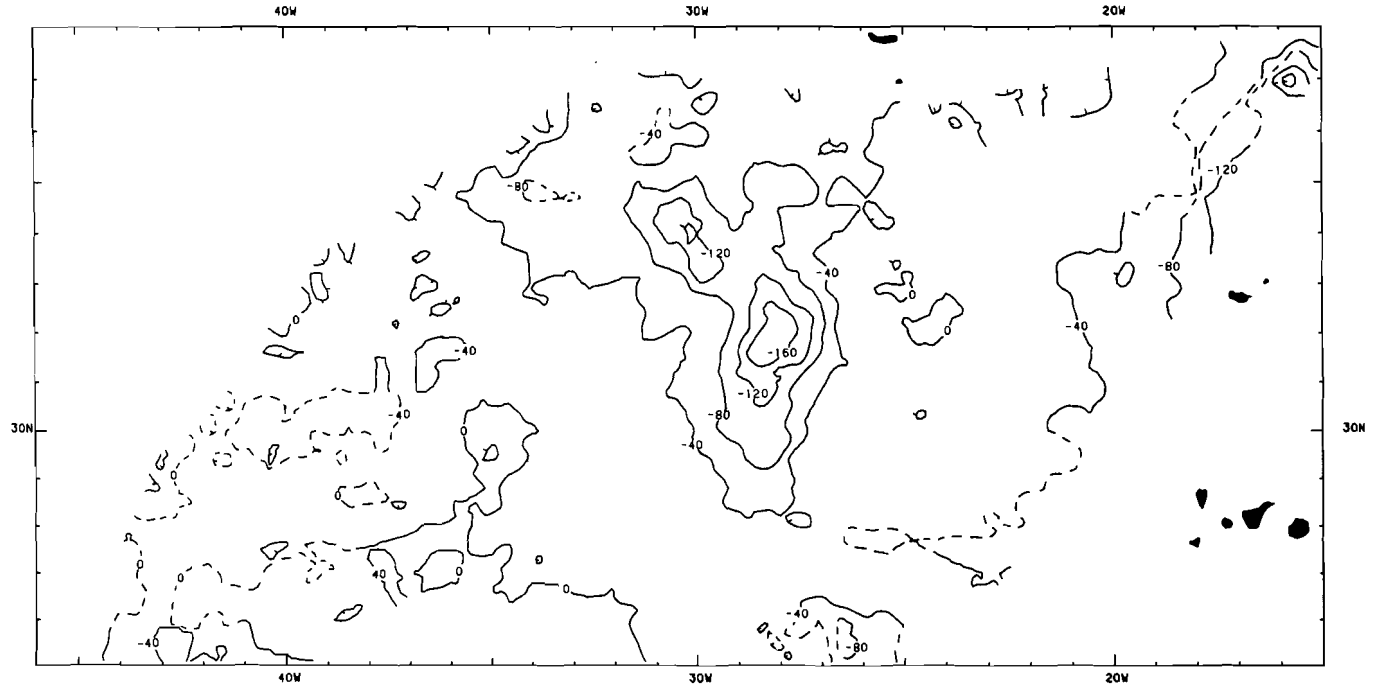

Figure 10: Gravity anomalies after correction for topography effect. Contour interval: 40 mGal. Dashed contours give places where correction is not accurate (scarce data).

The correction for the topography effects was done by assuming a density of 2.83 g/cm^3.

Residual anomalies

From the grid values giving the topography corrections we calculated profiles along the tracks with gravity data. We then calculated the residual, which was again contoured. Figure 10 gives the result. The seamount complex itself shows strong negative residuals, up to - 200 mGal. In the area around the seamount complex the residual is about -25 mGal. To the south, between 32° and 42°W we find positive residuals.

ISOSTATIC CORRECTIONS

Regional compensation

For the computation of the effect of isostasy we assumed regional isostatic compensation, after Vening Meinesz (1931). In this compensation system the topography constitutes a load on an elastic plate, which floats on a substratum. In order to calculate the flexure of an elastic plate for an arbitrary load we must know the response function of the system, i.e. the response of the elastic plate to a point load.

Flexure equation and solution for a point load

We consider an elastic plate, with thickness T, extending to infinite in the horizontal x and y directions. Take the positive z axis downward, with the origin in the middle of the plate, i.e. the upper side of the plate is at z= -T/2 and the lower side at z=+ T/2. The elastic plate floats on an incompressible fluid with density ρ_m. The response of the system on a load function p(x,y) will be w(x,y).

The basic equation for the flexure of the plate expresses the balance between the elastic forces, the buoyancy force and the load:

$$\nabla\cdot\nabla\, w(x,y) + 4\,\beta^4\, w(x,y) = p(x,y)/D \qquad (3)$$

with: $D = \dfrac{E.T^3}{12(1-\nu^2)}$ flexural rigidity (4)

E : Young's modulus

ν : Poisson ratio

$\nabla\cdot\nabla = (\partial^2/\partial x^2 + \partial^2/\partial y^2)^2$ biharmonic operator

$$4\beta^4 = \Delta\rho\, g/D \qquad (5)$$

g : acceleration due to gravity

$\Delta\rho$: density difference between the material below the elastic plate (ρ_m) and the material filling the moat caused by flexure (ρ_f).

In this definition β has as dimensions reciprocal distance (Vening Meinesz, 1931 uses $l^4 = 1/4\beta^4$,Walcott ,1970 $\alpha = 1/\beta$).

Several solutions to equation (3), using different load functions p have been given: e.g. Hertz (1884), Vening Meinesz (1941), Gunn(1943), Jeffreys (1959), Nadai (1963), Walcott(1970), Watts et al (1975), McNutt and Menard (1978) and Lambeck and Nakiboglu (1980). Most of the more recent flexural studies use two- dimensional load functions (e.g Watts and Cochran, 1974) or rotation symmetric load functions (e.g. McNutt and Menard, 1978; Lambeck and Nakiboglu, 1980). Watts et al (1975) used the series representation of the three-dimensional point load solution of Hertz (1884). They computed the flexure caused by the real topography of Great Meteor seamount.

We will use an equivalent form of the Hertz solution, now expressed in the zero order Kelvin function Kei, and convolve this solution with the load function formed by the seamount topography. The convolution will be performed in the Fourier domain.

In the case of a rotation symmetric load function, i.e. a disc load ($p(r)=p$, $r \leq A$ and $p(r)=0$, $r > A$, with A the radius of the disc),

and the boundary conditions: 1) flexure w and dw/dr finite under the center of the load, 2)flexure w and dw/dr continuous at edge of the load, 3) moments and stresses continue at edge of the load, 4) flexure w and 1/r dw/dr go to zero for r goes to infinite, the solution to (3) takes the form (e.g. McNutt and Menard, 1978; Lambeck and Nakiboglu, 1980):

$$\begin{aligned} w &= w_p.\{\ 1 + a.Ker'(a).Ber(\sqrt{2}\beta r) - a.Kei'(a).Bei(\sqrt{2}\beta r)\} \qquad r \leqq A \\ &= w_p.\{\ a.Ber'(a).Ker(\sqrt{2}\beta r) - a.Bei'(a).Kei(\sqrt{2}\beta r)\} \qquad r \geq A \end{aligned} \tag{6}$$

$$\text{with: } w_p = p/(4\beta^4 D)$$
$$a = \sqrt{2}\ \beta\ A \tag{7}$$
$$Ker'(a) = \{\ \partial/\partial x\ Ker(x)\}_{x=a}$$

the functions Ber, Bei, Ker and Kei are zero order Kelvin functions.

The solution for a point load follows from (6) by taking the limit of A to zero and keeping the load finite. The result is:

$$w(r) = -\frac{\beta^2 p}{\pi \Delta\rho g}\ .\ Kei(\sqrt{2}\ \beta r) \tag{8}$$

The maximum deflection occurs under the point load (r=0). With Kei(0)= $-\ \pi/4$ (Abramowitz and Segun, 1965) we find:

$$w(0) = \frac{\beta^2 p}{4\ \Delta\rho g} \tag{9}$$

An elegant solution of (3) for a point load, using zero order Hankel transforms, is given by Beaumont (1978).

Using an integral representation for the Kelvin function Kei(x) (e.g. Gradhsteyn and Ryzhik, 1965, point: 6.537) it can be shown, that the solution (8) is equivalent to:

$$w(r) = \frac{\beta^2}{\pi\Delta\rho g} \int_1^{\infty} \frac{e^{-\beta rt} \sin(\beta rt)}{(t^2 - 1)^{\frac{1}{2}}} \, dt \qquad (10)$$

This is the solution given by Hertz (1884). Note that in the original Hertz paper there is a misprint, an extra factor $\frac{1}{2}$, in his formula (2) (see also Beaumont, 1978 and Withjack, 1979).

We found with (8) the solution for the flexure of an elastic plate under a point load. The flexure of the plate under an arbitrary load can be found by the convolution of (8) with the load function.

Application of point load solution to an arbitrary load

Consider an arbitrary load with amplitude P(x,y), defined inside an area B. The flexure in an arbitrary point Q caused by the load P(x,y) will, in the case of a linear system, be given by the convolution of the response of the elastic plate to a point load (equation 8) with the load function P(x,y). If the load function P(x,y) is assumed to be zero outside the area B we can perform the convolution in the Fourier domain.

The procedure in the flexure calculations is as follows: first we calculate the solution (8) at grid points. We choose the origin in the center of the area. The Kelvin function Kei(x) is calculated from the polynomal approximations given by Abramowitz and Segun (1965, point: 9.11.4) for values of the argument smaller than 5. For larger values of the argument we use the asymptotic development of the function (Abramowitz and Segun, 1965, point: 9.10.4). Using standard 2D-FFT routines we obtain the Fourier transform of the point load solution which we correct for the shift of the origin.

The determination of the load in the case of a seamount is complicated by the fact that the deflection or moat around the base of the seamount is usually filled in by sediments and/or volcanic debris. If we only take the visible part of the seamount (see Figure 11) we underestimate the load. This problem can be solved if we assume that

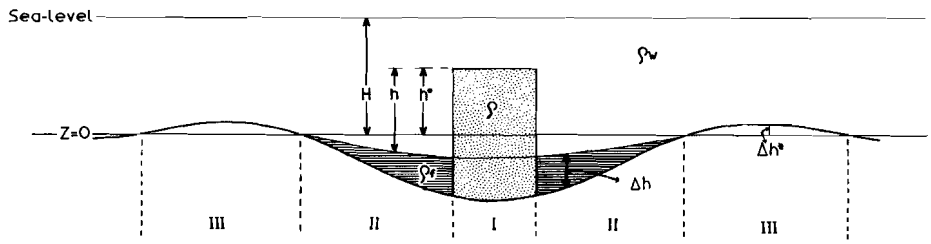

Figure 11: Illustration (not to scale) explaining the constants and the different areas used in the flexure calculations.

the density of the fill-in is equal to the density of the load. We follow Lambeck (1981):

Consider a cylindrical seamount with density ρ (Figure 11). The moat around the base of the seamount is filled in by material of density ρ_f up to a level Δh, which we take proportional to the deflection: $\Delta h = \alpha.w$. The load function now consists of three parts:

area I: within the area of the topographic feature

$$P_I = g\rho(h + \alpha w) + g\rho_w(H-h^*) \qquad (11)$$

area II: area outside topographic feature

$$P_{II} = g\rho_w\{H + (1 - \alpha)w\} + g\alpha w\rho_f \qquad (12)$$

area III: area with negative deflection (=uplift)

$$P_{III} = g\rho_w(H + w) \qquad (13)$$

With Lambeck we ignore the fact that the deflection again changes sign further away from the seamount, because here the deflections have become very small. The constant load $g\rho_w H$ results in a uniform

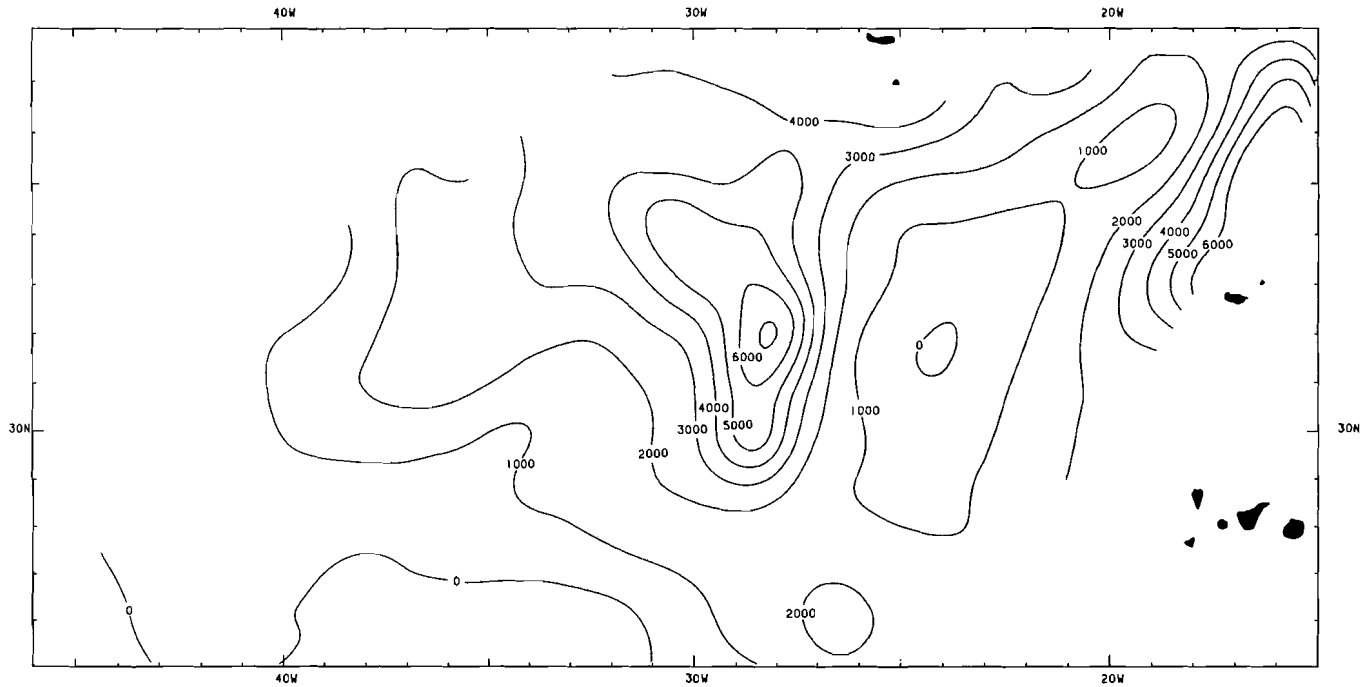

Figure 12: Deflection calculated for a plate thickness of 20 km. Contour interval 1000 m. The load is formed by all topography deviating from the Sclater curve.

compression and can be subtracted. We assume $\rho_f = \rho$ and $\alpha = 1 + \Delta h^* / w$, i.e. the fill-in continues up to the level of maximum uplift (Figure 11). With these assumptions we find:

area I: $$\nabla \cdot \nabla w + 4\beta^4 w = gh(\rho - \rho_w)/D \quad (14)$$

areas II and III: $$\nabla \cdot \nabla w + 4\beta^4 w = 0 \quad (15)$$

with: $$4\beta^4 = g(\rho_m - \rho)/D \quad (16)$$

In the above derived equations we correct for the load caused by the fill-inn and that part of the seamount below level Δh^* by an appropriate choice of the flexural parameter β.

In this study we chose the Sclater curve as the reference level instead of the seafloor. Topography deviating form the Sclater curve constitutes a load with amplitude:

$$P(x,y) = \rho' \, g \, h(x,y) \quad (17)$$

with: $\rho' = \rho - \rho_w$: relative density of load with respect to seawater.

$h(x,y)$: deviation of topography from Sclater-curve, i.e. depth anomaly.

Result flexure

Figure 12 shows the flexure of the elastic plate due to the load formed by the deviations from the Sclater-curve. The flexural rigidity in Figure 12 is $D = 5.7\ 10^{22}$ Nm, which with a Young's modulus $E = 8.\ 10^{10}$ N/m^2 and a Poisson ratio $\nu = .25$, corresponds with a plate thickness of 20 km. The load density was taken at 2.83 g/cm^3 and for the density contrast between material below the plate and the infill we took $\Delta\rho = 0.6$ g/cm^3. This indicates that we assumed the infill to consist of material with the same density as the load.

Figure 12 shows that the flexure increases to about 7 km under the center of the seamounts. We do not find separate maxima in the deflection under the different seamounts. This is caused by the high value of the flexural wavelength (= $2\pi/\beta$), which is about 495 km. To the south, between 31° and 40°W, there is an area with a negative flexure (= uplift). Another area with negative flexure can be found at 31°30'N/24°W. These areas indeed have a negative depth anomaly. The flexure is more than 1 km over a large area. This is caused by the fact that we took the total mass above the Sclater-curve as a positive load. This results in a load with a long wavelength for which the elastic plate has no resistance and which results in a change of level (= constant flexure).

Gravity effect of flexure

From the flexure given in Figure 12 we calculate the gravity effect. We assume that the normal density contrast is at 10 km below sealevel (see Figure 13). We now lower the flexural values to this

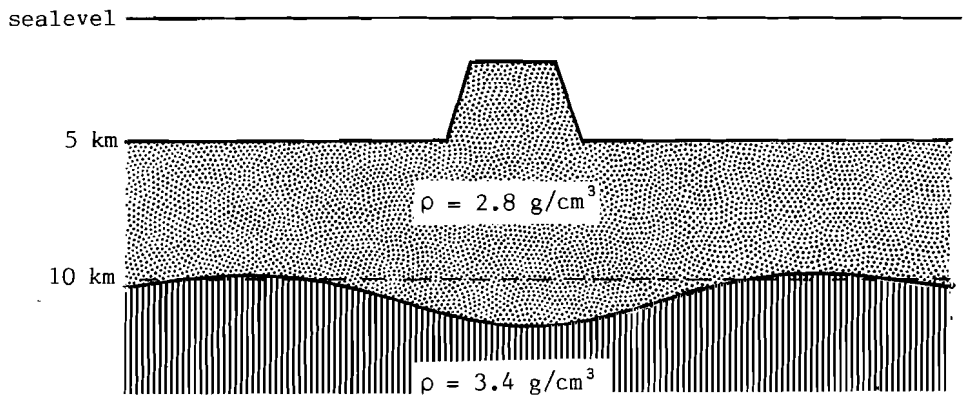

Figure 13: Illustration (not to scale) showing the density contrast which causes the gravity effect of flexure.

depth (density contrast -0.6 g/cm^3). The calculation of the gravity effect of flexure is analogous to the above described method for the topography corrections.

Contribution of Hayford zones 1-10

We have calculated for every point the gravity effect of all the topographic deviations from the Sclater-curve and the isostatic effect of the same deviations, assuming a regional compensation system. The corrections were calculated up to and including Hayford zone 11, i.e. inside a circle with a radius of 7°51' around the point. The contribution of the topography and its compensation outside this Hayford zone can be found in the topographic-isostatic maps of Niskanen and Kivioja (1951). These maps give the contribution assuming an Airy-Heiskanen compensation system. As the value for this contribution for a regional compensation system differs only slightly from the one for an Airy-Heiskanen system (Vening Meinesz, 1941) we used it in our study.

In the area around the Atlantis-Meteor seamount complex, Niskanen and Kivioja (1951) give, assuming a standard crustal thickness of 30 km, values ranging from -6 mGal in the western part to -5 mGal in the eastern part of the area. For a standard crustal thickness of 20 km the contribution changes to -4 mGal. We took the contribution for the standard crustal thickness of 30 km and because of the small variation over the area added -6 mGal to the isostatic effect.

Isostatic anomalies

We find the isostatic anomaly after correcting the residual anomalies, given in Figure 10, for the isostatic effect. Figure 14 shows the result. We eliminated the short wavelengths in Figure 14 by applying a two dimensional running mean procedure with a Gausian weight function (halfwidth: 55 km). The eliminated short wavelength anomalies have amplitudes between -10 and +10 mGal and are randomly

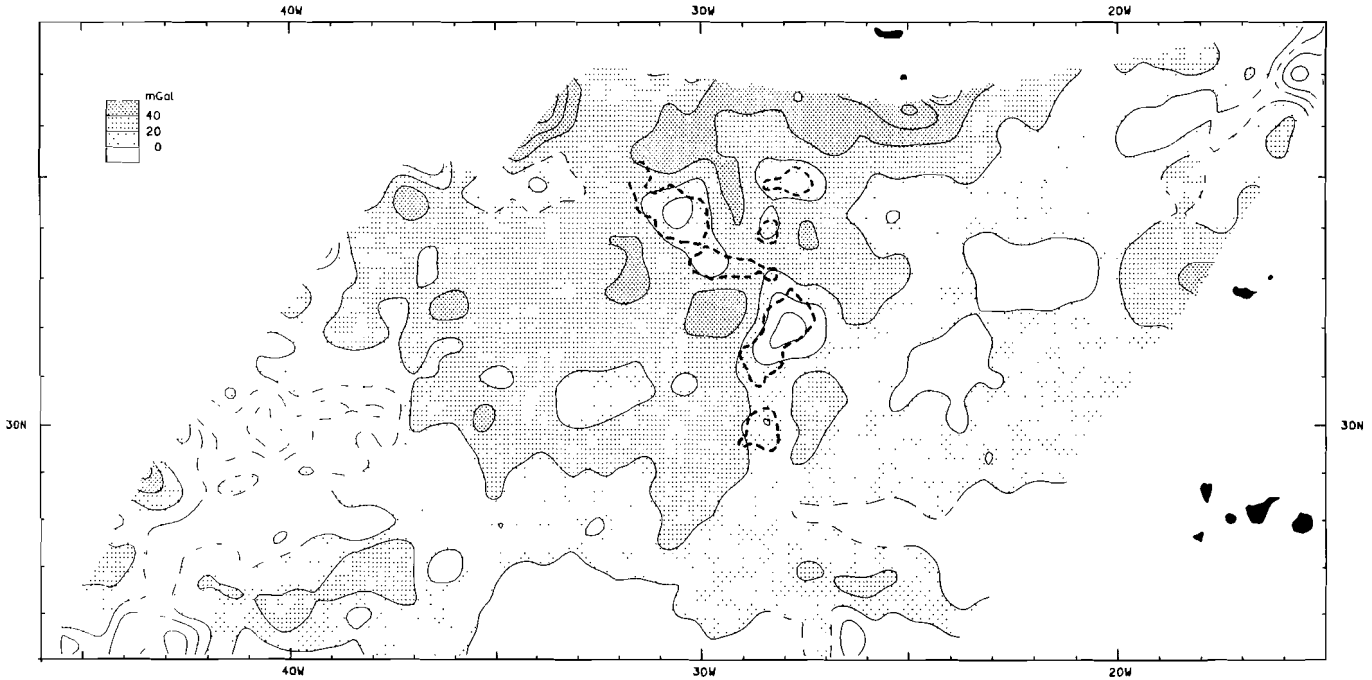

Figure 14: Isostatic anomaly for a plate thickness of 20 km. Contour interval: 20 mGal. Heavy dashed lines indicate the 3000 m corrected basement depth from Figure 2. Dashed contours give places where isostatic anomaly is not accurate (scarce data).

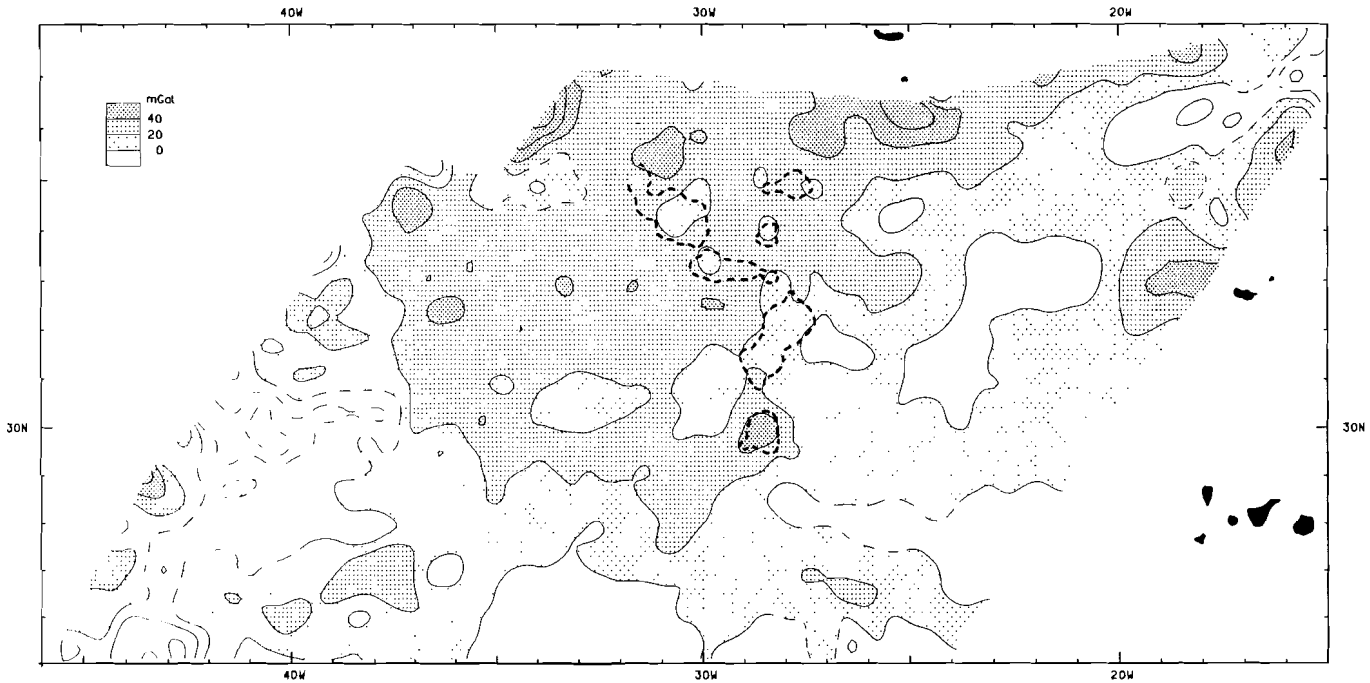

Figure 15: Isostatic anomaly for a plate thickness of 10 km. Contour interval: 20 mGal. Heavy dashed lines indicate the 3000 m corrected basement depth from Figure 2. Dashed contours give places where isostatic anomaly is not accurate (scarce data).

distributed over the area.

The central part of Figure 14 shows a regional positive isostatic anomaly with an amplitude of more than 20 mGal. The isostatic anomaly over Great Meteor seamounts has about the same value as the regional. All other seamounts clearly show a local minimum in the isostatic anomaly. This indicates that the assumed flexure is too small. Therefore we again calculated the isostatic correction for a flexural rigidity D= 7.1 10^{21} Nm, which is equivalent with a plate thickness of 10 km. Figure 15 shows the isostatic anomalies for this plate thickness.

Great Meteor seamount shows as a local maximum in the isostatic anomaly. Over the complex formed by Cruiser, Irving and Hyères seamounts the isostatic anomaly is close to the regional value, but the anomaly to the east of this complex has become negative. The western part of Plato seamount shows as a relative minimum in the isostatic anomaly, as well as Unnamed seamount and Atlantis seamount. The relative minima in the isostatic anomaly close to Tyro seamount are located outside the 3000 m contours of the seamount, i.e. on the flanks of the seamount.

Figure 16A shows the seamounts Atlantis, Plato and Unnamed in more detail with a contour interval of 10 mGal and still with a plate thickness of 10 km. Figure 16B gives the isostatic anomaly for an elastic plate thickness of 7 km (D= 2.4 10^{21} Nm). The larger part of the relative minimum in the isostatic anomaly over Atlantis seamount has now disappeared. Over the western part of Plato seamount we still have a local minimum in the isostatic anomaly. However more to the east the isostatic anomaly over Plato seamount increases to more than 40 mGal. Because gravity data over the western part of Plato seamount are scarce (see Figure 5) it is difficult to estimate the elastic thickness for this part of the seamount. Over Unnamed seamount we find with a plate thickness of 7 km a relative minimum in the isostatic anomaly. The position of this minimum has shifted towards the flanks of the seamount.

The relative minima in the isostatic anomaly which are located on

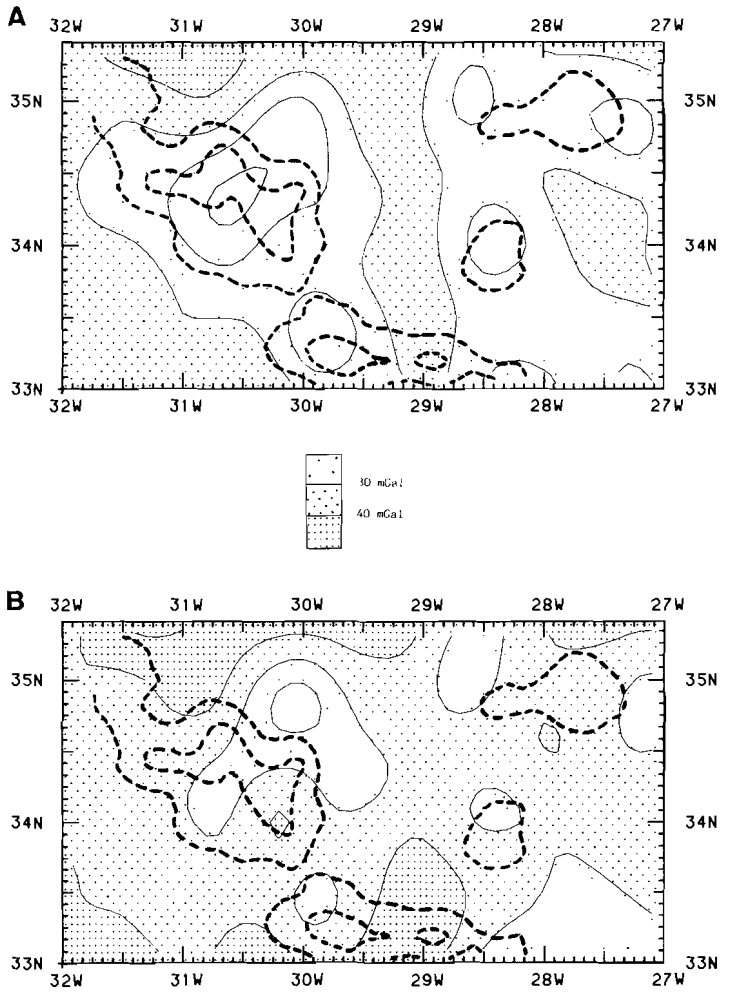

Figure 16: Isostatic anomaly around the Atlantis subgroup. Contour interval: 10 mGal. Heavy dashed lines indicate 2000 and 3000 m corrected basement depths from Figure 2. A): plate thickness 10 km; B): plate thickness 7 km.

the flanks of the seamount indicate that the isostatic effect is too high at these places. We took the value for the elastic plate thickness for which these minima appear as an estimate for the correct plate thickness under the seamount.

The isostatic anomaly in the area around the seamount complex is predominantly positive with an amplitude of more than 20 mGal (see Figures 14 and 15). The southern part of the area in general has a negative isostatic anomaly. Near Madeira and the Madeira Torre Rise we again have positive isostatic anomalies. In the western part of the area, between 27° and 31°N we find negative isostatic anomalies.

The results of the calculations of the isostatic anomaly can be resumed as follows: the elastic thickness under Great Meteor seamount is about 20 km (compare Figures 14 and 15). The resulting plate thickness agrees with the one found by Watts et al (1975), as could be expected, because their gravity data forms part of our data set from Figure 5. Under the complex formed by Cruiser, Irving and Hyères seamount we found an elastic thickness of 10 km. For Tyro seamount we find an elastic thickness of 10 km. The elastic thickness under Plato seamount is difficult to determine. Under the eastern part of this seamount a thickness of 10 km gives good results (Figure 15). Under the western part of this seamount a thickness of 7-10 km is needed. Unnamed seamount, as well as Atlantis seamount give a thickness of 7 km.

Age of seamounts

We calculated the elastic thickness of the lithosphere under the different seamounts. The results of several flexural studies lead to the suggestion, that the effective elastic thickness of the oceanic lithosphere increases with increasing age (e.g. Watts, 1978; Watts et al, 1980; Cazenave et al, 1980; Bodine et al, 1981; McNutt and Menard, 1982). When plotted as a function of lithospheric age the estimates of effective elastic thickness lie between the 300 and the 600° isotherm, calculated for a thermal plate model. Bodine et al (1981) suggested

that the relation between the effective elastic thickness (T_e) and the age (t) of the lithosphere for loads in the interior of the plate may be approximated by: $T_e = a.\sqrt{t}$ where *a* denotes a constant with a value dependent on the rheology. These authors found an overall fit with the observations for $a = 3.1 \pm 0.5$ (N.B. we corrected the value of *a* given by Bodine et al, 1981, for the different Young's modulus used in our study).

We calculated the ages of the seamounts of the Atlantis-Meteor complex (Table IV) using the above described relation between lithospheric age and elastic thickness of Bodine et al (1981). The result shows that there is no clear age migration pattern in the volcanism. The age of the Cruiser complex is higher than the age of the other seamounts.

TABLE IV: Age of seamounts

seamount:	age of oceanfloor*:	elastic thickness:	age of seamount:
Great Meteor	84 Ma	20 km	42 Ma
Cruiser complex	76 Ma	10 km	65 Ma
Plato (east)	58 Ma	10-15 km	34-47 Ma
Unnamed	55 Ma	7 km	48 Ma
Tyro	53 Ma	10 km	42 Ma
Plato (west)	52 Ma	7-10 km	41-47 Ma
Atlantis	43 Ma	7 km	38 Ma

*: age under center of the seamount.

Long wavelength anomalies

When discussing the isostatic anomalies in the area around the Atlantis-Meteor complex we described a regional positive anomaly. This suggests that the longer wavelengths of the anomalous depth are compensated at a deeper level. We examined the relation between the gravity anomalies and the corrected basement depth as a function of

the wavelength. For this we used the cross spectral or admittance technique. This method was developed by Dorman and Lewis (1970, see also Lewis and Dorman, 1970). The method was first applied to oceanic areas by McKenzie and Bowin (1976). These authors used a two-dimensional model. Three dimensional models, using contour charts in stead of profiles, were used by McNutt (1979) in the northeastern Pacific (Surveyor area) and by Sandwell and Poehls (1980) in the central Pacific.

Assuming that isostatic compensation is isotropic, the linear part of the relation between the gravity anomalies (G) and topography (T) in the wavenumber domain is given by (e.g. McNutt, 1979):

$$G(\vec{k}) = Z(k).T(\vec{k}) + I(\vec{k}) \qquad (18)$$

with k: wave number, $|\vec{k}| = (k_x^2 + k_y^2)^{\frac{1}{2}} = k$

$G(\vec{k})$ is the 2-D Fourier transform of the gravity. The part of the gravity anomalies, linearly related to the Fourier transform of the topography ($T(\vec{k})$) is given by: $Z(k).T(\vec{k})$. The part of the gravity anomalies which does not correlate, on the average, with the topography is $I(\vec{k})$. The assumption that the compensation is isotropic makes the admittance Z only a function of the amplitude of the wavenumber k.

By minimizing the sum of $I(\vec{k})$ squared the best estimate of the admittance or transfer function is given by (e.g. Sandwell and Poehls, 1980):

$$Z(k) = \mathrm{Re}\left(\frac{< G.T^* >}{< T.T^* >}\right) \qquad (19)$$

with T*: complex conjugate of T. The averaging, denoted by <>, is done over an annulus of width δk in the wave number domain. An estimate for the uncertainty in the transfer function is:

$$\sigma^2(k) = \frac{1}{2n - 1}\left\{\frac{< G.G^* >}{< T.T^* >} - Z^2(k)\right\} \qquad (20)$$

with n:number of complex numbers within the averaging interval.

We must perform the 2-D Fourier transform of the gravity anomalies and, in our case, of the corrected basement depth. Since we want to study the relation between the gravity anomalies and the topography for the longer wavelengths we took averages of 1°*1° of the observed gravity anomalies (Figure 6) and of the corrected basement depths (Figure 2) in the area 25°-37°N/22°-34°W. A best fitting plane was subtracted from both data sets and a cosinus taper applied. Figure 17 shows the admittance. We calculated the theoretical curves from the expressions of Karner (1982). The average depth was taken at 4.5 km, the thickness of the oceanic layer 5 km. Figure 17 shows that for wavenumbers larger than about .007 km^{-1} (wavelengths shorter than 900 km), the admittance closely follows a plate model curve, with a plate thickness of 10-12 km. For wavelengths larger than 900 km the admittance is higher than expected for a plate model. Here it seems

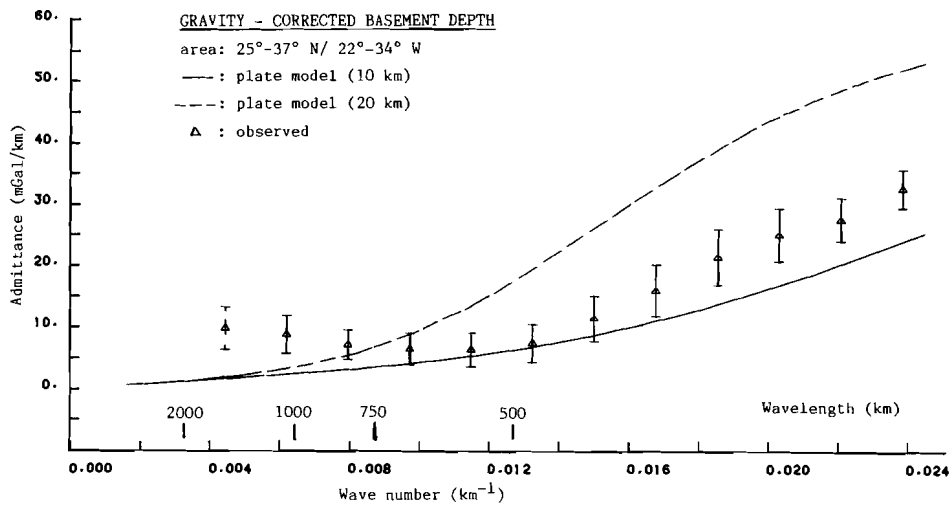

Figure 17: Admittance for wavelengths larger than 250 km. We plotted the observed values and the standard deviations (see text), together with theoretical curves for the plate model. Value with dotted standard deviation is only tentative.

that the compensation is situated at a deeper level. Our area is not large enough to get a good estimate of the depth of the compensation for these long wavelengths.

The theoretical admittance functions for a plate model given in Figure 17 are first order approximations. At places with high topographic relief, higher order terms might become important. We calcultated the effect of second order terms for a disc-shaped load. The results indicate that neglecting second order terms lead to a underestimation of the plate thickness in the wavelength band given in Figure 17. Thus the plate thicknesses as obtained from admittances are higher than those needed in the direct modelling, where we used 10 km for most of the seamounts. However Great Meteor seamount with a plate thickness of 20 km is also included in the area from which we calculated the admittances. The gravity anomaly over this seamount is the dominant feature in the area (see Figure 6), while its topographic expression is smaller than that over the Cruiser complex (see Figure 2). Thus the admittance being the quotient of the gravity and the bathymetry might be elevated over the whole wavelength band. In chapter 5 (Figures 1A and 1B) we show the depth anomaly and gravity anomaly of the area for wavelengths larger than 500 km. Even for these long wavelengths the gravity anomaly over Great Meteor remains the dominant feature in the area.

Geoid

From the available gravity data in the area around the Atlantis-Meteor seamount complex we calculated a detailed geoid . This was done with a method already used in several studies: e.g Talwani et al (1972) in the western North Atlantic, Kahle and Talwani (1973) in the Indian ocean, Watts and Leeds (1977) in the northwest Pacific, Albuisson et al (1979) and Chapman and Talwani (1979) in the North Atlantic. The geoid undulations are calculated from the Stokes formula (e.g. Heiskanen and Moritz, 1967). As the integration in this formula must be performed over the whole earth, the gravity anomalies must be

known all over the surface. In the area, where we want to calculate the detailed geoid, the gravity anomalies are given as .1°*.1° averages (see Figure 5). We assume, that the gravity anomalies outside this area are given by a spherical harmonic development of the geopotential complete to certain degree and order (e.g Lerch et al, 1979 ; Gaposchkin, 1980). The construction of the detailed geoid is made in six steps (e.g. Kahle and Talwani, 1973):

-1)calculation of 0.1°*0.1° averages (see Figure 5).

-2)calculation of free-air anomalies from the chosen spherical harmonic development: long wavelength gravity.

-3)the difference between 1) and 2) gives the short wavelength anomalies.

-4)from 3) we calculate the geoid undulations.

-5)from the spherical harmonics development we calculate the long wavelength geoid undulations.

-6)the summation of the results from 4) and 5) gives the detailed geoid.

As a long wavelength geoid we used the spherical harmonic development complete to order and degree 180 based on surface gravity data, altimeter data and other data (Rapp, 1981). The detailed geoid was calculated at a grid of 0.5° (Figure 18). Superimposed on the long wavelength trend of the geoid are local anomalies caused by the seamounts and the islands. Great Meteor seamount gives a geoid anomaly with an amplitude of about 12 m. The other seamounts have smaller geoid anomalies up to about 5 m.

Relation between geoid and topography

The relation between the geoid anomalies and the topography was studied for the longer wavelengths. Wavelengths shorter than the value corresponding with the spherical harmonic of degree 180 (wavelength 222 km) are calculated from the gravity data of Figure 5 and do not give new information. A comparative study of a detailed geoid based on the Gaposchkin (1980) long wavelength field (complete to order and

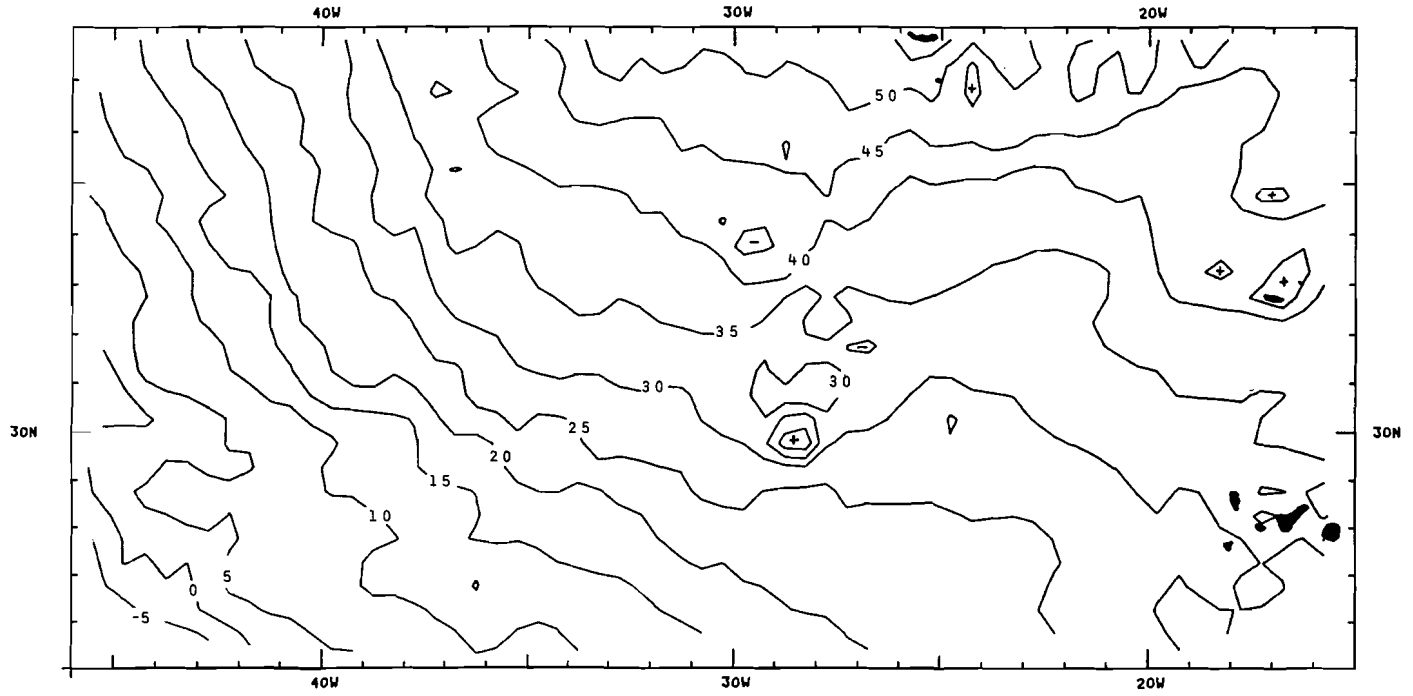

Figure 18: Detailed geoid. Contour interval 5m. The undulations are based upon the coefficients of the spherical harmonic development of the geopotential of Rapp (1981), together with the short wavelength undulations obtained from the surface gravity data in the area.

degree 30) and a detailed geoid based on the 180-field (Rapp, 1981) is in preparation (Verhoef and Van Es, in prep.).

The geoid undulations (N) and the corrected basement depths are compared using the cross-spectral method. We again calculated 1°*1° averages, following the same method as described above for the gravity anomalies. Figure 19 gives the resulting admittances, together with the theoretical curves for a plate model. We calculated these theoretical curves from those obtained for the gravity using the relation between geoid- and gravity admittances given by Chapman (1979, see also Watts, 1979). For wavenumbers larger than about .01 km-1 (wavelengths smaller than 630 km) the admittance follows a plate model with a thickness of 10-12 km. For the longer wavelengths we find, in agreement with the gravity results, an indication for a deeper compensation.

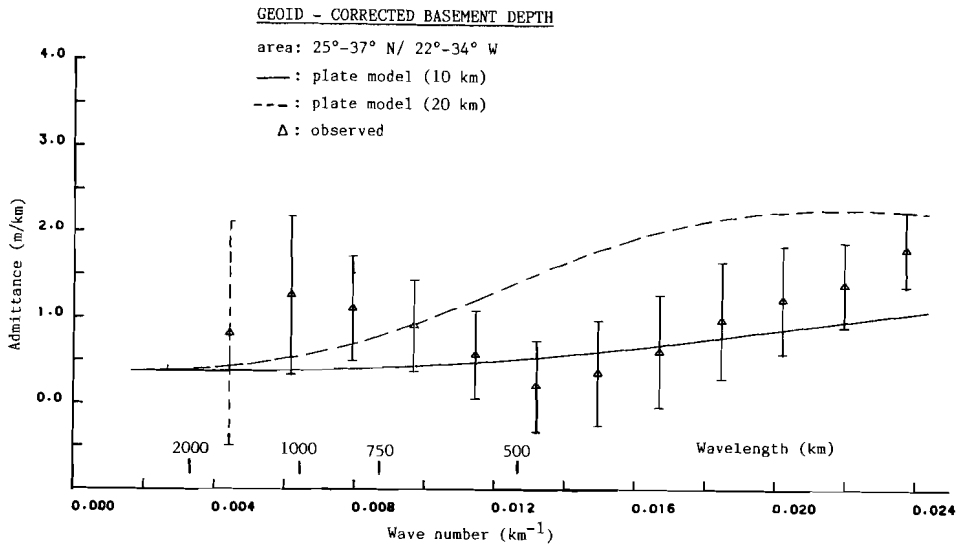

Figure 19: Admittance for geoid anomalies. We plotted observed values with standard deviations together with theoretical curves for a plate model. Value with dotted standard deviation is only tentative.

Conclusion

The calculation of the depth anomaly in the area around the Atlantis-Meteor seamount complex revealed that this area has a positive depth anomaly, i.e. the area is too shallow in terms of the depth-age curve given by Parsons and Sclater (1977).

From the gravity data we calculated the flexural rigidity under the seamounts as well as the isostatic anomaly in the area. The isostatic anomaly in the area around the seamounts is predominantly positive. The relation between the elastic thickness and age of the oceanic lithosphere, as originally proposed by Watts (1978, see also Watts et al, 1980) and elaborated by Bodine et al (1981), was used to obtain age estimations for the seamounts. The results make it unlikely that the seamounts originated on the Mid-Atlantic Ridge. A possible exception is formed by the Atlantis subgroup, whose elastic thickness suggests formation close to or on the spreading center. We do not find a clear age migration pattern for the volcanism. The age of the Cruiser complex is clearly larger than that of the other seamounts.

The relation between the long wavelength gravity anomalies and the bathymetry shows that the compensation closely follows a plate model. There are indications that the longest wavelengths are compensated at a deeper level. This result is sustained by the geoid anomalies.

CHAPTER IV

THE SEDIMENTATION PATTERN AROUND THE ATLANTIS-METEOR SEAMOUNT COMPLEX: A MODEL STUDY

Introduction

In this chapter we will investigate the sedimentary history of the area around the Atlantis-Meteor complex. An important aspect in this study forms the presence of a strong acoustic reflector, which is semi-opaque to opaque and which is often found in the surroundings of volcanic complexes (c.f. Collette et al, 1969; Laughton, Berggren et al, 1972; Tucholke, 1979). The thickness of the sediment above and below the acoustic reflector, as well as the total sediment thickness, will be given in the form of isopach maps. The sedimentary pattern around the Atlantis-Meteor seamount complex turned out to be related to the depth anomaly in terms of a depth dependent carbonate sedimentation.

The data

Figure 1 gives the tracklines in the area around the Atlantis-Meteor seamount complex. Until mid 1978 the Lamont air-gun was used as the seismic source (Ewing and Tirey, 1961), later on a 20 or 40 cu inch Bolt Par air-gun (Giles, 1968). During the 1980 expedition also a watergun was used (Sodera, 1979).

Figure 1 also gives the depth contours. The area around the seamounts (29°-35°30'N/ 25°-32°W) was contoured by hand, the remaining part by computer. The depth contours show the Atlantis-Meteor seamount complex as a general rising of the seafloor. To the north between 24° and 27°W this topographic high passes into the Azores. The regional NE-SW course of the depth contours (parallel to the Mid-Atlantic ridge) shows in the eastern part of the area. A description of the individual seamount groups can be found in chapter II.

We also indicated DSDP sites 137 and 138. DSDP site 136 is situated north of Madeira at about 34°N/ 16°W, i.e. outside the area shown in Figure 1. Other DSDP sites in the area are 332-335 and 411-413 close to and on the Mid-Atlantic Ridge in the FAMOUS area near 37°N. For a description of the sedimentary history around the

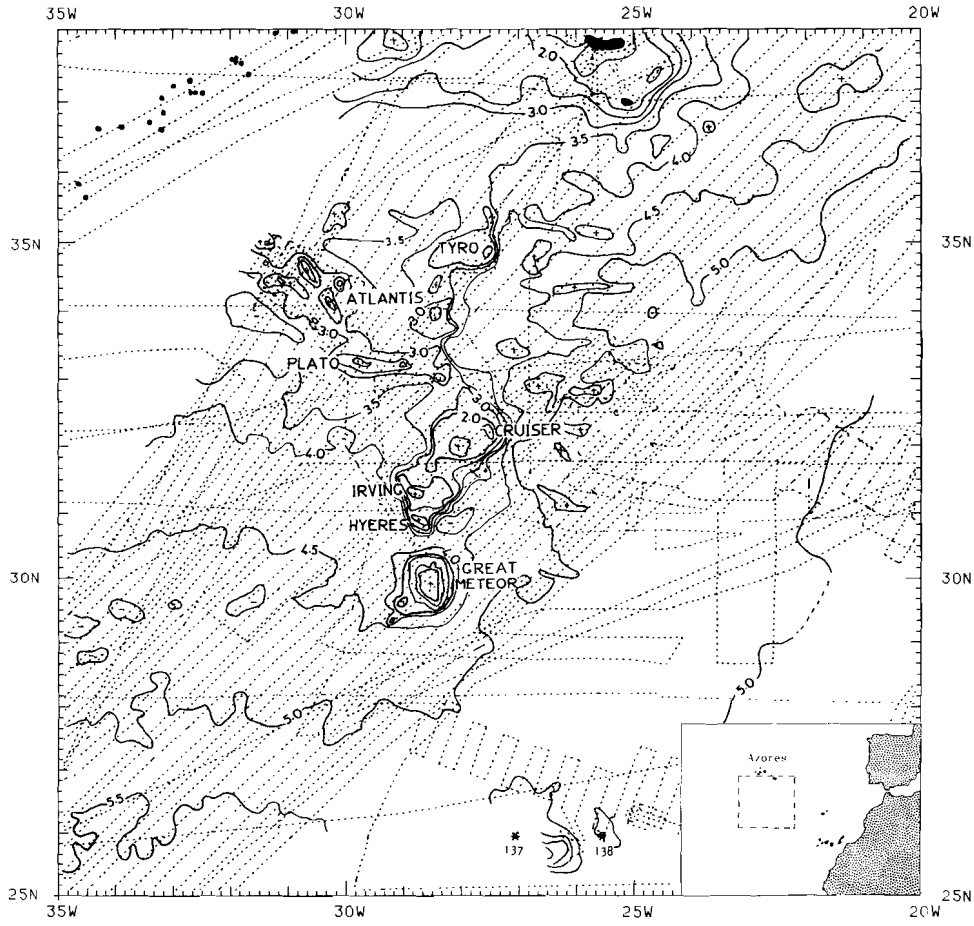

Figure 1: Contoured bathymetry in uncorrected kilometers together with the majority of the tracklines. Contour interval is 0.5 km. Because of the steep slopes an interval of 1 km was used for the areas shallower than 3 km. Dots in the northwestern part of the area denote earthquake epicenters. DSDP sites 137 and 138 are marked with an asterix.

seamounts these latter sites are of little use. The same is true for sites 136, 137 and 138 (Hayes, Pimm et al, 1972). The acoustic reflectors identified at these sites can not be followed into the seamount area. Dating of the strong acoustic reflector in this way therefore is not possible.

Volcano-clastic layer

In the area around the Atlantis-Meteor seamount complex and also to the north near the Azores, we find a strongly reflecting layer. The intensity of the reflections of this layer is often higher than of the oceanfloor. Reflectors of this type have been found at several places in the North Atlantic ocean, usually close to volcanic seamount complexes and volcanic islands. Collette et al (1969) found a reflective layer to the south of the island Sal (Cape Verde islands). They supposed that this strong reflector represents lava sheets interbedded in the sediments. At DSDP site 368, situated on the Cape Verde Rise diabase sills were found. These sills form a strong and discontinuous reflector on the seismic records (Lancelot, Seibold et al, 1977).

In the Iceland Basin, about 550 km to the south of Iceland, a strong acoustic reflector was found, which exceeds the seabed in strength. This reflector acts as an acoustic screen and obscures the deeper sediment horizons. At site 115 this layer was drilled and appeared to consist of indurated hyaloclastic volcanic sandstone deposited by turbidity currents. The limits of the occurrence of the strong reflector are related to the topography (Laughton, Berggren et al, 1972). On the Icelandic Plateau, to the NE of Iceland, the acoustical basement shows as an exceptional smooth opaque horizon (Eldholm and Windisch, 1974). Drilling at sites 348 and 350 showed that this opaque layer consists of basalt flows (Talwani, Udintsev et al, 1976).

Tucholke and Mountain (1979; see also Tucholke, 1979) describe the more important reflectors in the Western basin of the North Atlantic

ocean using the acoustic stratification and the results of several DSDP sites. Close to Bermuda a strong reflector is found which forms part of the horizon A complex. The strong reflector itself is A^v and masks deeper reflectors within 100 km of Bermuda. Horizon A^v was penetrated at site 386 about 140 km to the south of Bermuda (Tucholke, Vogt et al, 1979). It consists of coarse graded sands with a high impedance situated just above Upper Eocene to Upper Oligocene volcanoclastic turbidites deriving from Bermuda (Tucholke, 1979; see also Jansa et al, 1979).

Description of the seismic signature and geographical distribution of the layer

Figure 2 gives examples of seismic profiles which show the strong reflector. Figures 2A and 2B give profiles on two parallel tracks at a distance of about 10 km. Figure 2A shows a low frequency record and Figure 2B a high frequency record. Figures 2C and 2D give the same seismic profile, using alternatingly the Bolt Par air-gun and the watergun as sound source. Figure 2E shows a profile on which the layer reaches the surface.

The low frequency image of the layer (Figures 2A and 2C) shows a strong acoustic reflector with internal layering in the form of parallel reflectors. At some positions the internal reflectors are continuous (Figure 2C) but more often the lateral extent is short (Figures 2A and 2E). The highly reflective layer is in general very smooth and shows little or no resemblance with the "normal" oceanic basement. The high frequency image (Figure 2B and D) shows internal layering. Inside the layer there are small elements with a higher reflectivity than their surroundings. These small elements are not visible in the low frequency record.

Using the dataset of Figure 1 the strong reflector has been mapped. The following criteria have been used : the strong reflector is "present and opaque" if it is reflecting more energy than the seabed and at the same time shields almost all energy from possible

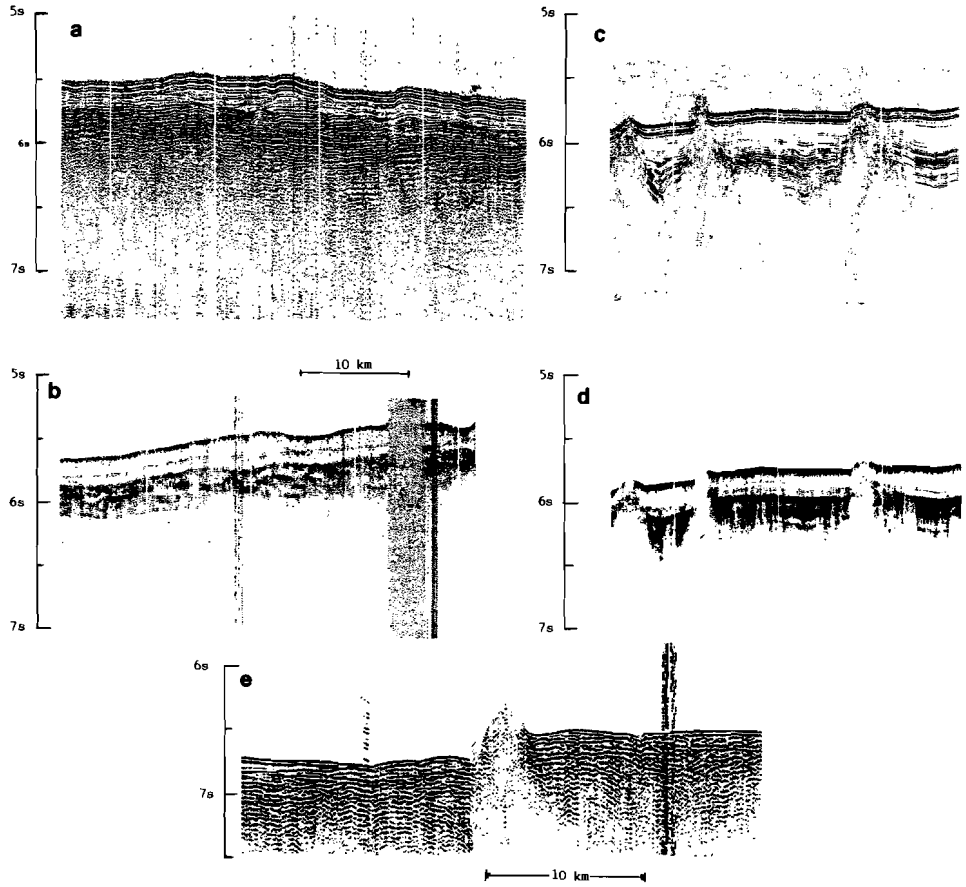

Figure 2: Seismic reflection profiles.

A: Seismic reflection profile recorded with a bandpass filter of 40-80 Hz. Soundsource: Bolt Par air-gun 40 cu in. (.66 l.).Depth is given in seconds two way travel time. Location of the profile between Hyeres and Great Meteor seamount.

B: Seismic reflection profile recorded with a bandpass filter of 200-2000 Hz. Soundsource: Watergun, 80 cu in. (1.32 l.). Location of the profile about 10 km away from the one shown in Figure 2A.

C: Seismic reflection profile recorded with a bandpass filter of 40-80 Hz. Soundsource: Bolt Par air-gun. Profile located to the west of Hyeres seamount.

D: Same seismic profile as in Figure 2C. Soundsource: Watergun. Filter: 200-1000 Hz.

E: Seismic reflection profile recorded with a bandpass filter of 40-200 Hz. On this profile located to the northeast of Cruiser seamount the volcano-clastic layer reaches the surface.

deeper reflectors including the oceanic basement. Where deeper reflectors become visible and the reflectivity of the layer is of the same strength as that of the seabed the layer will be called "present".

The results are given in Figure 3. In the southwestern part the limit of extent of the strong reflector is often determined by local topography. On several profiles the layer is present and opaque on the

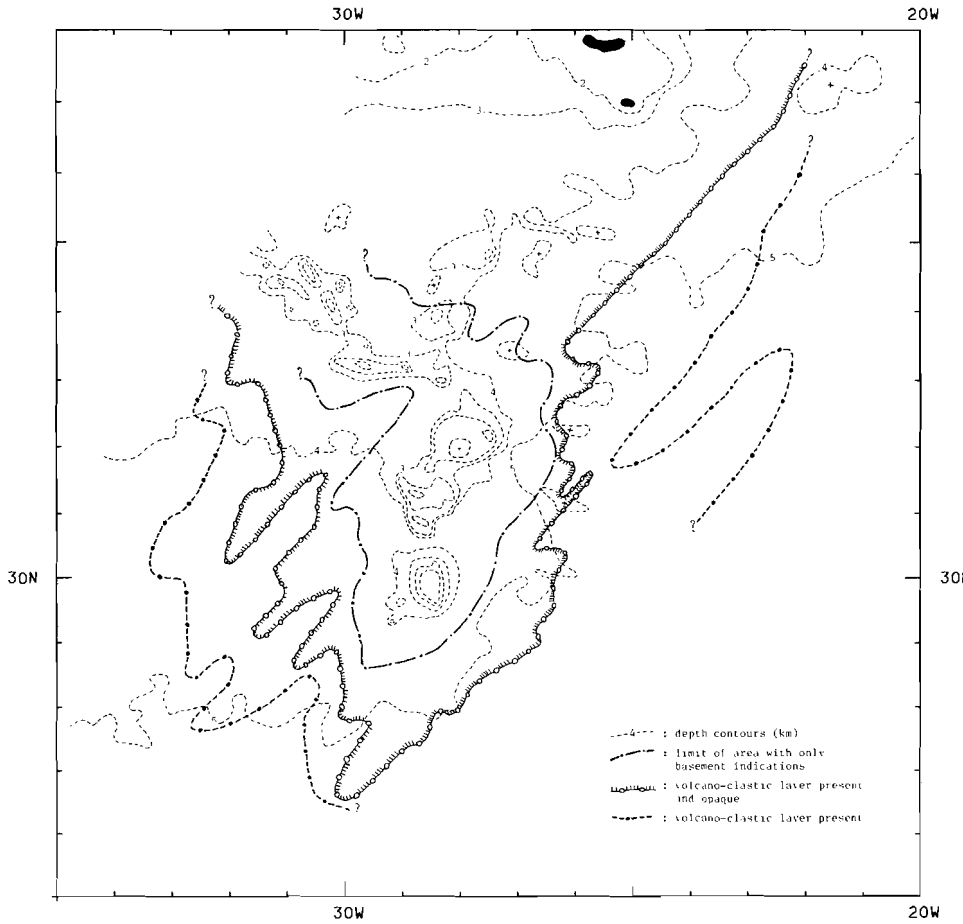

Figure 3: Area inside which the volcano-clastic layer is present and opaque together with the limit of the area of presence of this layer. Simplified bathymetry contours from Figure 1 give an indication of the seamounts. Close to the seamounts the area with no basement information is given.

side of a topographic high facing the seamounts. At the opposite side its opaqueness is less clear and the layer is defined as present. On profiles coming from the seamounts and going eastwards the the character of the layer changes gradually. Close to the seamounts the layer is strongly reflecting. Farther away it becomes as strong as the seabed (present) and gradually changes into a normal reflector in the abyssal plain. In this part of the area the limit between "present and opaque" and "present" and even more so between presence and absence is difficult to define. Here the quality of the seismic registrations is an important factor. In cases of doubt about the position of change in character we often compared several profiles to get a more systematic definition of this change.

The limit of the area inside which the strong reflector is present and opaque shows to the west of about 30°W an irregular NW-SE orientation. This direction is not reflected in the general depth contours. To the east of about 30°W the orientation of this limit is NE-SW with a clear relation to the general topographic trend. This relation stops north of about 35°N, where the depth contours change into an E-W direction. The limit of the area of presence of the layer runs roughly parallel to the limit of the area where the layer is present and opaque.

Figure 3 also gives the area inside which only locally indications of the oceanic basement are found. The limit of this area runs roughly parallel to the depth contours of the seamounts. The disappearance of the basement is also influenced by flexure as the oceanic lithosphere bends downwards under the load of the seamounts (see chapter III). The flexure causes moats around the seamounts which have been filled with sediments and/or volcanic material.

We can sum up the properties of the strong reflector in the area around the Atlantis-Meteor seamount complex as follows:
1):The layer is often opaque, with a higher reflectivity than the oceanfloor. Its low frequency image shows some internal reflectors, only with a small lateral extent. The high frequency image shows several reflectors all with different reflectivity (see Figure 2).

2):The area where the strong reflector was found is related to the seamounts in this area (see Figure 3).
3):The limit of extent of this reflector in the southwestern part is often related to local topography.

When comparing the literature results with the above described acoustic character of the reflector around the Atlantis-Meteor seamount complex leads to the following conclusions: The relation between the limit of extent and local topography in the southwest and the gradual change into a "normal" reflector points to a relation with the acoustic reflector found to the south of Iceland and near Bermuda. Because of the resemblance with the profile near the Cape Verde rise, the local presence of sills is probable.

We can sum up, in conclusion, that the strong often opaque reflector probably consists in general of material from the closeby seamounts. The local presence of sills is probable. The deposition takes place via turbidity currents that cause the relation of the limit of lateral extent with local topography. Just from the seismic registrations we cannot be sure whether the age of the volcano-clastic layer is the same over the whole area.

Total sediment thickness

Figure 4 gives the total sediment thickness in the area around the Atlantis-Meteor seamount complex. Since we did not attempt to convert the seismic registrations into depth-sections, thicknesses are expressed in time-units.

In the parts around the seamounts, where we did not find acoustic basement (see for location Figure 3) we took as total sediment thickness the difference between the oceanfloor and the deepest reflector. Here the sediment thickness is a minimum.

The contouring was done by computer with a cut-off wavelength of 55 km. In doing so we partly egalized the basement relief, which gave small wavelength changes in the sediment thickness. If one uses a filter, contours may shift where the thickness is small. Therefore the

zero contours were determined from the seismic profiles. Sediment-free areas with a diameter less than 20 km are not shown in Figure 4. In the southwestern part of the area we only find sediments in small basins. The lateral extent of these basins is so small that they disappear in the filtering proces.

The areas less deep than 3000 m without seismically detected sediments are hachured. Here reef sediments have been found (Hinz,

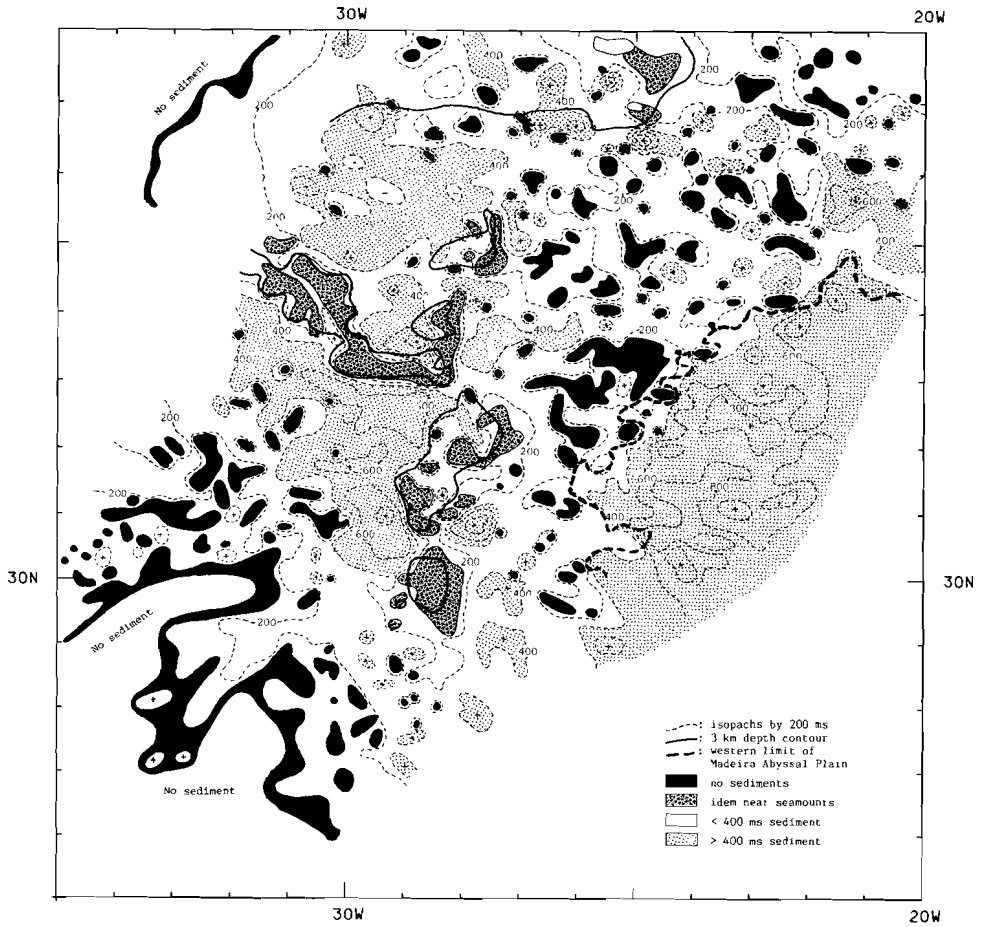

Figure 4: Isopachs of total sediment thickness. Contour interval of 200 ms two way travel time.

1969; Von Rad, 1974). In our seismic records we could not distinguish between volcanics and reefs. The majority of the area shallower than 3000 m is sediment free. Exceptions are found inside the complex formed by Cruiser, Irving and Hyères seamounts. Here we find sediments up to 400 ms. In the Atlantis seamountgroup an elongated structure is also found with sediments up to 200 ms.

In the eastern part of Figure 4 there is a large area with a sediment thickness of more than 400 ms. This area does not show any topographic relief due to turbiditic sedimentation coming from the NW African slope (Jones et al, 1966; Belderson and Laughton, 1966; Kuijpers, 1981). It forms the western extension of the Madeira abyssal plain. Using the seismic registrations from the Kroonvlag-project we indicated the western limit of the abyssal plain in Figure 4. Locally the turbidites protrude westwards in fracture zone valleys. Not counting the abyssal plain sediments, the sedimentation pattern around the Atlantis-Meteor seamount complex shows a great asymmetry: west of Cruiser, Irving and Hyères seamounts and south of Plato seamount we find a large area with a sediment thickness of more than 400 ms, while virtual no sediments occur east of these seamounts. Also to the northwest of Plato and Tyro seamounts there is an area with more than 400 ms of sediments.

Sediment thickness above the volcano-clastic layer

We also contoured the thickness of the sediments above the volcano-clastic layer, i.e. within the area shown in Figure 3. Figure 5 shows the result. In the southwestern part of the area and west of about 30° W the 200 ms isopach runs roughly NW-SE. East of about 29°W this orientation changes into NE-SW. At some places, close to the seamounts the thickness of the sediments above the volcano-clastic layer is more than 500 ms. Like in Figure 4 we see in Figure 5 an increase in sediment thickness going from east to west. This results into asymmetric sedimentation around the seamounts with in general more sediments above the volcano-clastic layer to the west of the

seamounts. This is also true in the northern part, where we find more sediments to the west of the islands Sao Miguel and Santa Maria. In the southern part of the area near Great Meteor seamount the greatest thickness of the sediments above the volcano-clastic layer lies to the northwest of this seamount.

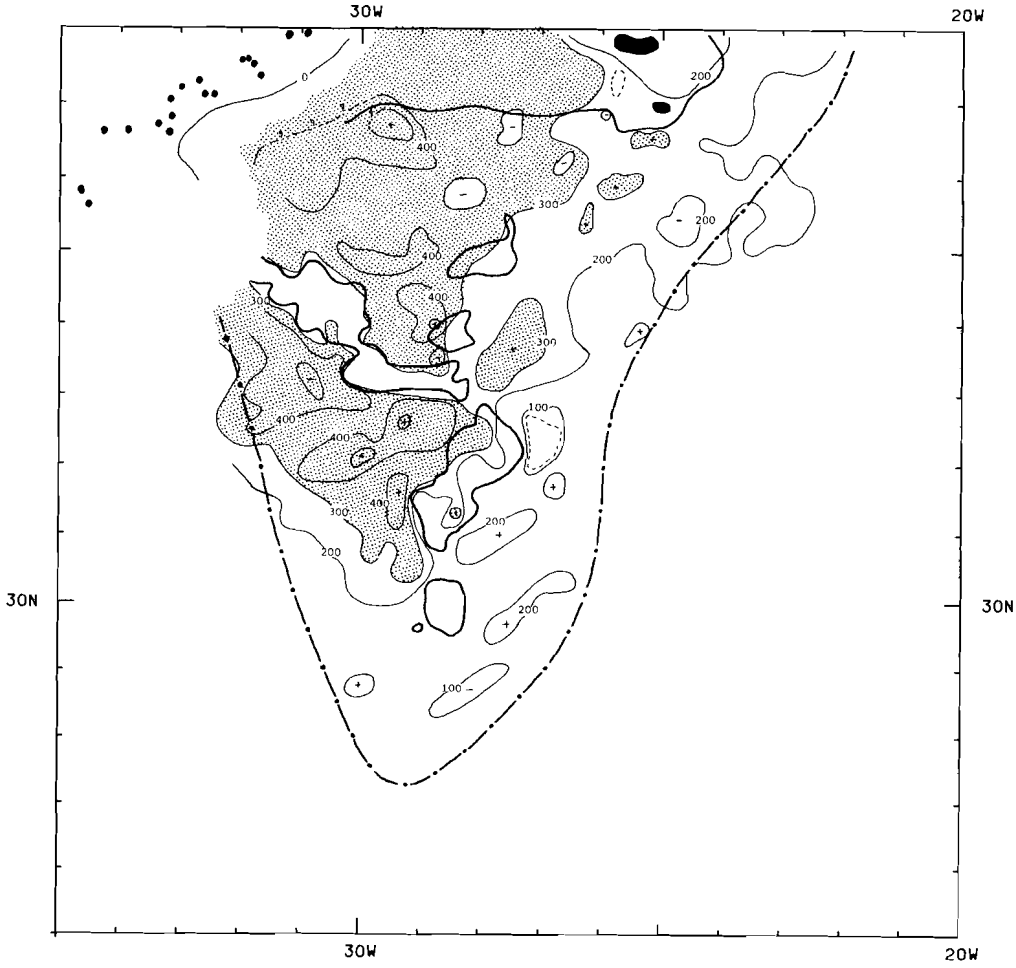

Figure 5: Isopachs of sediments above the volcano-clastic layer with an interval of 100 ms two way travel time. Heavy line denotes 3 km depth contour from Figure 1. Dots give the location of the earthquake epicentra. The line with dots gives the limit of extent of the volcano-clastic layer. Dashed contours denote places where volcano-clastic layer reaches the surface.

In Figure 5 the position of the Mid-Atlantic ridge has been indicated. In this part we only have a few track-lines (see Figure 1). The contours here are only tentative. Going west to the Mid-Atlantic ridge the thickness of the sediments above the volcano-clastic layer reduces to zero (the same is true for the total sediment thickness, see Figure 4).

Not taking into account small irregularities, there is a good correlation between the depth contours and the 200 and 300 ms isopachs in Figure 5. To the east of about 30°W they all show a NE-SW orientation. To the west of 30°W the isopachs have a NW-SE orientation. The depthcontours at first have the same orientation, but then change into an east-west orientation. The western part of the area has a depth between 3000 and 3500 m (see Figure 1) and a thickness of the sediments above the volcano-clastic layer of more than 300 ms.

In Figure 5 we also show two areas with a smooth oceanfloor where the volcano-clastic layer comes up to the surface. The larger area is located to the northeast of Cruiser seamount. Figure 2E shows a seismic profile from this area. The other area where the volcano-clastic layer reaches the surface lies to the south of Sao Miguel.

Sediments below the volcano-clastic layer

Within the area where we have found the volcano-clastic layer at some places a reflector is found underneath this layer. This reflector sometimes represents oceanic basement. The thickness of sediments underneath the volcano-clastic layer was determined where possible. Figure 6 shows the computer contour of this thickness (cut-off wavelength 55 km). Within the area where no oceanic basement was detected, shown in Figure 6 as the shaded part, no contours are given. In this area the load of the seamounts has bended the oceanic lithosphere downwards (see chapter III).

In the major part of Figure 6 the thickness of the sediments below the volcano-clastic layer has values between 200 and 300 ms.

Close to the shaded part several places with thicknesses of more than 400 ms are found: southeast of Tyro seamount, around 34°N/ 28°W and south of Plato seamount around 33°30'N/ 29°W. At the eastern limit of extent of the volcano-clastic layer there are some places with a thickness of this sediment unit of more than 300 ms. To the north, around 36°N and between 23°-27°W, there is a roughly east-west

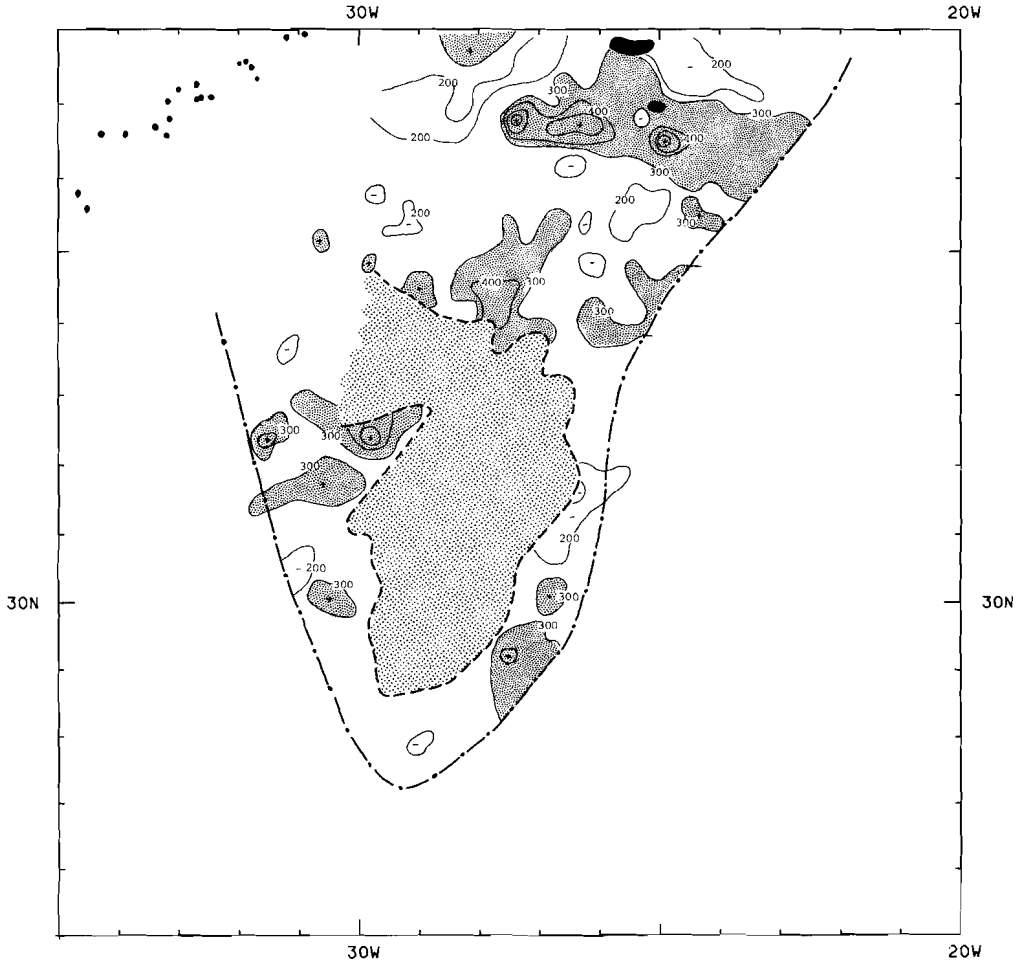

Figure 6: Sediments below the volcano-clastic layer. Interval: 100 ms. Central shaded part surrounded by heavy dashed line gives the area with only basement indication. Shaded parts have a thickness of more than 300 ms.

orientated area where the thickness of the sediments underneath the volcano-clastic layer is more than 500 ms.

Depth anomaly and relation to isopach maps

Figure 7 gives the depth anomaly of the area. A description of the depth anomaly can be found in chapter III. Especially to the west of 30°W the orientation of the isopachs of the sediment thickness above the volcano-clastic layer correlates better with the depth anomaly contour than with the direction of the depth contours. In almost the whole area with a depth anomaly of more than 1000 m, the thickness of the sediments above the volcano-clastic layer is more than 300 ms. An exception is formed by the northeastern part (east of 26°W) where the thickness of the sediments above the volcano-clastic layer has a value between 200 and 300 ms. Another exception is formed by the area around 36°N/ 29°W. Here the depth anomaly is less than 1000 m, while the sediment thickness above the volcano-clastic layer is more than 400 ms. The thickness of the sediments between the volcano-clastic layer and the oceanic basement in this area lies between 200 and 300 ms (see Figure 6). In this part of the area the East Azores fracture zone (the branch between Santa Maria and the Mid-Atlantic ridge) is situated. This causes the low values of the depth anomaly. Great Meteor seamount and its immediate surroundings form the third exception. Here we find a high positive depth anomaly combined with a thickness of the sediments above the volcano-clastic layer of less than 200 ms.

Paleodepth and sedimentation

Using paleodepth reconstructions we can model the relation between the depth anomaly and the sediment thickness. We reconstruct from the present depth the paleodepth in steps of 5 Ma. In that part of the area which lies above the average carbonate compensation depth

(CCD) for that period, carbonate sedimentation will occur. We have used the CCD-age curve for the North Atlantic ocean given by Berger and Von Rad (1972). This curve was calculated using DSDP results. During Eocene and Oligocene the CCD deepened from 3600 m to 4300 m. In the middle Miocene the CCD rose to 3600 m. Since then the CCD has deepened to its present value of 5000 m. To calculate the paleodepth

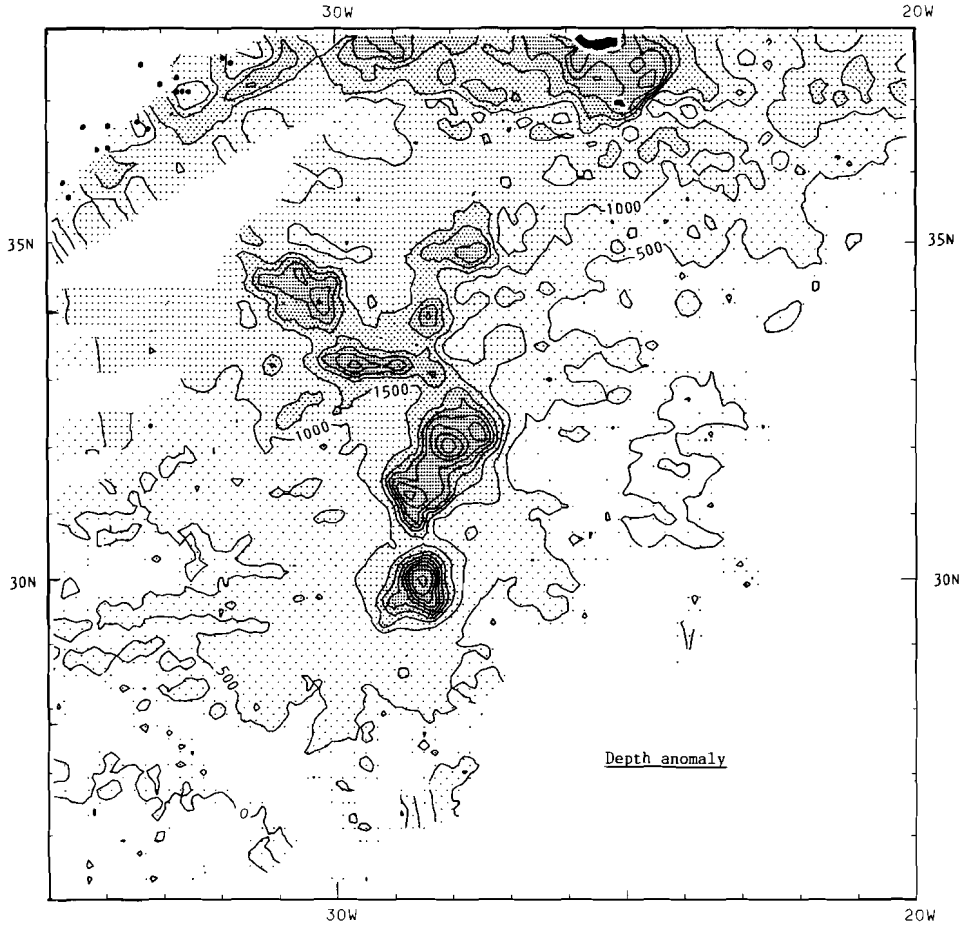

Figure 7: Depth anomaly contour chart. Interval: 500 m. Dots in the northwestern part of the area give the location of the earth quake epicentra. The topographic information around the islands Sao Miguel and Santa Maria was not used in the calculation. The white band around these islands gives the area inside which the contours are not reliable.

the depth-age curve given by Parsons and Sclater (1977) was used. However assuming that positive depth anomalies have been caused by a (thermal) rejuvenation (Detrick and Crough, 1978; Menard and McNutt, 1982), the subsidence of oceanfloor will not follow the slope of the depth-age curve belonging to the real age, but rather that of the apparent age. The apparent age has to be calculated from the real depth and the depth-age curve.

The procedure in calculating the paleodepths and model-isopachs was as follows: From the isopach map of the sediments above the volcano-clastic layer and from the one with the total sediment thickness we calculated 0.5°*0.5° averages (respectively Figure 8A and 8B). These generalized isopach maps give the sediment patterns that must be explained by the model.

The age of the oceanfloor and the depth anomaly were both calculated at 0.5°*0.5° averages (respectively Figures 8C and 8D). Using these two results we calculated the apparent age (Figure 8E). For positions with a depth anomaly of more than 2000 m, often corresponding with a seamount, we took 2000 m as the maximum depth anomaly. As starting depth for paleo reconstructions we took the bathymetry and added half of the thickness of the sediments above the volcano-clastic layer

The paleodepth was calculated at time intervals of 5 Ma using the apparent age for the uplift during the intervals. In Figures 8 F-I some examples are shown. Oceanfloor with an apparent age of zero was kept at the depth belonging to this age (= 2500 m) in the next reconstruction step. Figures 8F, G and H show that the area lying above the CCD has increased in the last 20 Ma. This is partly caused by the seafloor spreading process which causes the African plate to grow. But a more important factor is the deepening of the CCD (3700 m 20 Ma ago, to 5000 m at present). In the period 50-20 Ma ago the CCD-limit migrated in the direction of the ridge (compare Figures 8H with 8I).

For every time-interval we calculated at all points the amount of carbonate sedimentation. For this we used a simple sedimentation

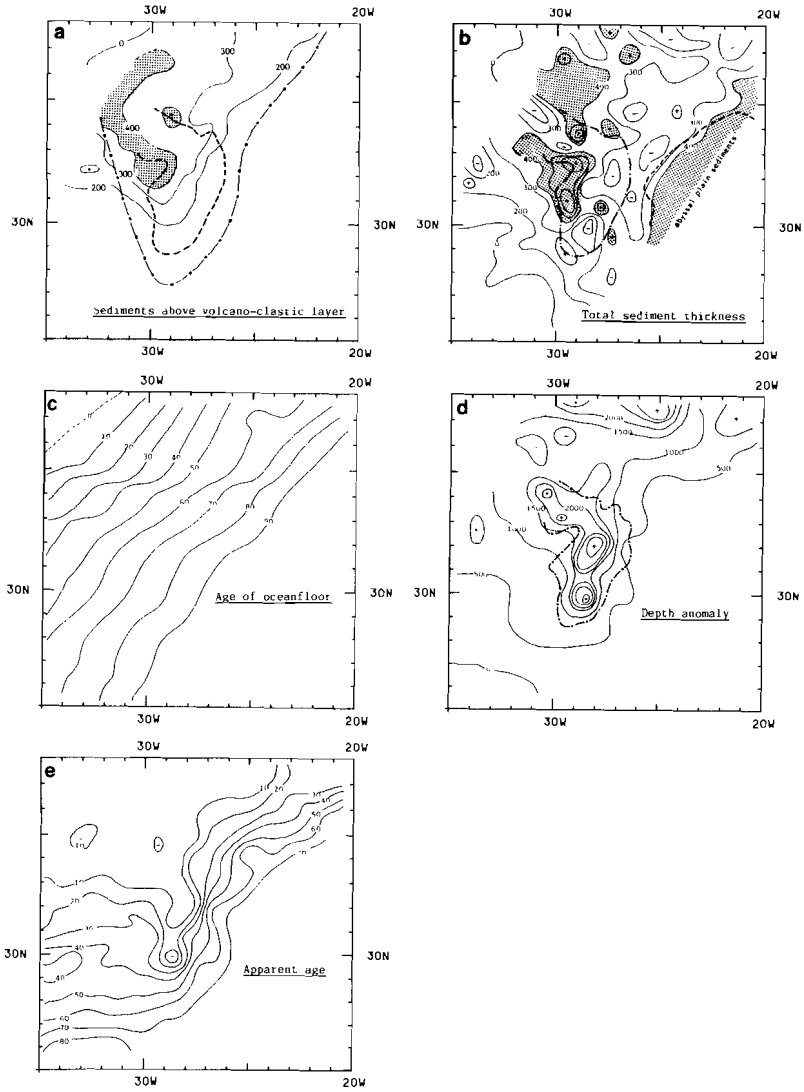

Figure 8: Paleodepths and sediment models on a .5.5 degree grid. Shaded parts have a thickness of more than 400 ms.*

A: Sediments above volcano-clastic layer. Line with dots gives the limit of extent of the volcano-clastic layer.

B: Total sediment thickness. Line with dots gives limit of area with only basement indications. Heavy dotted line gives the generalized western extension of the Madeira abyssal plain.

C: Age of the oceanfloor in intervals of 10 Ma.

D: Depth anomaly, interval: 500 m. Dotted line surrounds area with only basement indications.

E: Apparent age with an interval of 10 Ma.

model: The sedimentation rate is constant (1 unit per time-interval) down to a certain depth (lysocline, see Berger, 1970; Van Andel et al, 1977 and Sclater et al, 1979). From this depth to the CCD the sedimentation rate decreases linearly to zero. As depth for the lysocline we chose 500 m above the CCD. Figures 8J,K and L give the results. The model isopachs to the south and to the east have roughly the same orientation as the observed 200 and 300 ms isopachs. Deviations occur especially in the southwestern part of the area. Here the model isopachs have an east-west orientation, while the observed 200 and 300 ms isopachs show a NNW direction. The shape and position of the 400 ms isopach does not show in the model.

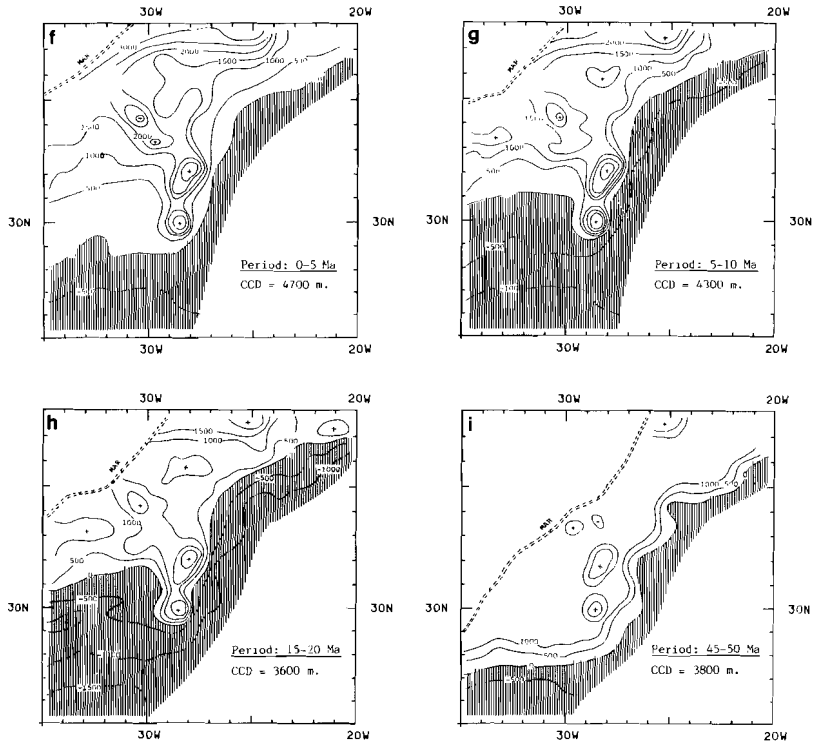

Figure 8 F-I: Paleodepths for respectively the periods:0-5 Ma, 5-10 Ma, 15-20 Ma and 45-50 Ma. Contourinterval:500 m. The paleodepth is plotted with respect to the average CCD of the period. Hachured parts are deeper than the CCD.

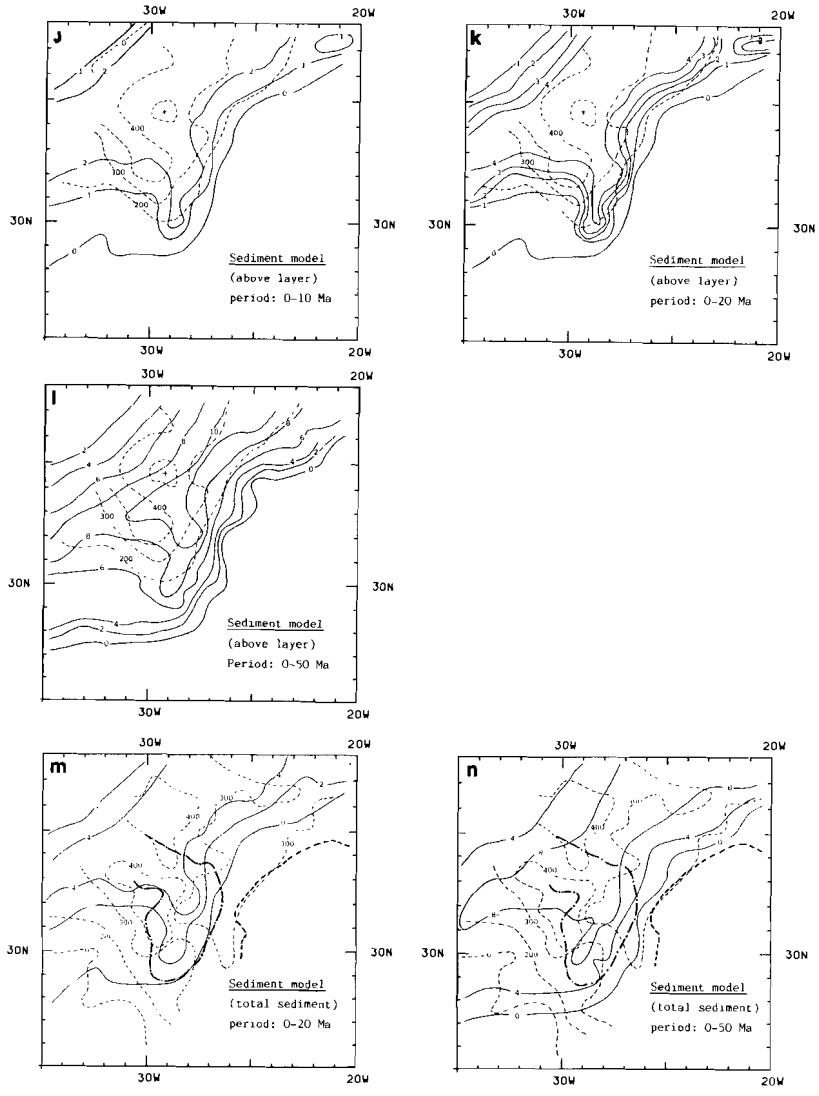

Figure 8 J-L: Models for the thickness of the sediments above the volcano-clastic layer. Model-isopachs are given for respectively the periods: 0-10 Ma, 0-20 Ma and 0-50 Ma. Dotted lines give the observed thickness from Figure 8A. The sedimentation rate was kept constant (1 unit per interval) till the lysocline and from that depth on till the CCD decreases linearly to zero. Depth of lysocline: CCD- 500 m.

M-N: Models for the total sediment thickness. Model-isopachs are given for respectively the periods: 0-20 Ma and 0-50 Ma. Dotted lines give the major observed isopachs from Figure 8B. Model used is the same as in Figure 8J.

In Figure 8K and L we increased the period during which deposition of sediments above the volcanoclastic layer took place. This implies an earlier origin of the volcano-clastic layer and of the anomalous depth of the area. An increase from 10 to 20 Ma gives an increase in sediment thickness in the model (compare Figure 8K with 8J). An increase of deposition time from 20 to 50 Ma shows, that the limit of the area of no sedimentation migrates to the south and to the east (compare Figure 8K with 8L). The asymmetric sedimentation pattern (i.e. more sediment to the west of the seamounts) clearly shows in the Figures 8J and 8K. In Figure 8L this aspect is hardly visible.

We have compared the model isopachs with the sediment-unit above the volcano-clastic layer. To make a comparison with the total sediment thickness possible we must use another starting depth for the paleo-depth reconstructions. This starting depth was calculated by adding half of the total sediment thickness to the bathymetric depth. Using this starting depth we calculated with the same model the amount of carbonate sediments. The results are given in Figures 8M and 8N .

To the east of about 28°W the observed 300 ms isopach has a NNE direction, which is in agreement with the model isopachs. In this model an increase in the time of sediment accumulation implies an earlier origin of the anomalous depth of the area. An increase of 20 to 50 Ma gives a migration of the model isopachs to the area where virtually no sediments were observed (compare Figure 8M with 8N). The total sediment thickness in the area close to the seamounts cannot be determined by the model study. Here flexure will occur and the resulting moat will be filled with sediments.

Discussion

The dating of the volcanism in the study area is incomplete. Dredged basalts from the flanks of Great Meteor seamount give ages of 11 and 16 Ma (Wendt et al, 1976). The top of Great Meteor seamount is covered with Miocene sediments (Von Rad, 1974). The beginning of the volcanism on the Azores, which is still active is not known (c.f.

Ridley et al, 1973; Feraud et al, 1980). For an estimation of the age of the volcano-clastic layer, which near the Azores might be considerably younger than near the Atlantis-Meteor complex, we only could use recent sedimentation rates (Von Stackelbergh et al, 1976 and 1979; Kuijpers 1981). However these sedimentation rates show a great variation over the area. Extrapolation of these values over the whole period after the origin of the volcanism will cause such an uncertainty that an hereupon based age determination based has no value.

Since no closeby DSDP sites exist, the sedimentation pattern around the Atlantis-Meteor seamount complex offers a welcome opportunity to at least estimate the age of the volcanism.

The sediment model we have used explains the increase in the thickness of the sediments above the volcano-clastic layer going from east to west in the area to the north of about 30°N and to the east of about 28°W. The model isopachs and the observed isopachs run almost parallel here. In the soutwestern part of the area there is an increase in the thickness of the sediments above the volcano-clastic layer going form south to north. Here the model isopachs show the same trend. However the orientation of the model isopachs here is east-west, while the orientation of the observed isopachs is NW-SE. An increase in the age of the volcano-clastic layer results in an increase in the period of deposition of sediments above the layer. An increase from 10 to 20 Ma only gives an increase in sediment thickness. The limit of the area inside which we find carbonate sediments migrates to the south in the southwestern part and to the southeast in the northeastern part of the area. This migration outwards starts as the total time of sediment accumulation increases to more than about 20 Ma (see Figures 8H and 8I). This is about the same time as the deepening of the CCD starts (Berger and Von Rad, 1972). This seems to point at a start of the sediment accumulation above the volcano-clastic layer not much before Miocene.

In Figures 8J,K and L we have given the zero model isopach. This isopach lies within the limit of extent of the volcano-clastic layer

(see Figure 8D). The observed sediment thickness (Figure 8A) has almost everywhere values of more than 100 ms. The model only gives the carbonate sedimentation, while there is also a, be it small, depth independent sedimentation of pelagic clay. This sedimentation, not taken into account in the model, will give a roughly constant background level over the whole area.

There are several aspects in the sedimentation pattern which are not accounted for by the model: a): The sedimentation around the Great Meteor seamount is larger in the model than observed. This difference is partly caused by the lack of basement information in this part. Because of this the calculated depth anomaly is too high, which causes the apparent age to be too small. In the paleodepth reconstructions this part of the area rises too fast and gains too many sediments. b): The large sediment thickness in the northwestern part of the area and to the southwest of Plato seamount are not predicted by the model. A redeposition of sediments from the seamounts by turbidity currents seems to have caused these large deposits. The area close to the seamounts especially to the west is for the greater part very smooth. c): To the east of the Azores there is an area where the thickness of the sediments above the volcano-clastic layer is smaller than predicted by the model. The thickness of the sediments between this layer and the oceanic basement here is larger than on the average (see Figure 6). This might point to a younger age for the volcano-clastic layer there. d): The discrepancy in orientation between the model isopachs and the observed isopachs in the southwestern part of the area cannot be explained by using the real age of the oceanfloor in the paleodepth reconstructions. A paleodepth reconstruction using the real age causes the paleodepth contours to bend southwards. This is caused by an increase in the rising velocity to the west i.e. to a younger age. The orientation of the model isopachs can change by applying a change of the CCD over the area. We tried a CCD, with a minimum at the Mid-Atlantic ridge and a linear increase to the east with isolines parallel to the ridge. We took for the increase a variation of 1500 m keeping the CCD in the central part of the area

equal to the one given by Berger and Von Rad, 1972). The model isopachs now run rougly parallel to the observed ones.

Variations in carbonate sediment input, which we kept constant in the model, will hardly influence the orientation of the isopachs. Only the positions of the isopachs will change. Also a change in the depth of the lysocline compared to the CCD will have the same effect. A decrease in the age of the volcano-clastic layer going from east to west will give NW-SE oriented, isopachs but cannot explain the high values to the south of the Atlantis seamount group.

The pattern of the sediments above the volcano-clastic layer gives an age indication for this layer. We also modeled the pattern of the total sediment thickness. Here the observed isopachs can only be compared with the model in the southwestern part. In this part of the area both the observed and the model isopachs have a clear NW-SE orientation. An increase in the age of the anomalous depth gives rise to carbonate sedimentation in that part of the area with virtually no observed sediments. The sedimentation in this part of the area starts in the model when the age increases to more than 20 Ma. This might indicate, that the time at which the anomalous depth in this area originated cannot be much before Miocene.

The sedimentation above the volcano-clastic layer leads to the conclusion, that the age of this layer cannot be much older than Miocene. The absence of sediments in the southwestern part of the area (see Figure 8L) indicates that the anomalous depth of the area cannot have originated much before Miocene. These indications of age are rough, but make it unlikely, that the volcanism in this area and the depth anomaly of it originated on the Mid Atlantic ridge. The sediment model is not sensitive enough to detect variations in age between the different seamounts belonging to the Atlantis-Meteor complex.

Conclusions

The strong, often opaque acoustic reflector in the area around the Atlantis-Meteor seamount complex probably consists of volcanic

material deposited by turbidity currents. Locally the presence of sills cannot be excluded.

The isopachs of the sediments above the volcano-clastic layer correlate with the depth contours. However a better correlation with the depth anomaly contours exists in the southwestern part of the area. This leads to a simple sedimentation model based on depth-dependent carbonate sedimentation.

The carbonate sedimentation model based upon paleodepth reconstructions leads to the following conclusions: 1): The sedimentation above the volcano-clastic layer has not started before the Miocene. This outcome is corraborated by the absence of sediments in the southwestern part of the area. 2): In view of these results it seems unlikely, that the volcanism in this area and its anomalous depth have originated on the spreading centre.

CHAPTER V:

THE ATLANTIS-METEOR DEPTH ANOMALY, A DISCUSSION

Introduction

In this study we have described the Atlantis-Meteor seamount complex and noticed that it is surrounded by a positive depth anomaly. The Atlantis-Meteor complex consists of elongated structures, a pattern suggestive to extension. Indirect age determinations of the volcanoes do not lead to a clear age migration pattern of the volcanism.

In this chapter we will describe several studies of intra-plate volcanism. Results from these studies will be compared with those from the Atlantis-Meteor complex. We will calculate the stresses caused by the bending of the lithosphere under the seamounts. Using these stresses we will discuss the validity of the elastic approach. It will be shown that, similar to the Atlantis-Meteor complex, there are other volcanic complexes which show lineations but no clear age migration pattern of the volcanism. The results obtained in this study make the simple hot-spot hypothesis an unlikely explanation for the origin of the Atlantis-Meteor complex. An alternative explanation will be discussed.

Studies of depth anomalies and their relation with gravity

During the last decade there has been particular interest in examining the correlation between gravity and depth anomalies. Menard (1973) calculated depth anomalies in the eastern Pacific and found a weak correlation between depth anomalies and gravity anomalies. Sclater et al (1975) showed that in the North Atlantic residual elevation anomalies with wavelengths of more than 400 km are superimposed upon the subsidence curve, which are linearly related to regional variations in the free-air gravity field.

Watts (1976) examined the relation between gravity and bathymetry in the central Pacific. He found, that the observed correlation between 5°*5° averages over the Hawaiian swell can be explained by a model for the gravity effect of the swell and its compensation.

Cochran and Talwani (1977) examined 5°*5° average depth anomalies and residual gravity anomalies throughout the world's oceans. They found, that many of the correlations observed between residual gravity and depth anomalies arise from areas of extensive intraplate volcanism. In some of the locations where the correlation is observed, such as over Bermuda and aseismic ridges, the active volcanism has ceased long ago. The long wavelength component of the earth's gravity field (>4000 km) is characterized by large areas in which significant anomalies of a constant sign are found. There is no apparent relationship between the long wavelength gravity anomalies and depth anomalies. Exceptions are formed by the southeastern Indian ocean and by the North Atlantic ocean, the latter is the largest in extent. In a second study Cochran and Talwani (1978) describe the North Atlantic gravity high, i.e. the broad high in the gravity field to the north of near 30°N (see also Talwani and Le Pichon, 1969). To the south of the Azores the gravity high is centered over the Atlantis-Meteor complex. North of the Azores there is no direct relationship between the gravity and depth anomalies, although both are consistently positive over the same regions.

In addition to the above described observations several recent studies of depth anomalies, associated with intra-plate volcanism, all show the correlation between the depth anomalies and gravity or geoid anomalies (e.g. McKenzie et al, 1980; Sandwell and Poehls, 1980; Mammerickx, 1980; Crough and Jarrard, 1981 and Crough, 1982).

The relationship between gravity anomalies and depth anomalies is not a simple one. Depth anomalies associated with volcanism show a direct correlation with gravity anomalies. Depth anomalies with a larger extent, e.g. the North Atlantic high, only show a correlation with gravity in that they both are consistently positive over the same area. From these observations the suggestion follows, that we must

distinguish two types of depth anomalies: Depth anomalies, or mid-plate swells, associated with volcanism, showing a direct correlation with gravity, and depth anomalies, usually of larger extent than the first type, which show no systematic correlation with gravity.

The Atlantis-Meteor depth anomaly

The correlation between the Atlantis-Meteor depth and gravity anomalies has already been discussed in chapter III. Here we want to show that this correlation also exists for the longer wavelengths. For this, we first eliminated the short wavelengths by applying to both data sets a low-pass two dimensional Butterworth filter with a cut-off wavelength of 500 km, 6 dB/octave roll off. Application of this filter removes most of the effects related to flexure. To avoid edge effects we extended the depth anomaly data set where necessary with the data used for the calculation of the topography corrections (see chapter III). The gravity data set was extended using the 1°*1° averages from Cochran and Talwani (1977). Figures 1A and 1B show the resulting long wavelength depth anomalies and residual gravity anomalies. The residual gravity anomalies have been corrected for the indirect effect and for the ridge effect (see chapter III). There is a general correlation between the depth anomalies and the residual anomalies, e.g. the 500 m depth anomaly contour and the 20 mGal residual gravity anomaly contour. The gravity anomaly over Great Meteor seamount is much larger than the anomalies over the other seamounts.

The correlation between depth anomalies and gravity anomalies for the longer wavelengths has implications for the compensation mechanism. We show this using the isostatic response function (e.g. Walcott, 1976). This function is defined as the ratio between the combined gravity effect of topography and its compensation and the gravity effect of the topography alone. The isostatic response function depends on wavelength and can be calculated from the formulas used in the theoretical admittance calculations (e.g. Karner, 1982). Figure 2 shows some examples of the isostatic response function for

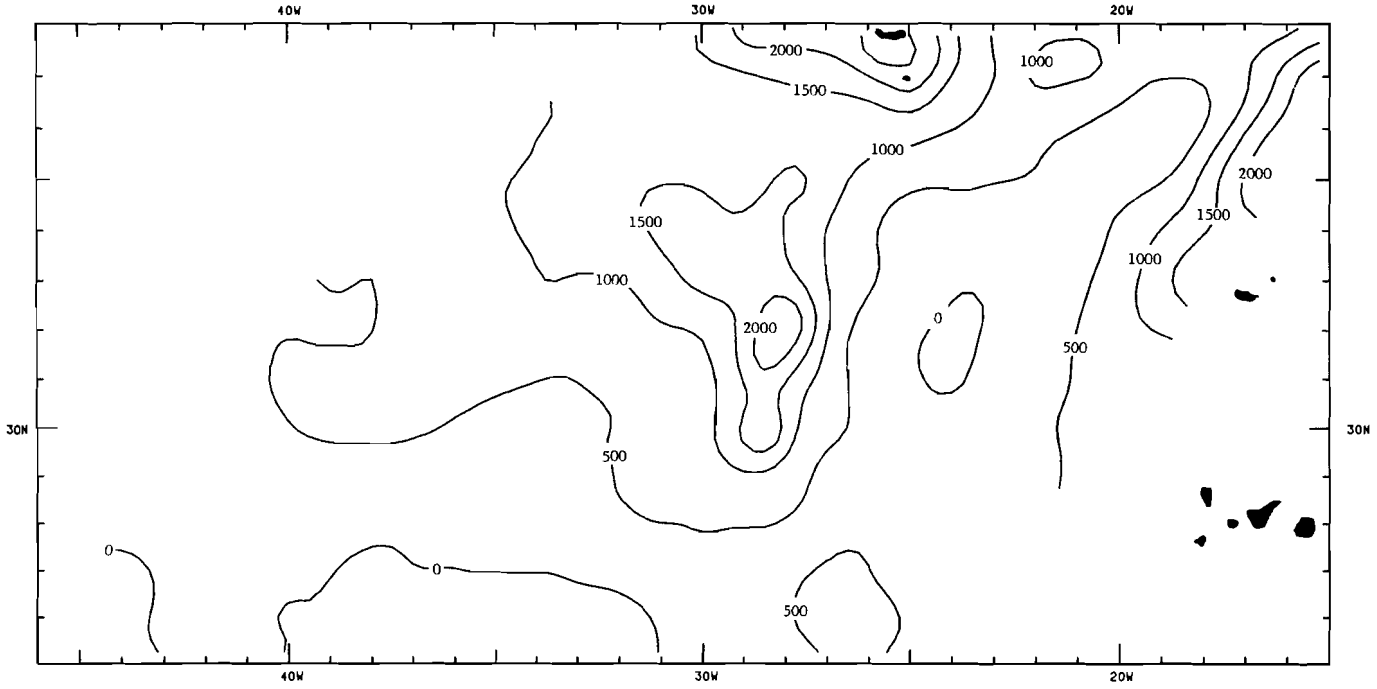

Figure 1A: Depth anomaly filtered with a two-dimensional Butterworth filter, cut-off wavelength 500 km. Contour interval: 500 m.

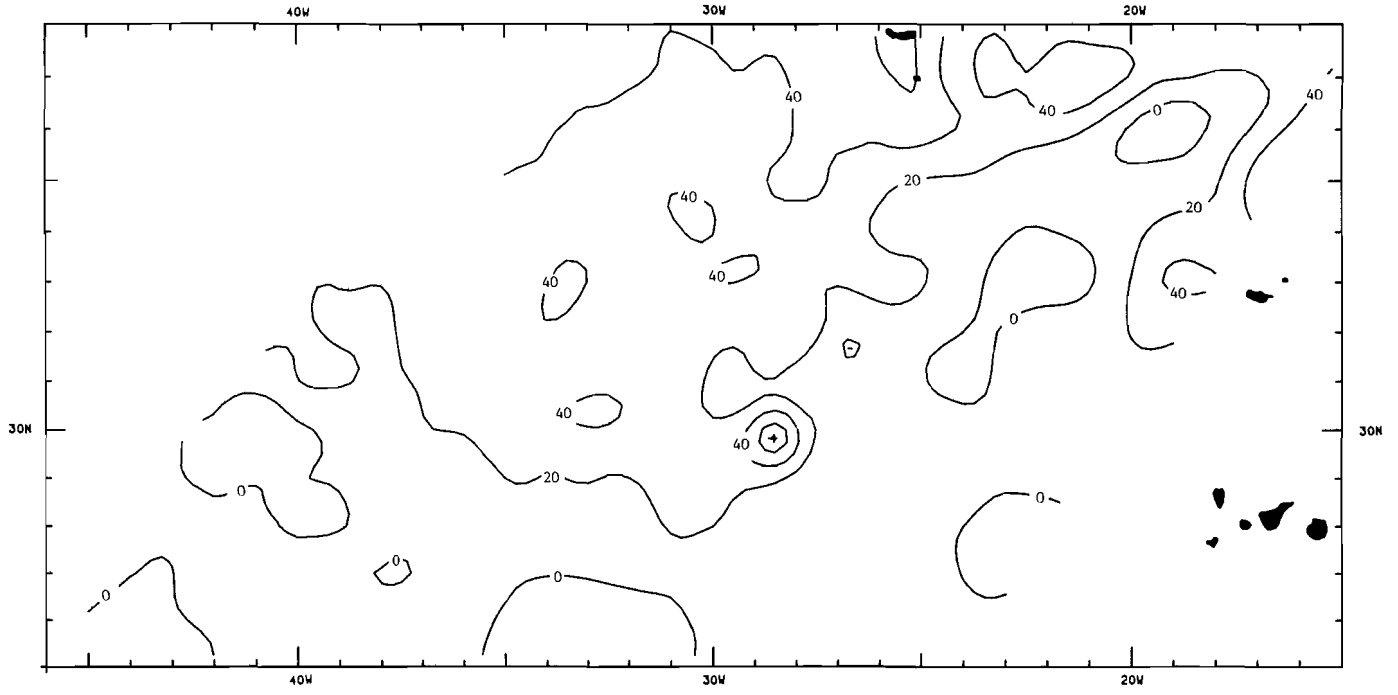

Figure 1B: Gravity anomalies filtered with a two-dimensional Butterworth filter, cut-off wavelength 500 km. Contour interval: 20 mGal. The gravity anomalies have been corrected for the indirect effect and for the ridge effect (see chapter III).

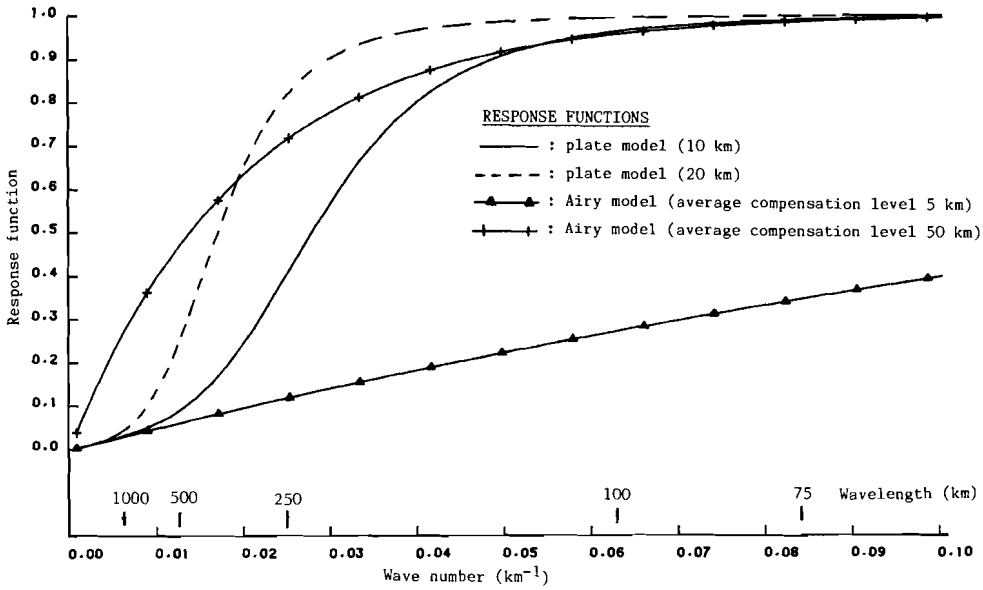

Figure 2: Isostatic response functions for different isostatic compensation models. A value of 1.0 for the response function indicates that the compensation effect is negligible compared to the gravity effect of topography. A value close to zero indicates that the compensation effect is about equal, with opposite sign, to the gravity effect of topography.

different compensation models. Plate models in general show a small compensation effect for wavelengths shorter than about 100 km. For an isostatically compensated feature with a wavelength of more than about 1000 km the resulting gravity anomaly is close to zero, if we assume a plate model or an Airy type compensation, both with a thickness of the oceanic layer of 5 km. An increase in the response function for these wavelengths can result from an increase in compensation depth (e.g. Airy model with a contrast depth of 50 km in Figure 2). Figure 1B shows the residual gravity anomaly for wavelengths larger than 500 km. For these wavelengths the isostatic response function, assuming a plate model with a thickness of 20 km, is larger than for the one with 10 km. Therefore the large anomaly over Great Meteor seamount, larger then the anomalies over the other seamounts, is an indication for a

thicker lithosphere under this seamount (see Table IV, chapter III for the elastic thicknesses under the seamounts).

Depth of compensation

From the gravity and/or geoid anomalies over mid-plate swells one can, in principle, obtain the average depth of the compensation of the swell. Since this depth might discriminate between possible ways by which depth anomalies are created, the determination of the compensation depth has been the subject of several mid-plate swell studies. First the question must be answered whether the depth anomalies are compensated at all. The gravity effect of an uncompensated uplift (or depression) of the lithosphere can be approximated by that of a Bouguer plate. We thus find for the gravity effect of a simple 1 km uplift of the lithosphere (density 3.4 g/cm^3) a value of about 95 mGal. The gravity anomalies over mid-plate swells are much smaller than this predicted uncompensated value (e.g. Watts, 1976, Cochran and Talwani, 1978). This can also be seen from Figures 1A and 1B, which show an uplift of about 1.0 km and a gravity anomaly of about 30 mGal. It can thus be concluded that the anomalous mass associated with depth anomalies is at least in part balanced by a compensating mass.

Talwani and Le Pichon (1969) found that part of the compensation in the North Atlantic must take place at depths larger than 30 km. Sclater et al (1975) found in the North Atlantic from 5°*5° averages an average compensation depth of about 100 km. Watts (1976) calculated over the Hawaiian swell from 5°*5° averages an average compensation depth larger than 120 km. Detrick and Crough (1978) concluded from the same data, that the average depth of compensation is between 50 and 100 km. The difference with Watts's result was ascribed to a difference in the assumed half-wavelength of the swell (Watts used 2200 km, Detrick and Crough used 1200 km).

Haxby and Turcotte (1978) explained the geoid anomaly over the Bermuda Rise by assuming a Pratt compensation, with a compensation

depth of 100 km. Crough (1978) used gravity-height ratios for Hawaii, Cook-Austral swell, Cape Verde Rise and Bermuda Rise and found that they are all supported by density anomalies 50 to 100 km deep.

Cochran and Talwani (1978), in their study of the North Atlantic, assumed that in the anomalous region, i.e. to the north of 30°N, the first 500 m of excess elevation was compensated by a low density body at depths larger than 100 km. The remaining part of the excess elevation must be compensated by variations in the crustal thickness. The implication of these models is that the overall elevation of the North Atlantic high results from mass deficiencies at greater depths (up to 300 km). Cochran and Talwani (1978) explain the mass deficiency by an increase in temperature of about 75°C.

Sandwell and Poehls (1980) showed that in the Central Pacific the shorter wavelength topography ($<$1100 km) is compensated at shallow depths (14 km). The longer wavelength topography is compensated at depths between 40 and 80 km. Crough and Jarrard (1981) found for the Marquesas-Line swell a local compensation with an average root depth of about 40 km. Over the Cape Verde Rise Crough (1982) found an average compensation depth of about 40 km.

The results of studies of the average compensation depth of positive depth anomalies do not yet lead to a simple model. The conclusion seems warranted that most of the compensation of positive depth anomalies takes place at shallow depths, i.e. by means of crustal thickening. The longer wavelengths are compensated at a deeper level. The evidence is increasing that this level is situated in the lower part of the "normal" lithosphere. Some results indicate a depth between 100 and 300 km for the deep compensation.

Compensation of Atlantis-Meteor depth anomaly

We have examined the relation between corrected basement depth and gravity anomalies in the Atlantis-Meteor area as a function of wavelength using the admittance method (see chapter III). We found, that this relation can be explained by a plate model compensation

model for wavelengths smaller than about 900 km. The data suggest a deeper compensation level for the longer wavelengths, but the study area is not large enough to give an estimate of this depth. The admittance obtained from the geoid anomalies also suggests a deeper compensation level for the longest wavelengths.

Lithospheric thinning, thermal rejuvenation

In 1978 Detrick and Crough, in a study on the long term subsidence of several western Pacific islands, introduced the concept of lithospheric thinning. They found, that the subsidence of these islands, all situated on the Hawaiian swell, is much more than would be expected from the age of the underlying lithosphere and the Sclater-curve. They proposed, that the Hawaiian swell is formed as the isostatic response of the lithosphere to an increase in basal heat flux. The increase in basal heat flux thins the lithosphere, whose lower boundary is assumed to be defined by an isotherm, by driving this isotherm upward and thus resetting the "thermal clock" to a younger age. This thermal rejuvenation causes the lithosphere to subside at faster rates than would be expected from the crustal age. One of the implicit assumptions in this model is that the depth of the density contrast, i.e. the raised lithosphere/asthenosphere boundary, should be within the thickness of the lithosphere as calculated from the crustal age.

Although this model explains several observations, some major problems remain unsolved. The Hawaiian swell actually rises near Hawaii over about 1 km (from 5.3 km to 4.3 km) in 3-5 Ma (Detrick and Crough, 1978). The transfer of the amount of heat, necessary for the uplift, from the upper mantle to relatively shallow depths in such a short time by conductive transport requires an increase in the basal heat flux of about 40 times (Detrick and Crough, 1978). Such an increase in the basal heat flux, if realistic, would lead to a, be it delayed, increase of surface heat flow of about the same factor (Crough and Thompson, 1976). Heat flow measurements along the Hawaiian

swell show a systematic increase in heat flux from near normal near Hawaii (youngest part of swell) to values near Midway (about 27 Ma old) which are only about 20-25 % higher than normal (Detrick et al, 1981; Von Herzen et al, 1982). Crough (1978) examined the effects of different reheating mechanisms on the subsidence and the heat flow and argued that the reheating must be confined to the lower part of the lithosphere. The available heat flow data fit a reheating model with about 50 % of lithospheric thinning (Von Herzen et al, 1982). In this model only the process after the reheating is considered.

A convective heat transfer model for lithospheric thinning was examined by Withjack (1979, c.f. Spohn and Schubert, 1982). In the model the rate of lithospheric thinning depends on the rate of magma intrusion, which causes the convective heat transfer. The model assumes a random magma entry up to an eruption depth, taken at 25 km. This is the depth at which significant volumes of magma are transported to the surface through volcanic conduits. Withjack (1979) assumes, that at the eruption depth the lithospheric thinning ceases. With a rate of magma entry of 2. 10^{-8} cm/s, the model suggests that the Hawaiian swell could form in less than 6 Ma.

The lithospheric thinning model can explain the observed subsidence of atolls and the observed heat flow values if we assume that the lithosphere is thinned to a depth L by some not yet specified process and study the decay of the thinned lithosphere to a "normal" one. The depth L can in principle be obtained from the uplift of the area and the delay time of the surface heat flux (e.g. Von Herzen et al, 1982). The process, responsible for the thinning, that reconciles both the surface heat flux and the rate of thinning has not yet been quantified. Withjack (1979) does not explain why some places are more favorable to thinning than others. We think that tectonic fracturing of the lithosphere may play an important role.

Consequences of inelastic deformation and thermal rejuvenation for the calculated ages of seamounts

In calculating the ages of the seamounts from the flexural rigidity we assumed that the behaviour of oceanic lithosphere, when loaded by a seamount, can be modelled with a homogeneous elastic plate which floats on an incompressible asthenosphere. From matching model calculations of gravity anomalies to those observed, we obtained the flexural rigidity of the plate. Empirical studies have shown that the base of the elastic plate corresponds to an isotherm (450°±150°C) in the oceanic lithosphere at the time the lithosphere was loaded (e.g. Watts et al, 1980). Bodine et al (1981) and McNutt and Menard (1982) used laboratory data on brittle and ductile rock failure to explain the thermal control of the elastic thickness. From the empirical relation and the elastic thickness we can calculate the age of the lithosphere at the time of loading, as was done in chapter III. Inelastic deformation and temperature perturbations of the lithosphere arising from thermal rejuvenation may lead to deviations from the above described relation.

Bending stresses

The equilibrium equation for an elastic plate (equation 3, chapter III) was derived under the assumption that a surface in the plate, which is parallel to the central surface (= neutral plane), will remain parallel to this surface when the plate is deformed. Thus on loading a vertical cross-section will only rotate with respect to the neutral surface, i.e. elements above this surface undergo compression and elements below tension. The neutral surface itself undergoes no longitudinal strain. The bending stresses have maxima at the upper surface (compression) and at the lower surface (tension) of the plate. We calculated these stresses, using the formulas given by Fung (1965, see also Timoshenko, 1941), and transformed them to the principal stresses: σ_1 and σ_2. If the bending stresses surpass a yield criterium inelastic deformation occurs. We used the Von Mises yield

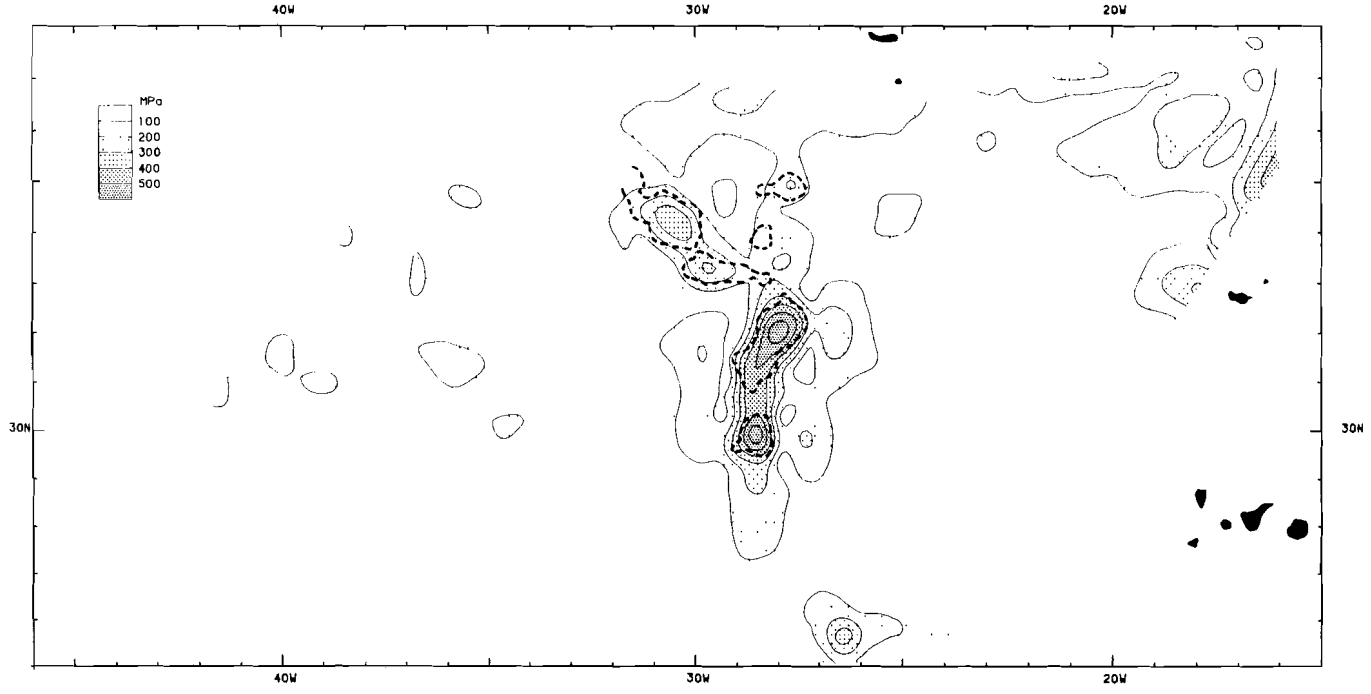

Figure 3: Bending stresses for a plate thickness of 20 km. Contour interval is 100 MPa (1kbar). Heavy dashed line indicates 3000 m corrected basement depth form Figure 2, chapter III.

criterium. In the absence of bending stresses in the z direction the expression is:

$$\{ (\sigma_1 - \sigma_2)^2 + \sigma_1^2 + \sigma_2^2 \} = \sqrt{2} \cdot \sigma_0 \qquad (1)$$

where σ_0 is the yield stress for uniaxial compression or tension (Jaeger and Cook, 1976). We calculated the left side of equation (1) and divided this value by $\sqrt{2}$ to obtain $\underline{Y}$: a value comparable to results in other studies. Figure 3 gives the contours of $\underline{Y}$ resulting from the flexure given in Figure 14, chapter III (plate thickness 20 km). Under Great Meteor seamount and the Cruiser complex $\underline{Y}$ is about 600 MPa (6 kbar). The other seamounts give values of about 300 MPa. Table I gives the values of $\underline{Y}$ under the center of the seamounts for the plate thicknesses found in chapter III.

Table I: Value of Y under center of seamounts.

seamount	*plate thickness*	*value of Y (MPa)*
Great Meteor	20 km	610
Cruiser complex	10 km	960
Plato (east)	10-15 km	260-210
Unnamed	7 km	450
Tyro	10 km	420
Plato (west)	7-10 km	670-530
Atlantis	7 km	680

These values are calculated under the assumption that the deflections are small. Before comparing these values with other results we will discuss some restrictions of the flexure equations.

Large deflections

The computed deflections for plate thicknesses of 10 km and less reach a significant fraction of the thickness. In this case the small deflection (linear or Poisson-Kirchoff) theory leads to inaccuracies

both in the computed deflections and in the stresses. In the linear theory one assumes that there is no stretching of the middle plane during deformation. This assumption is not valid for large deflections. The equilibrium equations of the plate for large deflections are given by two coupled non-linear fourth order differential equations: the Von Karman equations (e.g. Fung, 1965). For general loading conditions these equations do not lend themselves to analytical and closed form solutions.

Ribe (1982) found an elegant solution for the case of a one dimensional harmonic load. For this load function the resulting deflections using Von Karman's equations are always smaller than the corresponding results of the linear theory. The amount of reduction decreases with increasing plate thickness. For a plate thickness of 10 km the reduction reaches values of 20% for a deflection of about 8 km. The bending stresses also are reduced about the same amount.

Lambeck and Nakiboglu (1980) used a perturbation scheme for solving the Von Karman equations in the case of an axisymmetrical loading. Their solutions indicate that the linear theory underestimates the deflections, a result contradicting with Ribe (1982). Notwithstanding this, they conclude in agreement with Ribe that the linear theory overestimates the bending stresses. However, one of the assumptions in the calculations of Lambeck and Nakiboglu (1980), i.e. the neglection of part of the homogeneous solution for the stress potential in the outer region, is not entirely correct. This may lead to inaccuracies in their results.

Following Ribe (1982), when we use the linear theory, we overestimate the calculated deflections and the bending stresses. By comparing the calculated gravity effect of the flexure with the observed gravity anomalies this results in an overestimation of the plate thicknesses, especially for plate thicknesses of 10 km and less. This implies that the bending stresses for the "real" plate thickness are comparable in size to those calculated from the linear theory, using the overestimated plate thickness.

The bending stresses under the seamounts as given in table I are, with the exception of the ones under the Cruiser complex, comparable in magnitude to those found in other studies (e.g. Watts et al, 1980; Cazenave et al, 1980). The estimates of the thickness T_e used by Bodine et al (1981) to establish their relation between the elastic thickness and the age of the lithosphere are calculated from the elastic model. Thus we can, in principle, compare our results with this relation to obtain the ages of the seamounts.

The estimates of bending stresses cannot be applied directly to the state of stress in the oceanic lithosphere. The elastic model is based on a simple homogeneous plate model, i.e. we neglect that the rheological properties of the lithosphere are a function of the temperature and thus depth dependent. Several attempts have been made to model lithospheric flexure using a more complex rheology (e.g. Watts et al., 1980; Lago and Cazenave, 1980; Bodine et al, 1981; McNutt and Menard, 1982). In these models a yield strength envelope is used to estimate the bending stresses developed in the plate. The yield strength of the oceanic lithosphere is a strong function of the age. It ranges from values of a few kbar for young lithosphere up to about 10 kbar for older lithosphere (e.g. Watts et al, 1980; Cloetingh, 1982). The resulting stresses from these models are considerably smaller than those obtained in the elastic model, but still amount more than 100 MPa (1 kbar) for Hawaii (Watts et al, 1980). Visco-elastic relaxation may lead to a time-dependent and load-size dependent flexural rigidity (e.g. Lambeck and Nakiboglu, 1981). Bodine et al (1981) found that the mechanical thickness of the lithosphere, which determines the effective flexural rigidity is only weakly dependent on load size and duration for times greater than 1-10 Ma.

The elastic thickness under the Cruiser complex leads to bending stresses of about 1000 MPa (see table I). This value is much higher than that usually found from flexure. From Figure 3 it follows that the bending stresses under Great Meteor seamount and under the Cruiser complex are about equal for the same plate thickness. This makes it

unlikely, that the Cruiser complex seemingly gives too low a value because of high bending stresses. A possible cause for the large flexure of this complex might be found in fractures under the complex (e.g. Walcott 1970, who suggested this mechanism for Hawaii). In the case of a two dimensional model, fracture of the lithosphere will increase the flexure with a factor of 2. The stresses reduce with a factor of 2.5 (e.g. McNutt, 1980).

Consequences of thermal rejuvenation

If thermal rejuvenation affects the mechanical properties of the lithosphere, the age of the lithosphere at the time of loading calculated from the flexure will be too small. We show the influence of thermal rejuvenation on the upper mechanical layer by using Crough's solution to the lithospheric thinning model (plate model solution, see Von Herzen et al, 1982, c.f. Menard and McNutt, 1982). Figure 4A shows the depth of the 450°C isotherm as a function of the time after loading and of the thickness of the lithosphere after thinning (L). Figure 4B shows the depth of the ocean before and after reheating. In these models we assumed that the age of the oceanfloor at the time of reheating is 60 Ma. We will apply these results to Great Meteor seamount. For this seamount we found an elastic thickness of 20 km. Assuming that this represents the minimum value of the 450°C isotherm we derive from Figure 4A that the lithosphere under this seamount must have been thinned to about 35 km. From Figure 4B we see that for L=35 km, the depth anomaly over Great Meteor, with an age of the oceanfloor of 84 Ma, would be about 600 m. From a profile taken from Figure 1A we measured a depth anomaly of about 800 m. An age of the oceanfloor at the time of reheating less than 60 Ma results in a smaller depth anomaly. From this model it follows that the age of Great Meteor seamount is about 20 Ma, substantially less than the 42 Ma found in chapter III.

The conclusion from the above mentioned is, that the relation between elastic thickness and age of the oceanic lithosphere, as

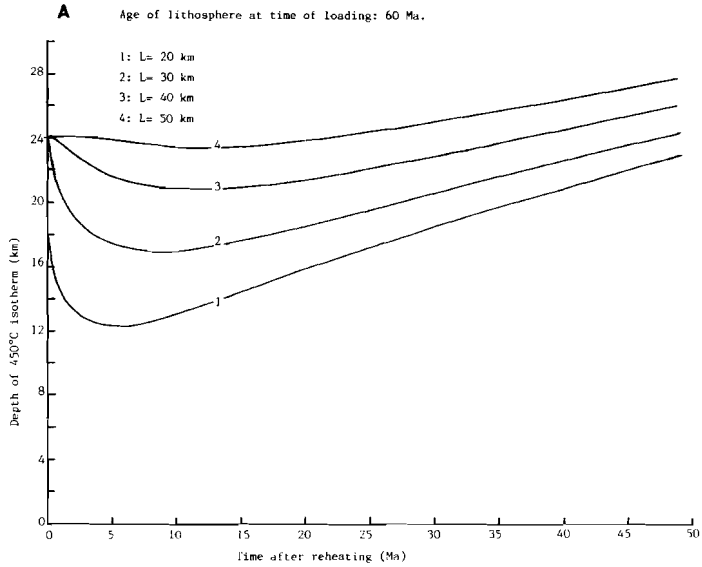

Figure 4A: Depth of 450°C isotherm after lithospheric thinning. L denotes thickness of lithosphere after thinning. Solution for the depth of the isostherm after Von Herzen et al (1982).

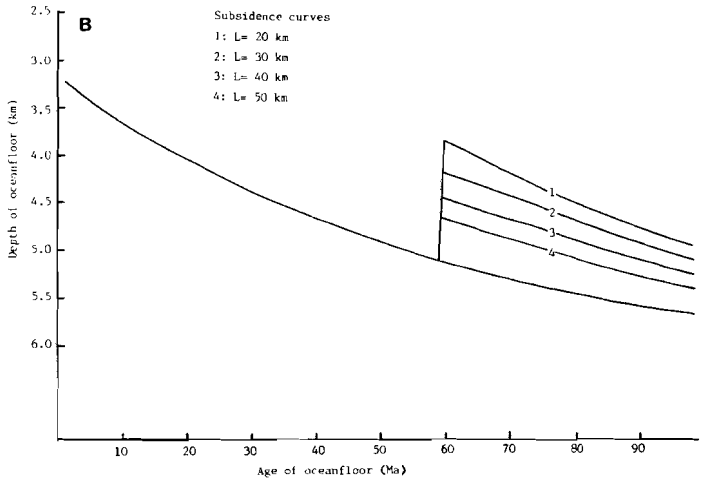

Figure 4B: Depth of oceanfloor before and after thermal rejuvenation for different values of the thinned lithosphere (L).

originally found by Watts (1978) and elaborated by Bodine et al (1981), is at this moment the best available. It may, however, not be expected that age estimates from this relation are accurate. However, inelastic deformation in general leads to an underestimation of the elastic thickness in a simple elastic model (e.g. McNutt and Menard, 1982). Visco-elastic relaxation and thermal rejuvenation also lead to an underestimation of the elastic thickness. It therefore seems reasonable to conclude, that the ages obtained for the seamounts in the Atlantis-Meteor complex are maximum estimates. A calculation of the real stresses under the seamounts makes a depth dependent rheology necessary. For this we analytical methods are no longer appropriate and we must use numerical methods (e.g Cloetingh, 1982).

Age variations of volcanoes over depth anomalies

A prediction of the hot-spot model (e.g. Wilson, 1963) is that the ages of volcanoes within a chain should increase continuously along the chain. Changes in trend along a chain reflect a change in plate motion relative to the underlying deep mantle. Chains formed at the same time, on the same plate, should all reflect the same motion with respect to the deep mantle. Small deviations can be accounted for in the hot-spot theory by allowing the sources to move slightly with respect to each other.

Age estimates from the seamounts of the Hawaiian-Emperor chain indicate an increase in age away from the present volcanism, i.e away from Hawaii (e.g. Wilson, 1963; Jarrard and Clague, 1977; McDougall and Duncan, 1980). The migration rate of the volcanism along the Hawaiian-Emperor chain follows a linear model (e.g McDougall and Duncan, 1980), a result confirmed by recent DSDP results (Jackson, Koisumi et al, 1980). Several other chains in the Pacific also show a systematic age increase (Jarrard and Clague,1977; McDougall and Duncan, 1980).

McDougall and Duncan (1980) also notice that the simple picture of a monotonic increase in age is not so evident along the chain

formed by the Austral and Cook islands (see also Turcotte and Oxburgh, 1978). Haggerty et al (1982) showed the existence of Late Cretaceous volcanism close to Caroline island (Pacific, at about 9°S, 150°W). With this result the nearly synchronous Late Cretaceous volcanism occurred over a distance of about 2500 km along the Line Islands chain. This makes a single hot-spot model an unlikely explanation for the origin of the Line Islands (Haggerty et al, 1982). The Eastern-Nazca trace forms another complication for the simple hot-spot hypothesis (e.g. Pilger and Handschumacher, 1981). Here recent volcanic activity occurred at several places along the trace, which led Bonatti et al (1977) to assume that this trace is the expression of a "mantle hot line" in stead of a mantle plume. Menard and McNutt (1982), in a study on thermal rejuvenation, found that most of the long and apparently continuous volcanic lineations in the Pacific in fact are composed of short segments. These segments are favorable sites for volcanism ("hot lines", see Bonatti et al, 1977).

Earlier explanations for the origin of the Atlantis-Meteor complex

Explanations of the origin of the Atlantis-Meteor complex, or part of this complex, up to now often related its origin to the Corner seamounts. The Corner seamounts form a complex in the western North Atlantic, situated between 34° and 36°N and from 47'30° to 52°W (McGregor and Krause, 1972). Pitman and Talwani (1972) suggested as a possible origin for Corner, Cruiser and Great Meteor seamounts a leaking transform fault as a result of changes in the pole of rotation. McGregor and Krause (1972) suggested a hot-spot origin for the Corner seamounts and also for Great Meteor, Cruiser and Plato seamounts. In this model the hot-spot would first be situated under the American plate giving birth to the Kelvin- New England seamounts and the western Corner seamounts. Then in Late Cretaceous times the hot-spot, now located under the Mid Atlantic Ridge, could have created the eastern Corner seamounts as well as Great Meteor, Cruiser and Plato seamounts. After this formation the less active hot-spot

migrated to the vicinity of the Azores where it might be presently located. A similar model has been proposed by Crough et al (1980). However these authors consider Great Meteor seamount to be the site of an active hot-spot.

The results in our study are not in agreement with the earlier explanations for the origin of the Atlantis-Meteor complex. First, it is unlikely that the seamounts originated on the spreading center as is assumed in the earlier explanations. Secondly, no clear age migration pattern of the volcanism has been detected. There is a third objection to the above mentioned hot-spot explanation. Studies of hot-spot lineations on the African plate (e.g. Duncan, 1981) suggest a general NE movement of the African plate with respect to the hot-spots. This movement is incompatible with the lineations found in the Atlantis-Meteor seamount complex. We therefore think it an unlikely explanation, in view of the results in this study, that the Atlantis-Meteor seamount complex originated from a movement of the African plate over a "fixed " hot-spot.

An alternative hypothesis for the origin of the complex

Turcotte and Oxburgh (1973, see also 1978) proposed as an alternative hypothesis for intra-plate volcanism, lithospheric fracturing, allowing magmas from the asthenosphere to penetrate into the lithosphere. They suggested that the cause for the tensional stresses responsible for the fracturing can be found in the thermal contraction of the oceanic plate or in 'membrane tectonic' stresses due to a change in the radius of curvature caused by the ellipticity of the earth. Tensional failure allows the hydrostatic head to drive the magma into the lithosphere (e.g Turcotte et al, 1977). The rising velocity of the magmas can be estimated (e.g. Turcotte et al, 1977). With a viscosity of the astenosphere of $1.5\ 10^{19}$ stokes (Collette et al, 1980), an average lithospheric thickness of 80 km and a pressure available to drive the material through the lithosphere of 40 MPa (Turcotte et al, 1977) we find, that rising diapirs must have

dimensions of about 7 km to allow rising velocities of 1 cm/a.

In chapter II it was concluded that the lithosphere under the Atlantis-Meteor complex primarily underwent an extension in a general NE-SW direction, leading to faulting and volcanism. In order to accomodate this extension Verhoef and Collette (1983) postulated the existence of one or more shear faults with a NE-SW strike joining the Azores-Gibraltar plate boundary. An upper limit for the extension can be found in the accuracy of the reconstruction of the seafloor spreading pattern (Collette et al, 1984). This leads to the conclusion that the amount of extension cannot be more than a few to ten kilometers.

Collette et al (1984) suggested that the extension might result from thermal contraction in the horizontal plane beyond the transform domain. Their analysis of the fracture zone pattern showed that the N-S component of this contraction still must be effective beyond the transform domain of the large-offset fracture zones in the adjustment of the flow-lines to a small circle pattern. If this adjustment leads to a concentration of tensional stresses in specific areas, an appropriate source of extension would be present, which could explain the observed tectonization. The measured extent of the deformation from horizontal thermal contraction is 2%. About half of this contraction will concentrate in the tramsform domain of the fracture zones. This leaves a N-S contraction of about 1% for deformation beyond the transform domain. On a distance of 1000 km this gives 10 km. This is also about the maximum estimated N-S error in the reconstruction of the flow line pattern of the fracture zones. Note that the uncertainty in the E-W direction is not accounted for in the reconstruction by Collette et al (1984). The tolerance in a NE-SW direction therefore may be more, say between 10 and 20 km. We estimate that this is enough to start the lithospheric thinning process.

In this model there is no need to postulate faulting beyond the area of the seamounts. However, the question of which process is responsible for the concentration of tension in a specific area is not clarified. External factors may be involved and as such we can think

of a reorganization of the spreading process with temporarily active offshoots of the European-African plate boundary. Such an offshoot then must lie to the N or E of the Atlantis-Meteor area proper. Up to now no indications for a hidden fault have been found but a transcurrent fault would be extremely difficult to detect, especially under the sediments of the Madeira abyssal plain. A more refined reconstruction of the fossil spreading pattern involving data of the American plate at these latitudes might help to formulate a definite answer of the question whether the occurrence of the Atlantis-Meteor seamount complex is due to an intra-plate process, or whether inter-plate factors are involved.

Conclusion

In this chapter we summarized several studies on depth anomalies. We argued that, looking at the correlation between gravity anomalies and depth anomalies we must distinguish two types of depth anomalies. The first type is related to intra-plate volcanism and mid-plate swells. It has, in general, a direct relationship with gravity with moderately shallow isostatic compensation. The second type, often of larger extent than the first type, also goes accompanied by gravity anomalies but the isostatic compensation is deeper and cannot be seated in the lithosphere.

The Atlantis-Meteor complex belongs to the former type of depth anomalies. The wavelengths shorter than about 1000 km follow the elastic plate compensation. The average compensation depth of the wavelengths longer than about 1000 km is situated in the lower half of the lithosphere. Still longer wavelengths in the gravity spectrum are of the second type and may be indicative for interaction with the Azores high.

We discussed the lithospheric thinning model. Convective heat transfer (by intrusion) is probably the process which is responsible for the thinning. We think that tectonic fracturing of the lithosphere may play an important rol (stoping).

There is no indication for a systematic variation of the age, or migration, of the volcanism of the Atlantis-Meteor complex. Age variations of the volcanism are systematic along the Hawaiian-Emperor chain. However several other lineations in the Pacific do not show a clear age migration pattern. The absence of a migration pattern in the Atlantis-Meteor complex combined with its mosaic pattern makes a hot-spot origin unlikely for this complex. As an alternative hypothesis we discussed lithospheric fracturing.

The Atlantis-Meteor complex does not stand alone as a volcano-tectonic structure in the North Atlantic (cf. Gebco sheet 5.08, 1982). The other island and submarine volcano groups are e.g. Azores, Canary Islands, Madeira archipelago and Cape Verde Islands. The tectonic setting of these volcanic groups is not identical and only some of these features can be considered as ridge flank volcanism. A comparitive study of the volcanism and the tectonics of these areas may eventually lead to an answer of the question whether lithospheric fracturing can be an explanation for all these volcanic phenomena in the Atlantic and what the interaction between intra- and interplate processes is.

References

-*Abramowitz M., Segun I.A., 1965. Handbook of Mathematical Functions., Dover, New York.*

-*Albuisson M., Monget J.M., Balmino G., Moynot B., Reigber Ch., 1979. Detailed gravimetric geoid for the North Atlantic, Bull. Geod., 53, 1-10.*

-*Anderson R.N., McKenzie D., Sclater J.G., 1973. Gravity, bathymetry and convection in the earth., Earth Planet Sci lett., 18, 391-407.*

-*Anonymous, 1967. "NAVADO III Bathymetric, magnetic and gravity investigations HNMS Snellius 1964-1965, Hydrographic Newsletter, special publication number 3.*

-*Aric K., Hirschleber H., Menzel H., Weigel W., 1970. About the structure of the Great Meteor seamount after seismic results., Meteor Forschungsergebnisse, Reihe C, 3, 48-65.*

-*Baranov V., 1957. A new method for interpretation of aeromagnetic maps: pseudo-gravimetric anomalies., Geophysics, 22, 359-383.*

-*Bhattacharyya B.K., 1965. Two-dimensional harmonic analysis as a tool for magnetic interpretation., Geophysics, 30, 829-857.*

-*Beaumont Ch., 1978. The evolution of sedimentary basins on a viscoelastic lithosphere: theory and examples. Geophys. J.R. astr. Soc.,55 , 471-497.*

-*Belderson R.H., Laughton A.S., 1966 Correlations of some Atlantic turbidites, Sedimentology, 7, 103-116.*

-*Berger W.H. 1970. Planktonic foraminifera: selective solution and the lysocline., Mar. Geol., 111-139.*

-*Berger W.H., Von Rad U., 1972. Cretaceous and Cenozoic sediments from the Atlantic Ocean., in: Hayes D.E., Pimm A.C., et al, 1972, Initial Reports of the Deep Sea Drilling Projext, vol XIV, Washington (U.S. Government Printing Office), 787-954.*

-*Bodine J.H., Karner G.D., 1981. Gravity effect of axially symmetric bodies using one-dimensional FFT., Geophys. J., R. astr. Soc., 67, 747-754.*

-*Bodine J.H., Steckler M.S., Watts A.B., 1981. Observations of flexure and the rheology of the oceanic lithosphere., J. Geophys. Res., 86, 3695-3707.*

-*Bonatti E., Harrison C.G.A., Fisher D.E., Honnorez J., Schilling J.G., Stipp J.J., Zentilli M., 1977. Easter volcanic chain (southeast Pacific): a mantle hot line.*

-*Bracewel R.N., 1978. The Fourier transform and its application., 2nd edition, McGraw-Hill, New York.*

-*Bullard E.C., Mason R.G., 1963. The magnetic field over the oceans., in: The Sea, vol 4-II, Maxwell A.E., ed., Wiley-Interscience, New York, pp 175-217.*

-*Cazenave A., Lago B., Dominh K., Lambeck K., 1980. On the response of the oceanic lithosphere from Geos-3 satellite radar altimeter observations., Geophys. J. R. astr. Soc., 63, 233-252.*

-*Chapman M.E., 1979. Techniques for interpretation of geoid anomalies., J. Geophys. Res., 84, 3793-3803.*

-Chapman M.E., Bodine J.H., 1979. Considerations of the indirect effect in marine gravity modelling., J. Geophys. Res., 84, 3889-3893.
-Chapman M.E., Talwani M., 1979. Comparison of gravimetric geoids with Geos 3 altimetric geoid., J. Geophys. Res., 84, 3803-3817.
-Cloetingh S.A.P.L., 1982. Evolution of passive continental margins and initiation of subduction zones., PhD thesis, Geologica Ultraiectina, 29, Utrecht.
-Cochran J.R., Talwani M., 1977. Free-air gravity anomalies in the world's oceans and their relationship to residual elevation., Geophys. J. R. astr. Soc., 50, 495-552.
-Cochran J.R., Talwani M., 1978. Gravity anomalies, regional elevation and the deep structure of the North Atlantic., J. Geophys. Res., 83, 4907-4924.
-Collette B.J., Ewing J.I., Lagaay R.A., Truchan M., 1969. Sediment distribution in the oceans: The Atlantic between 10° and 19° N., Mar. Geol., 7, 279-345.
-Collette B.J., Verhoef J., Mulder A.F.J., 1980. Gravity and a model of the median valley., J. Geophys., 47, 91-98.
-Collette B.J., Slootweg A.P., Verhoef J., Roest W.R., 1984. Geophysical investigations of the floor of the Atlantic Ocean between 10° and 38°N (Kroonvlag-project), Proc. Ned. Akad. Wet., series B, 1-76
-Crough S.T., 1978. Thermal origine of mid-plate hot-spot swells., Geophys. J. R. astr. Soc., 55, 451-469.
-Crough S.T., 1982. Geoid height anomalies over the Cape Verde Rise., Mar. Geophys. Res., 5, 263-271.
-Crough S.T., 1983. The correction for sediment loading on the seafloor., J. Geophys. Res., 88, 1236-1244.
-Crough S.T., Thompson G.A., 1976. Numerical and approximate solutions for lithospheric thickening and thinning., Earth Planet. Sci. Lett., 31, 397-402.
-Crough S.T., Morgan W.J., Hargraves R.B., 1980. Kimberlites: their relation to mantle hotspots., Earth Planet. Sci. Lett., 50, 260-275.
-Crough S.T., Jarrard R.D., 1981. The Marquesas-Line swell., J. Geophys. Res., 86, 11763-11771.
-Detrick R.S., Crough S.T., 1978. Island subsidence, hot spots and lithospheric thinning., J. Geophys. Res., 83, 1236-1244.
-Detrick R.S., von Herzen R.P., Crough S.T., Epp D., Fehn U., 1981. Heat flow on the Hawaiian swell and lithospheric reheating. Nature, 292, 142-143.
-Dietrich D., 1939. Einige morphologische Ergebnisse der Meteor fahrt Januar bis May 1938., Ann. Hydr., Beiheft, Januar.
-Dorman L.M., Lewis B.T.R., 1970. Experimental isostasy, 1: Theory of the determination of the earth'isostatic respons to a concentrted load., J. Geophys. Res., 75, 3357-3365.
-Duncan R.A., 1981. Hotspots in the southern oceans. An absolute frame of reference for motion of the Gondwana continents, Tectono-physics, 74, 29-42.
-Eldholm O., Windisch Ch.C., 1974. Sediment distribution in the Norwegian-Greenland Sea., Geol. Soc. Amer. Bull., 85, 1661-1676.

-Ewing J.I., Tirey G.B., 1961. Seismic Profiler., J. Geophys. Res., 66, 2917-2927.
-Feraud G., Kaneoka I., Allegre C.J., 1980. K-Ar ages and stress pattern in the Azores: Geodynamic implications., Earth Planet. Sci. Lett., 46, 275-286.
-Fermont W.J.J., Troelstra S.R., 1983. Early Miocene larger foraminifera from the Cruiser-Hyères seamount complex (Eastern North Atlantic)., Proc. Ned. Ak. Wet., series B, 86, 243-253.
-Fleischer U., Meyer O., Schaaf H., 1970. On the structure of the submarine tablemounts south of the Azores as derived from a gravimetric-magnetic north-south profile across the Grosse Meteor Bank., Meteor Forschungsergebnisse, Reihe C, 3, 37-48.
-Fox P.J., Schroeder F.W., Moody P.H., Pitman III W.C., Hoose P.J., in preparation. The bathymetry of the Oceanographer fracture zone and Mid-Atlantic ridge at 35°N with implications for the Central North Atlantic plate motion.
-Franceteau J., Harrison C.G.A., Sclater J.G., Richards M.G., 1970. Magnetization of Pacific seamounts: a preliminary polar curve for the Northeastern Pacific., J. Geophys. Res., 75, 2035-2061.
-Fung Y.C., 1965. Foundations of solid mechanics, Prentice-Hall, Englewood Cliffs, N.Y.
-Galdeano A., Rossignol J.C., 1977. Contribution de l'areomagnetisme a l'etude du Golfe de Valence (Mediterranee Occidentale)., Earth Planet. Sci. Lett., 34, 85-99.
-Gaposchkin E.M., 1980. Global gravity field to degree and order 30 from Geos 3 satellite altimetry and other data., J. Geophys. Res., 85, 7221-7234.
-GEBCO or General Bathrymetric Chart of the Oceans, 1982. Sheet 5.08, Hydrographic Chart Distribution Office, Ottawa.
-Giles B.F., 1968. Pneumatic acoustic energy source., Geophys. Prosp., 16, 21-53.
-Gradhsteyn I.S., Ryzhik I.M., 1965. Table of integrals, series and products., 4th edn, Academic Press, New York.
-Gunn R.A., 1943. A quantitive study of isobaric equilibrium and gravity anomalies in the Hawaiian islands., J. Franklin Inst., 238, 373-396.
-Haggarty J.A., Schlanger S.O., Premoli Silva I., 1982., Late Cretaceous and Eocene volcanism in the southern Line Islands and implications for the hotspot theory., Geology, 10, 433-437.
-Haut F.R., 1973. Auswertung und Interpretation einer geomagnetischen Vermessung der Groszen Meteor Kuppe., Dipl. Arb. Inst. Geophys. T.U., Claustal, 62 pp.
-Haxby W.F., Turcotte D.L., 1978. On isostatic geoid anomalies., J. Geophys. Res., 83, 5473-5478.
-Hayes D.E., Pimm A.C., et al, 1972. Initial Reports of the Deep Sea Drilling Project, vol XIV, Washington (U.S. Government Printing Office).
-Heezen B.C., Hollister C.D., 1971. The faces of the deep, Oxford University Press, New York.

-Heezen B.C., Ewing M., Ericson D.B., Bentley C.R., 1954. Flat topped Atlantis, Cruiser and Great Meteor seamounts (abstract), Bull. Geol. Soc., Amer., 65, 1261.
-Heiskanen W.A., Moritz H., 1967. Physical Geodesy., W.H. Freeman, San Francisco.
-Hertz H., 1884. Uber das Gleichgewicht schwimmender elastischen Platten, in Gesammelte Werke von Heinrich Hertz, vol. 1, 288-294.
-Hinz K., 1969. The Great Meteor seamount. Results of seismic reflection measurements with a pneumatic sound source and their geological interpretation., Meteor Forschungsergebnisse, Reihe C, 2, 63-77.
-IAGA Division I Working Group I, 1981. International Geomagnetic Reference Fields: DGRF 1965, DGRF 1970, DGRF 1975 an IGRF 1980, EOS, 62, 1169.
-Jackson E.D., Koisumi I., et al, 1980. Initial Reports of the Deep Sea Drilling Project, vol 55, Washington (U.S. Government Printing Office).
-Jaeger J.C., Cook N.G.W., 1976. Fundamentals of Rock Mechanics., John Wiley & Sons, Inc., New York.
-Jansa L.F., Enos P., Tucholke B.E., Gradstein F.M., Sheridan R.E.,1979. Mesozoic-Cenozoic sedimentary formations of the North American Basin, Western North Atlantic, in: Deep drilling results in the Atlantic Ocean, Continental margins and paleo-environment, ed. Talwani, Hay, Ryan., Maurice Ewing series vol 3, Am. Geophys. Un., 1-53.
-Jarrard R., Clague D. A., 1977. Implications of Pacific island and seamount ages for the origin of volcanic chains., Rev. Geophys. Space Phys., 15, 57-76.
-Jeffreys H., 1959. The Earth, 4th edin, Cambridge university press, London.
-Jones E.J.W., Laughton A.S., Hill M.N., Davies D., 1966. A geophysical study of part of the western boundary of the Madeira-Cape Verde Abyssal Plain., Deep Sea Res., 13, 889-907.
-Kahle H.G., Talwani M., 1973. Gravimetric Indian ocean geoid., Z. Geophys., 39, 167-187.
-Karner G.D., 1982. Spectral representation of isostatc models., B.M.R. J. of Australian Geology & Geophysics, 7, 55-62.
-Kuijpers A., 1981. The sedimentology of two Northeast Atlantic study areas: the Western Abyssal Plain and the area West of Great Meteor seamount. Progress Report 1981, Internal Report Rijks Geologische Dienst, Haarlem.
-Kuijpers A., Schuttenhelm R.T.E., Verbeek J. (eds), in prep., Geological studies in the Eastern Atlantic, in Mededelingen Rijks Geologische Dienst.
-Kukkamaki T.J., 1955. Gravimetric reductions with electronic computers., Publ. Isos. Inst.I.A.G (Helsinki), no 30.
-Lago B., Cazenave A., 1980. State of stress of the oceanic lithosphere in response to loading., Geophys. J. R. astr. Soc., 64, 785-799.

-Lambeck K., 1981. Flexure of the oceanic lithosphere from island uplift, bathymetry and geoid height observations: the Soceitty islands., Geophys. J. R. astr. Soc., 67, 91-114.
-Lambeck K., Nakiboglu. S.M., 1980. Seamount loading and stress in the ocean lithosphere., J. Geophys. Res., 85, 6403-6418.
-Lambeck K., Nakiboglu S.M., 1981. Seamount loading and stress in the ocean lithosphere, 2: viscoelastic and elastic-viscoelastic models., J. Geophys. Res., 86, 6961-6985.
-Lancelot Y., Seibold E., et al, 1977. Initial Reports of the Deep Sea Drilling Project., vol XLI, Washington (U.S. Government Printing Office).
-Laughton A.S., Berggren W.A., et al, 1972. Initial Reports of the Deep Sea Drilling Project., vol XII, Washington (U.S. Government Printing Office).
-Laughton A.S., Whitmarsh R.W., 1974. The Azores-Gibraltar plate boundary, in: Geodynamics of Iceland and the North Atlantic area, L. Kristjansson, ed., D. Reidel, Dordrecht, 63-81.
-Le Mouel J.L., Galdeano A., Le Pichon X., 1972. Remanent magnetization vector direction and the statictical porperties of magnetic anomalies., Geophys. J. R. Astr. Soc., 30, 353-371.
-Lerch F.J., Klosko S.M., Laubscher R.E., Wagner C.A., 1979. Gravity model improvements using Geos 3 (Gem 9 and 10)., J. Geophys. Res., 84, 3897-3916.
-Lewis B.T.R., Dorman L.M., 1970. Experimental isostasy, 2: An isostatic model for the U.S.A. derived from gravity and topographic data., J. Geophys. Res., 75, 3367-3386.
-Lowrie W., Alvarez W., 1981. One hundred million years of geomagnetic polarity history., Geology, 9, 392-397.
-Mammerickx J., 1981. Depth anomalies in the Pacific: active, fossil and precursor., Earth Planet. Sci. Lett., 53, 147-157.
-McDougall I., Duncan R.A., 1980. Linear volcanic chains- recording plate motions?, Tectonophysics, 63, 275-297.
-McGregor B.A., Krause D.C., 1972. Evolution of the seafloor in the Corner seamounts area., J. Geophys. Res., 77, 2526-2534.
-McKenzie D.P., Bowin C., 1976. Relationship between bathymetry and gravity in the Atlantic ocean., J. Geophys. Res., 81, 1903-1915.
-McKenzie D.P., Watts A.B., Parsons B., Roufousse M., 1980. The plan form of mantle convection beneath the Pacific ocean., Nature, 288, 442-442.
-McNutt M.K., 1979. Compensation of oceanic topography: An application of the response function technique to the Surveyor area., J. Geophys. Res., 84, 7589-7598.
-McNutt M.K., 1980. Implications of regional gravity for state of stress in the earth's crust and upper mantle., J. Geophys. Res., 85, 6377-6397.
-McNutt M.K., Menard H.W., 1978. Lithospheric flexure and uplifted atolls., J. Geophys. Res., 83, 1206-1212.
-McNutt M.K., Menard H.W., 1982. Constraints on yield strength in the oceanic lithosphere derived from observations of flexure., Geophys. J. R. astr. Soc., 71, 363-394.

-Menard H.W., 1973. Depth anomalies and the bobbing motion of drifting islands., J. Geophys. Res., 78, 5128-5138.
-Menard H.W., McNutt M.K., 1982. Evidence for and consequences of thermal rejuvenation., J. Geophys. Res., 87, 8570-8580.
-Morelli C. et al, 1974. The International Gravity Standarization Net 1971 (I.G.S.N.71), Publ. Bureau central de l'association internationale de geodesie, Paris.
-Morgan W.J., 1968. Rises, Trenches, Great Faults and Crustal Blocks., J. Geophys. Res., 73, 1959-1982.
-Morgan W.J., 1971. Convection plumes in the lower mantle., Nature, 230, 42.
-Morgan W.J., 1972. Plate motion and deep mantle convection. Mem Geol. Soc. Am., 132, 7-22.
-Nabighian M.N., 1972. The analytical signal of two-dimensional magnetic bodies with polygonal cross-section: its properties and use for automated anomaly interpretation., Geophysics, 37, 507-517.
-Nadai A., 1963. Theory of flow and fracture of solids., McGraw-Hill, New York.
-Niskanen E., Kivioja L., 1951. Topographic-isostatic world maps of the effect of the Hayford zones 10 to 1 for the Airy-Heiskanen and Pratt-Hayford systems., Publ. Isos. Inst. IAG (Helsinki),no: 28.
-Parsons B., Sclater J.G., 1977. An analysis of the variation of ocean floor bathymetry and heat flow with age., J. Geophys. Res., 82, 803-828.
-Perry R.K., Fleming H.S., Vogt P.R., Cherkis N.Z., Feden R.H., Thiede J., Strand J.E., Collette B.J., 1981. Bathymetry and plate tectonic evolution., Geol. Soc. Am., Map and chart series, MC-35.
-Pilger R.H., Handschumacher D.W., 1981. The fixed-hotspot hypothesis and the origin of the Easter-Sala y Gomez- Nazca trace., Geol. Soc. Amer. Bull., 92, 437-446.
-Pitmann III W.C., Talwani M., 1972. Sea-floor spreading in the North Atlantic., Geol. Soc. Amer. Bull., 83, 619-646.
-Plaumann S., 1974. Zur gravimetrische Bestimmung der Dichte von Seamounts mit Anwendung auf die Kleine und Grosse Meteor Kuppe, Geol. J.B., E2, 99-110, Hannover.
-Pratt R.M., 1962. Great Meteor seamount., Deep Sea Res., 10, 17-25.
-Prince R.A., Forsyth D.W., submitted. A simple objective method for minimizing crossover errors in marine gravity data.
-Rabinowitz P.D., Cande S.C., Hayes D.E., 1979. The J-anomaly in the central North Atlantic ocean., in: Initial reports of the Deep Sea Drilling Project, vol 43, Tucholke B.E., Vogt P.R. et al, 1979, Washington (U.S. Government Printing office), 879-885.
-Rad U. von, 1974. Great Meteor and Josephine seamounts (eastern North Atlantic): Composition and origin of bioclastic sands, carbonate and pyroclastic rocks., Meteor Forschungsergebnisse, Reihe C, 19, 1-62.
-Rapp R.H., 1981. The Earth's grevity field to degree and order 180 using Seasat altimeter data, terrestrial gravity data and other data. Dept. of Geodetic Science Report No 322., The Ohio State University, Colombus, Ohio.

-Ribe N.M., 1982. On the interpretation of frequency respons functions for oceanic gravity and bathymetry., Geophys. J. R. Astr. Soc., 70, 273-294.
-Ridley W.I., Watkins N.D., MacFarlane D.J., 1973. in: The ocean basins and margins, A.E.M. Nairn and F.G. Stehli, eds, Plenum New York, vol 2, 445-483.
-Sandwell D.T., Poehls K.A., 1980. A compensation mechanism for the Central Pacific., J. Geophys. Res., 85, 3751-3758.
-Schouten J.A., 1971. A fundamental analysis of magnetic anomalies over oceanic ridges., Mar. Geophys. Res., 1, 111-144.
-Sclater J.G., Francheteau J., 1970. The implications of terrestrial heat flow observations on current tectonic and geochemical models of the crust and upper mantle of the earth., Geophys. J. R. astr. Soc., 20, 509-542.
-Sclater J.G., Lawver L.A., Parsons B., 1975. Comparisons of long wavelength residual elevations and free-air gravity anomalies in the North Atlantic and possible implications for the thickness of the lithospheric plate., J. Geophys. Res., 80, 1031-1053.
-Sclater J.G., Boyle E., Edmond J.M., 1979. A quantitive analysis of some factors affecting carbonate sedimentation in the oceans., in: Deep drilling results in the Atlantic ocean, eds: Talwani M., Hay W., Ryan W.B.F., Mauric Ewing series vol 3, Amer. Geophys. Un., 235-249.
-Searle R.C., 1980. Tectonic pattern of the Azores spreading centre and triple junction., Earth Planet. Sci. Lett., 51, 415-434.
-Slootweg A.P., 1978. Computer contouring with a digital filter., Mar. Geophys. Res., 3, 401-405.
-Slootweg A.P., Collette B.J., in preparation. Crustal structure and spreading history of the central North-Atlantic in the Cretaceous Magnetic Quiet Period (African Plate).
-Sodera, 1979. Watergun documentation.
-Spohn T., Schubert G., 1982. Convective thinning of the lithosphere: a mechanism for the initiation of continental rifting., J. Geophys. Res., 87, 4669-4681.
-Stackelbergh U. von, Rad U. von, Zobel B., 1976. Asymmetric distribution of displaced material in calcareous oozes around Great Meteor seamount (North Atlantic), Meteor Forschungsergebnisse, Reihe C, 25, 1-46.
-Stackelbergh U. von, Rad U. von, Zobel B., 1979. Asymmetric sedimentation around Great Meteor seamount (North Atlantic)., Mar. Geol., 33, 117-133.
-Talwani M., 1973. Computer usage in the computation of gravity anomalies, in: Methods in computational physics, 13, edited by B. Bolt, 343-389, Academic, New York.
-Talwani M., Le Pichon X., 1969. Gravity field over the Atlantic Ocean, in The Earth's crust and upper mantle, Geophys. Monogr. Ser., vol 13, ed: Hart P.J., AGU, Washington D.C., pp 341-351.
-Talwani M., Poppe H., Rabinowitz P., 1972. Gravimetrically determined geoid in the western North Atlantic, sea surface topography from space, NOAA tech. Rep., ERL-228-AOML 7-2, part 2, 1-34, Nat. Oceanic and Atmos. Admin., Boulder, Colorado.

-Talwani M., Udintsev G., et al, 1976. Initial Reports of the Deep Sea Drilling Project, vol XXXVIII, Washington (U.S. Government Printing Office).
-Timoshenko S., 1940. Theory of plates and shells., McGraw-Hill, New York.
-Tucholke B.E., 1979. Relationship between acoustic stratigraphy and lithography in the western North Atlantic basin, in: Tucholke B.E., Vogt P.R., et al, 1979, Initial Reports of the Deep Sea Drilling Project, vol 43, Washington (US. Government Printing Office),827-847.
-Tucholke B.E., Mountain G.S., 1979. Seismic stratigraphy, lithostratigraphy and paleasedimentation patterns in the North American basin, in: Deep Drilling results in the Atlantic ocean, Talwani M., Hay W., Ryan W.B.F., eds, Maurice Ewing series, vol 3, Am. Geophys. Un., Washington, 58-87.
-Tucholke B. E., Vogt P.R., et al, 1979. Initial Reports of the Deep Sea Drilling Project, vol XLIII, Washington (U.S. Government Printing Office).
-Turcotte D.L., Oxburgh E.R., 1973. Mid-plate tectonics., Nature, 244, 337-339.
-Turcotte D.L., Haxby W.F., Ockendon J.R., 1977. Lithospheric instabilities, in: Talwani M. and Pitmann III W. (eds), Island arcs, deep sea trenches and back-arc basins, Washington D.C., AGU, Maurice Ewing Series, vol 1, pp 63-69.
-Turcotte D.L., Oxburgh E.R., 1978. Intra-plate volcanism., Phil. Trans. R. Soc. London A., 288, 561-579.
-Twigt W., 1980. Magnetic anomalies over fracture zones in the central North Atlantic ocean., Ph.D. thesis, Geologica Ultraiectina, 26, Utrecht.
-Twigt W., Verhoef J., Rohr K., Mulder Th.F.A., Collette B.J., 1983. Topography, magnetics and gravity over the Kane fracture zone in the Cretaceous Magnetic Quiet Zone (African Plate)., Proc. Kon. Ned. Ak. Wet., series B, 86 (2), 181-210.
-Ulrich J., 1971. On the topography and morphology of the Great Meteor seamount., Meteor Forschungsergebnisse, Reihe C, 6, 48-68.
-Van Andel T.H., Thiede J., Sclater J.G., Hay W.G., 1977. Depositional history of the South Atlantic ocean during the last 125 million years., J. of Geol., 85, 651-698.
-Van den Berg J., 1979. Paleomagnetic data from the western Mediterranean: a review., Geol. Mijnbouw, 58, 161-174.
-Vening Meinesz F.A., 1931. Une nouvelle methode pour la reduction isostatique regionale de l'intensite de la pesanteur., Bull. Geod., 29.
-Vening Meinesz F.A., 1941. Tables for the regional and local isostatic reduction (Airy system) for gravity values, Publ. Neth. Geod. Comm., Waltmann, Delft.
-Verhoef J., Collette B.J., 1983. A tear fault system beneath the Atlantis-Meteor seamount group., Ann. Geophys.,1,199-206.
-Verhoef J., Scholten R.D., 1983. Cross-over analysis of marine magnetic anomalies ., Mar. Geophys. Res., 5, 421-435.

-*Von Herzen R.P., Detrick R.S., Crough S.T., Epp D., Fohn U., 1982. Thermal origin of the Hawaiian swell: heat flow evidence and thermal models., J. Geophys. Res., 87, 6711-6723.*
-*Walcott R.I., 1970. Flexure of the lithosphere at Hawaii., Tectonophys., 9, 435-446.*
-*Walcott R.I., 1976. Lithospheric flexure, analysis of gravity anomalies and the propagation of seamount chains., Int. Woolard Symp., AGU Monogr. 19, pp 431-438.*
-*Watts A.B., 1976. Gravity and bathymetry in the Central Pacific ocean., J. Geophys. Res., 81, 1533-1553.*
-*Watts A.B., 1978. An analysis of isostasy in the world's oceans, 1: Hawaiian-Emperor seamount chain., J. Geophys. Res., 83, 5889-6004.*
-*Watts A.B., 1979. On geoid heights derived from Geos3 altimeter data along the Hawaiian-Emperor seamount chain., J. Geophys. Res., 84, 3817-3827.*
-*Watts A.B., Cochran J.R., 1974. Gravity anomalies and flexure of the lithosphere along the Hawaiian-Emperor seamount chain., Geophys. J. R. astr. Soc., 38, 119-141.*
-*Watts A.B., Cochran J.R., Selzer G., 1975. Gravity anomalies and flexure of the lithosphere: A three-dimensional study of the Great Meteor seamount, Northeast Atlantic., J. Geophys. Res., 80, 1391-1398.*
-*Watts A.B., Leeds A., 1977. Gravimetric geoid in the Northwest Pacific ocean, Geophys. J. R. astr. Soc., 50, 249-278.*
-*Watts A.B., Bodine J.H., Steckler M.S., 1980. Observations of flexure and the state of stress in the oceanic lithosphere., J. Geophys. Res., 85, 6369-6376.*
-*Wendt I., Kreuzer H., Muller D., Rad U. von, Raschka H., 1976. K-Ar age of basalts from Great Meteor and Josephine seamounts (eastern North Atlantic)., Deep Sea Res., 23, 849-862.*
-*Williams C.A., Verhoef J., Collette B.J., 1983. Magnetic analysis of some large seamounts in the North Atlantic., Earth Planet. Sci. Lett., 63, 399-407.*
-*Wilson J.T., 1963. A possible origin of the Hawaiian islands., Can. J. Phys., 41, 863-870.*
-*Wilson J.T., 1973. Mantle Plumes and plate motions., Tectonophysics, 19, 146-164.*
-*Withjack M., 1979. A convective heat transfer model for lithospheric thinning and crustal uplift., J. Geophys. Res., 84, 3008-3022.*

CURRICULUM VITAE

De schrijver van dit proefschrift behaalde in 1967 het diploma MULO-B aan de Christelijke MULO te Ermelo en in 1970 het diploma HBS-B aan het Christelijk College Nassau-Veluwe te Harderwijk. In 1970 werd begonnen met de studie natuurkunde aan de Rijksuniversiteit Utrecht. Na het behalen van het kandidaatsexamen N4 (natuurkunde en scheikunde met bijvak wiskunde) in 1973, werd in 1977 het doctoraalexamen experimentele natuurkunde met als groot bijvak scheikunde afgelegd. In 1978 werd een aanvullend doctoraalexamen met groot bijvak fysica van de vaste aarde gedaan. Van december 1978 tot april 1984 is de auteur werkzaam geweest bij de afdeling Mariene Geofysica aan de Rijksuniversiteit Utrecht in dienst van de Nederlandse organisatie voor zuiver-wetenschappelijk onderzoek. Gedurende die periode werd deelgenomen aan een zestal expedities.